Ricardo Oliveira Gomes

STUDY CASE OF IMPACTS IN POWER QUALITY AND ANALYSIS OF TIME VARYING HARMONICS PRODUCED BY PHOTOVOLTAIC INVERTERS UNDER TRANSIENT CONDITIONS

Brasil

2019

Ricardo Oliveira Gomes

STUDY CASE OF IMPACTS IN POWER QUALITY AND ANALYSIS OF TIME VARYING HARMONICS PRODUCED BY PHOTOVOLTAIC INVERTERS UNDER TRANSIENT CONDITIONS

Dissertação submetida à Coordenação de Pós-Graduação em Engenharia Elétrica da Universidade Federal de Itajubá, como parte dos requisitos para a obtenção do título de Mestre em Ciências em Engenharia Elétrica.

Universidade Federal de Itajubá – UNIFEI

Programa de Pós-Graduação

Supervisor: Paulo Fernando Ribeiro

Co-supervisor: Carlos Augusto Duque

Brasil

2019

ACKNOWLEDGEMENTS

At first, I thank my family for their support. Even far from home, I have always received attention and encouragement during the development of this work. Special thanks to my mother that even in the face of difficult moments she always supported me.

Thanks to my supervisor Prof. Paulo Fernando Ribeiro who always attended me with great attention and dedication at all times, not only technically but personally.

I thank Matheus Zambroni for sharing his knowledge and contributing for the development of this work.

To the laboratory technician Lucio for the support in the assembly and installation of the measuring equipment described in this work.

To all of UNIFEI who contributed directly and indirectly to this work and the organization CAPES for financial support.

"Look again at that dot. That's here. That's home. That's us."
Carl Sagan, Pale Blue Dot: A Vision of the Human Future in Space.

ABSTRACT

As renewable energy use increases mainly by photovoltaic generation, a large number of inverters are connected to the grid creating harmonic distortion. Each inverter topology and control methodology has advantages and disadvantages. A comparative study was carried out between the three main internal inverters topologies, analyzing their content and harmonic distortion (THD). A second study was carried out on two models of Fronius inverters, located at an university building with photovoltaic plant of 27kWp. Measurements were taken at the building substation and directly at inverters outputs analyzing standard operation, startup, shutdown and energy variation due to solar irradiation. To perform these analyzes, time-frequency analysis techniques such as STFT, Wavelet and Wavelet Packet were used. The techniques are effective to analyze and identify the harmonic system components, as well as increase in magnitude over time. In addition, the techniques were also effective on identifying the behavior of other loads and their harmonics propagation in the grid.

Keywords: Inverters, Harmonic distortion, Harmonic decomposition, Multi-resolution analysis, Wavelet transform , STFT, Time-varying harmonics

LIST OF FIGURES

LIST OF TABLES

LIST OF ABBREVIATIONS AND ACRONYMS

AC	Alternating Current
ASD	Adjustable Speed Drivers
CWT	Continuous Wavelet Transform
DC	Direct Current
DWT	Discrete Wavelet Transform
DFT	Discrete Fourier Transform
DWT	Discrete Wavelet Transform
FACTS	Flexible AC Transmission Systems
FFT	Fast Fourier Transform
FT	Fast Transform
MPPT	Maximum Power Point Tracker
PD	Phase Disposition
PWM	Pulse-Width Modulation
PV	Photovoltaic
RTDS	Real Time Digital Simulator
SPWM	Sinusoidal Pulse-Width Modulation
STFT	Short-Time Fourier Transform
THD	Total Harmonic Distortion
UPS	Uninterrupted Power Supply
VSI	Voltage Source Inverter

CONTENTS

1 INTRODUCTION

With the increase power electronic devices there is a greater insertion of non-linear loads in the electric system. These devices generate voltage and current harmonic distortions that are responsible for thermal losses, equipment damage, switching protection malfunction and degradation of power quality [1, 2].

Distributed generation uses these devices to perform the necessary electrical energy conversions for use and connection to the grid. Inverters are largely used for this applications [3, 4] since they use semiconductor switches. In their construction, the type of topology adopted influences harmonic contribution [5], which are how these switches are grouped to generate the sine-wave voltage output. The control strategy and techniques have an impact on the switching frequency [6], where high frequencies are used and the harmonics are concentrated around these frequencies.

Manufactures datasheet usually report the level of distortion, but this information refers to the outputs under normal operating conditions. Since there are variations at system currents and also variations in harmonics, conventional methods of analysis such as the Fourier transform may inform data that do not correspond to the reality of the measured signal [7]. A better investigation of these phenomena is necessary.

This dissertation proposes the use of time-frequency techniques to perform analysis of the behavior of harmonics caused by the inverter of a PV system. Most commonly used inverter topologies are compared using simulation using MATLAB/Simulink.

Following, two models of Fronius inverters are analyzed, located at an university building with photovoltaic plant of 27kWp. Standard conditions are analyzed during startup, shutdown and energy variation due to solar irradiation. Using the same techniques it is possible to perform the event identification using the time-varying harmonics such as load activation or harmonics propagation in the grid.

1.1 Motivations and Objectives

Power quality is an important factor when it comes to electrical systems. With the increase of nonlinear loads and distributed generation, harmonic distortion can affect the grid power quality.

When installing a PV plant, there is no previous concern of the impacts of the harmonics that this system can inject in the grid. Manufacturers often show distortion data available in their datasheets, which are within acceptable standards. However, in practice the impacts of power quality after installation are not analyzed, or if they are, do

not take into account the transient operating conditions of the inverters, such as startup, shutdown and energy output variations.

In this way, a study on the harmonic contributions generated by the inverters in a real photovoltaic installation, using tools of time-frequency analysis, allowing to follow the harmonic spectrum in the time, contemplated both the regular conditions and the transient ones, help us to understand better the procedures to be taken and which impacts on the power quality occur after the installation of a solar generation.

This work contributes to the presentation of signal processing tools applied to current measurements at photovoltaic generation inverters in several operational conditions, presenting these inverters behavior and its particularities. The impacts caused on power quality when inserting the generation in the system are also discussed. Another contribution is the possibility to detect load activation events in the system by using the signal processing tools.

1.2 Literature review

The application of inverters as voltage source (Voltage Source Inverter - VSI) is one of the most used, especially nowadays due to the increase in renewable energy. Both mono phase and three phase grid connections have been used to produce alternating voltages in various types of applications like adjustable speed drives (ASD) [8], power active filters [9], Flexible AC transmission systems (FACTS) [10], battery banks, wind turbines [11], AC motors speed control [12] and PV systems [13, 14].

The electrical production from PV modules generates DC voltage. In order to use this energy for AC applications it is necessary to use an inverter to convert output voltage to the alternate form. There are several topologies of inverters [15] that can be symmetrical [16] or asymmetrical and have varying levels of output voltages [17].

Multi-level inverters for AC generation have several advantages, like eliminating the number of power transformers and minimizing the filter requirements as it improves the quality of voltage output [18].

The analysis of the harmonic content due to the modulation and topology adopted proves essential [4]. According to the location and amplitude of the harmonic components (voltage and current) the performance and stability of electrical systems that use these types of inverters can be compromised.

The micro residential solar generation has grown each year, leads to a concern on the impacts that a large number of inverters installed on a region can cause in the grid, especially in power quality [19, 20]. For the power quality it's important to analyze the level of voltage and current harmonic distortion on the grid caused by the inverter due to

the switching of the electric current, when flowing through impedance's, induces harmonic distortion in voltage. Another drawback of inverters is grid voltage elevation, caused by the peak voltage during the MPPT (Maximum Power Point Tracking) voltage rise cycle [21].

The energy generated by PV modules depends on a number of factors such as irradiation, temperature, which can change DC voltage output. In order to provide a stable grid connection, the use of DC to DC Boost converter combined with a MPPT algorithm help provides a more stable DC output [22–24].

These non-linear loads connected to the grid have a harmonic signature, which can be used to perform a non-invasive monitoring of these loads [2, 25], allowing the identification of the connected equipment and the moment in which it was operated.

Time-frequency techniques are used to obtain information on signal frequencies in the time domain. Thus, one can extract the frequency components of the signal and observe their variations, magnitude and duration over time.

One of these techniques is the STFT, where the reference [26] makes use to fault detection in transmission lines and [27] in distribution.

Another technique, the Wavelet transform, is well conceptualized in the detection of events in power systems [28–32], being used to identify several types of events such as sag, swell, interruption, flicker, notch, oscillatory transients and harmonics [33]. Reference [34] classify four classes of events: generator outage, 3-phase fault, load rejection, and capacitor outage. Some references use Wavelet in conjunction with neural networks for real-time classification of events [29, 35].

A variation of the Wavelet transform, the Wavelet Packet can be used to produce uniform frequency bands, favoring its use at harmonic signals analysis. At [36] the Wavelet Packet is used to detect island for grid-connected photovoltaic systems.

1.3 Structure of dissertation

The work was divided into 7 chapters as follows.

Chapter 1 presents an introduction, motivations and bibliographic review.

Chapter 2 presents the entire theoretical basis used in this work as signal processing techniques and power quality.

Chapter 3 describes three some types of inverters topologies and their control method.

Chapter 4 presents measurements methodology and simulations of inverters topologies and comparison of harmonic distortion levels.

Chapter 5 presents results of time-frequency techniques at inverter measurements

under standard operation and under transient conditions.

Chapter 6 presents the conclusions of the study.

Chapter 7 presents the future work.

2 THEORETICAL FOUNDATIONS

2.1 Fourier Transform (FT)

The Fourier Transform (FT) is a mathematical procedure to determine the frequencies contained in a given signal [37]. It is defined by the equation:

$$X(f) = \int_{-\infty}^{\infty} f(t).e^{-j.2\pi.f.t}dt \tag{2.1}$$

The Fourier series can be used to find the harmonic's magnitude and phase for periodic signals. The FT provides the general frequency response, and in cases where the signal is periodic, the FT are impulses which the areas are related to the Fourier series.

2.2 Total Harmonic Distorcion (THD)

The THD is a parameter used to indicate the percentage of deformation of a waveform [38]. The higher the level of distortion the greater its value. The equation 2.2 represents the calculation of this parameter:

$$THD\,(\%) = \frac{\sqrt{\sum_{k=2}^{N} V_k^2}}{V_1} \tag{2.2}$$

The RMS voltage V_1 is the fundamental voltage and V_k is the RMS of the harmonic order k.

2.3 Discrete Fourier Transform (DFT)

The Fourier transform is used to analyze time continuous domain signals in the frequency domain. When it is applied to a periodic signal, it provides the magnitudes and phases of the fundamental and its harmonic components. The Discrete Fourier Transform (DFT) is the digital version of the Fourier transform, where both time and frequency are discrete, and can be implemented in digital processor. The mathematical expression for DFT is given by [39]:

$$X(m) = \sum_{n=0}^{N-1} x(n).e^{-i2\pi n\frac{m}{N}}\ (m = 0, 1, \ldots, N-1) \tag{2.3}$$

Where N is the number of frequency bins. The graph representation by this technique displays the amplitudes of the frequencies contained in the signal (Fig. 1).

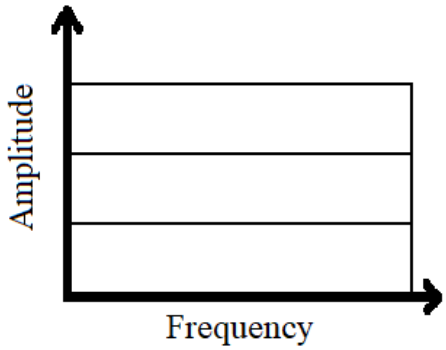

Figure 1 – Amplitude vs Frequency (DFT).

For periodic signals, harmonics can be analyzed using the Discrete Fourier Transform (DFT), which is computationally optimized by the Fast Fourier Transform (FFT). The Fig. 2(a) shows a sum of sine waves at 60, 180, 300, 420 and 540 Hz and Fig. 2(b) the magnitude of DFT.

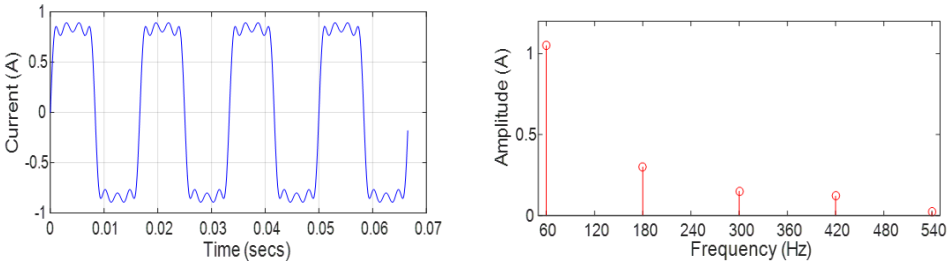

(a) Fundamental signal with odd harmonics.

(b) Amplitude of harmonic frequencies.

Figure 2 – Periodic signal and FFT analysis.

However, this method is not very efficient when applied to a wave with time varying components (where the amplitude and/or, phase and/or frequency are time function). Another important point is the Fourier transform does not carry time information and is not possible to identify, from the spectrum, the time instant that some changing happens in the component. [40]. The example is represented by the equation 2.4:

$$\begin{cases} f(t) = sin(2 * pi * 60 * t), 0 \leq t \leq 0.033 \\ f(t) = sin(2 * pi * 60 * t) + sin(2 * pi * 300 * t), 0.033 > t \leq 0.066 \\ f(t) = sin(2 * pi * 60 * t) + sin(2 * pi * 300 * t) + sin(2 * pi * 540 * t), 0.066 > t \leq 0.1 \end{cases} \tag{2.4}$$

The Fig. 3(a) contains a signal with time varying frequencies, from 0 to 0.033s at 60Hz, from 0.034 to 0.066s added 300Hz and from 0.067s added 540Hz. When this signal is analyzed using FFT (Fig. 3 (b)), the spectrum leakage effect occurs, displaying frequencies that does not exist in the original signal.

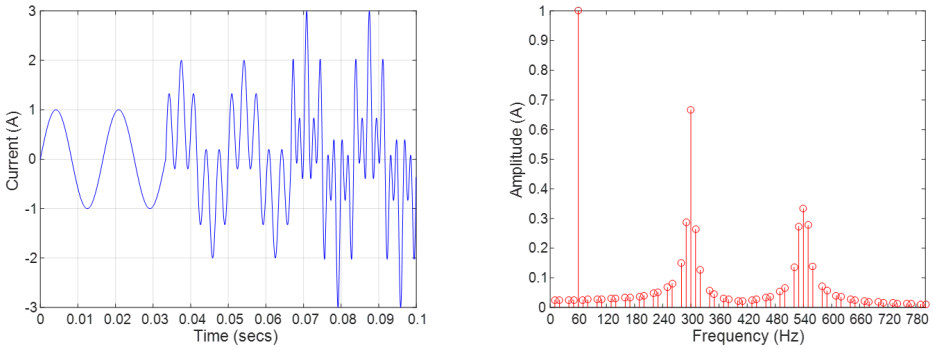

(a) Signal with varying frequencies (60, 300 and 540Hz).

(b) FFT analysis spectrum result with leakage effect.

Figure 3 – FFT spectrum analysis.

2.4 Short-Time Fourier Transform (STFT)

In power systems, the voltage and current distortion levels are continually changing in time, this is due to the fact that the grid configuration usually changes and its linear and nonlinear loads vary all the time [41,42]. When the FFT is applied to these signals, the frequency components are obtained, but the information in time is lost, so it is not possible to determine when a variation of the spectral content has occurred [43]. An alternative to this type of analysis was proposed by Gabor [44] as an adaptation of the Fourier transform, where a signal is multiplied by a sliding windowed function in time.

The time signal is subdivided into fixed length and short duration windows (Fig. 4(a)), where a new FFT is calculated for each window. Thus, we obtain a result in two dimensions, time and frequency [45] (Fig. 4(b)), allowing to observe the evolution of the harmonic components over time, such as analysis and detection of events in the power system. The drawback of this technique is the fixed size windows for all frequencies in time-frequency analysis. To obtain different resolutions in the analysis of a signal it is necessary to reapply the STFT with different windows sizes.

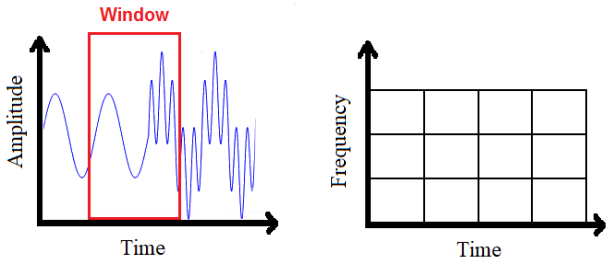

(a) Signal with sliding window.

(b) Frequency x Time.

Figure 4 – STFT window example and result graph.

The STFT is used in non-stationary signals and is defined as:

$$X_n\left(e^{j\omega_k}\right) = \sum_m x(m).w\left[n-m\right].e^{-j\omega_k m} \tag{2.5}$$

Where $w_k = 2\pi k/N$ is the frequency in radians ($k = 0, 1, ..., N-1$), N is the number of frequency bands, $w[m]$ is a limited size L window (Ex: Hamming), where $L \leq N$.

In Fig. 5 and Fig. 6, the moment in which frequencies of 300hz and 540hz are added to the signal are identified at approximately 0.033s and 0.066s. The sliding window causes a bit of leakage between the windows, making detail analysis less accurate, for example discontinuity recognition, among others. Thus, a suitable window should be chosen to obtain a better result in the spectogram of the analyzed signal.

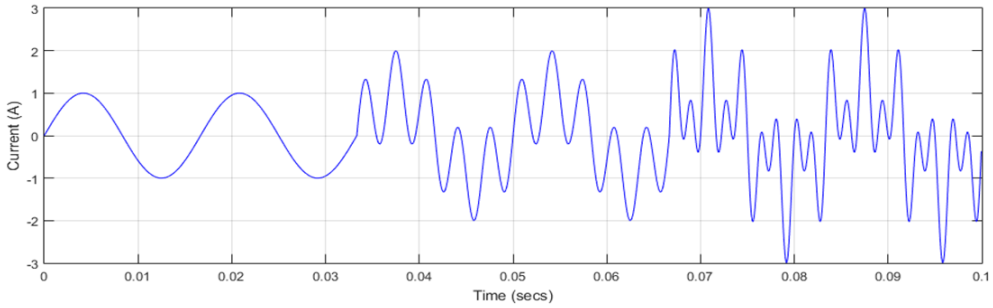

Figure 5 – Signal with varying frequencies (60, 300 and 540Hz).

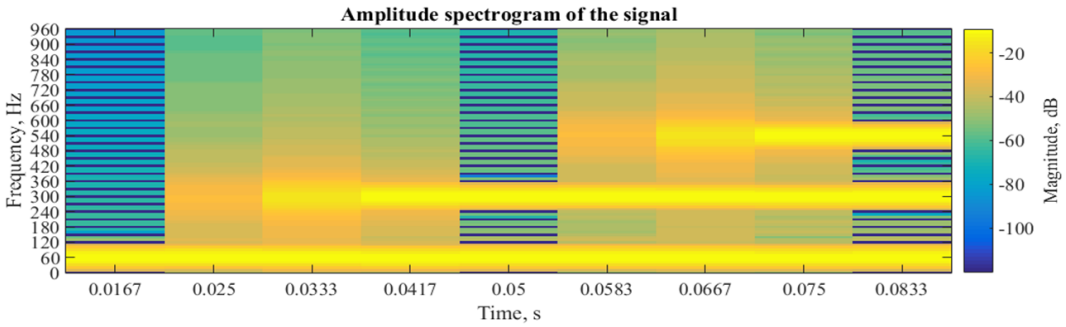

Figure 6 – STFT spectrogram.

2.5 Wavelets

A Wavelet can be classified as a wave with finite energy and mean equal to zero [46], represented by equations:

$$\int_{-\infty}^{\infty} |\psi(t)|^2 dt \neq \infty \tag{2.6}$$

$$\int_{-\infty}^{\infty} \psi(t)\, dt = 0 \tag{2.7}$$

There are different families of wavelets, like Haar, Morlet, Daubechies, among others. The choice of the mother wavelet depends on the application and different families can be used to detect events in power systems [35, 47–54]. Some examples of the families of wavelets are shown in Fig. 7.

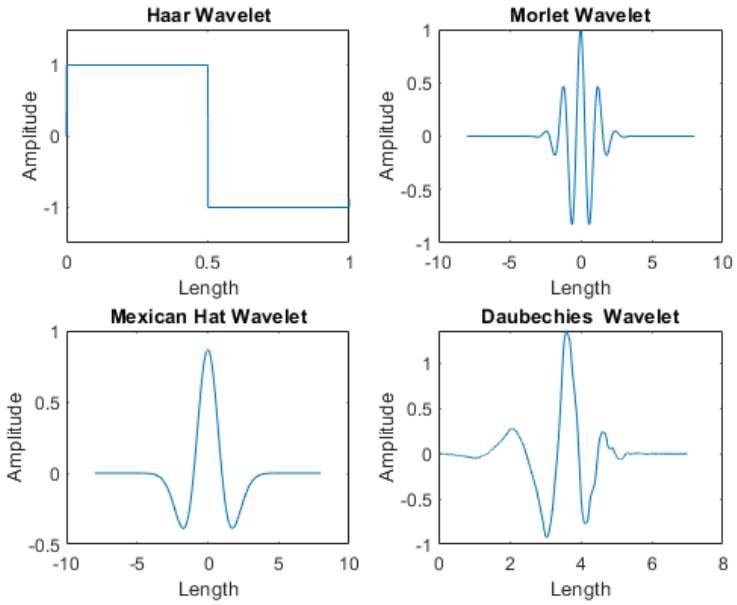

Figure 7 – Wavelets Families.

A Wavelet Transform allows both decomposition (analysis) and signal reconstruction (synthesis) of the analyzed signal.

2.5.1 Continuous Wavelet Transform (CWT)

The Wavelet's Transform decomposes a time domain signal into the time domain and the frequency domain. It is defined as:

$$W(a,b) = \int_{-\infty}^{\infty} f(t) \frac{1}{\sqrt{|a|}} \psi^* \left(\frac{t-b}{a} \right) dt; a, b \in R \tag{2.8}$$

Defining the function $\psi_{a,b}(t)$ as:

$$\psi_{a,b}(t) = \frac{1}{\sqrt{|a|}}\psi^* \left(\frac{t-b}{a}\right) dt \tag{2.9}$$

Rewriting the equation 2.8 as an internal product of the functions $f(t)$ and $\psi_{a,b}(t)$:

$$W(a,b) = \int_{-\infty}^{\infty} f(t)\psi^*_{a,b}(t)dt \tag{2.10}$$

The CWT compares the signal to shifted and compressed or stretched versions of a wavelet. The parameter a indicate a scale factor. The smaller the scale factor, the more "compressed" the wavelet and its corresponds to high frequencies. The larger the scale, the more "stretched" the wavelet and its corresponds to low frequencies. The position of the function $\psi(t)$ on the axis t is indicated by parameter b.

The mother wavelet is defined when the function $\psi(t)$ equals to $\psi_{1,0}(t)$, for the others values of the function parameters, these are called daughter wavelets, their format descends from the mother wavelet.

The CWT scalogram for the Daubechies (db4) wavelet is shown in Fig. 8.

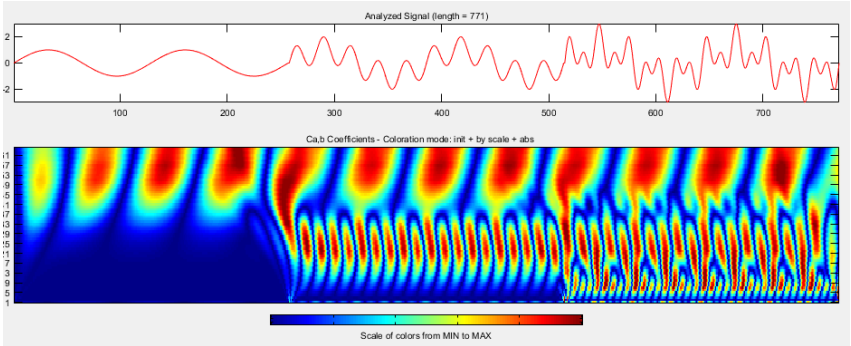

Figure 8 – CWT scalogram.

2.5.2 Discrete Wavelet Transform (DWT)

The wavelet's transform main characteristic is the multi-resolution analysis, which consists of the signal's decomposition into sub-signals of different resolution levels, being scaled and translated versions of wavelet functions. The STFT can be used to provide temporal information. However, since it uses a fixed size window for the entire analysis it is difficult to obtain a window size that provides good time and frequency information. In the wavelet transform this limitation was overcame, allowing the visualization of the signal in different frequency scales [43].

The Discrete Wavelet's Transform is a modified version of the CWT it is defined as:

$$X_{DWT}(n,k) = \int_{-\infty}^{\infty} x(t) h_k \left(2^k n T_s - t\right) dt, n, k \in Z \tag{2.11}$$

The DWT uses a filter bank to process the signal $x[n]$. In successive filtering the signals are subsampled by a factor of 2. The Fig. 9 shows the scale versus frequency representation:

$$y_{high}[n] = \sum_{k=-\infty}^{\infty} x(k) .h(2n-k) \tag{2.12}$$

$$y_{low}[n] = \sum_{k=-\infty}^{\infty} x(k) .g(2n-k) \tag{2.13}$$

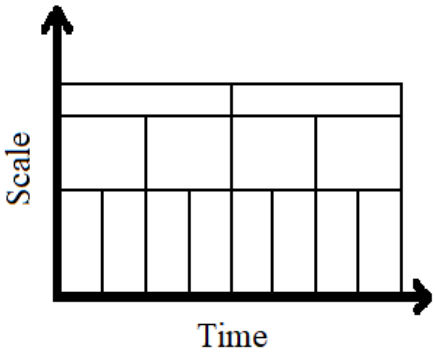

Figure 9 – Scale x Time.

The g[n] (Eq. 2.12) filter decomposes the signal resulting in components signal approximation (low frequencies) and the h[n] (Eq. 2.13) filter (high-pass) results in detail components (high frequencies). At each iteration only the approximation component is subdivided. Fig. 10 illustrate the decomposition structure and Fig. 11, the frequency spectrum resulting from the filters bank.

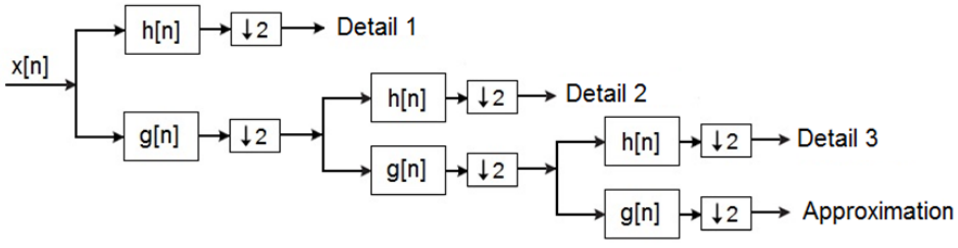

Figure 10 – Discrete Wavelet Transform decomposition tree.

The Fig. 12 shows the application of DWT to the signal of equation 2.4 for the Daubechies‘ mother wavelet(db4) of 5 levels of decomposition. At levels d1, d2 and d3 one can clearly see the frequency changes in time on the signal.

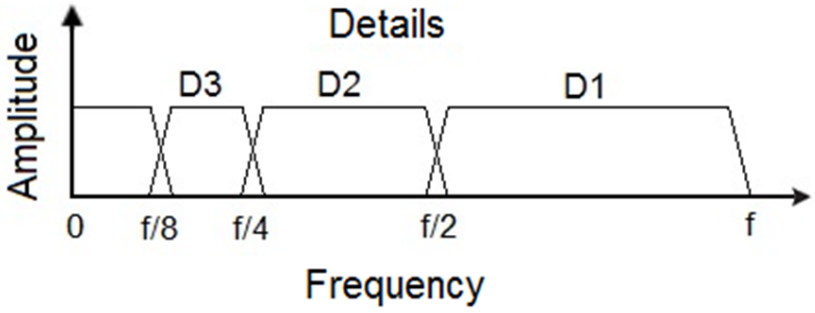

Figure 11 – DWT frequency spectrum. (Detail 1 – D1, Detail 2 – D2 e Detail 3 – D3).

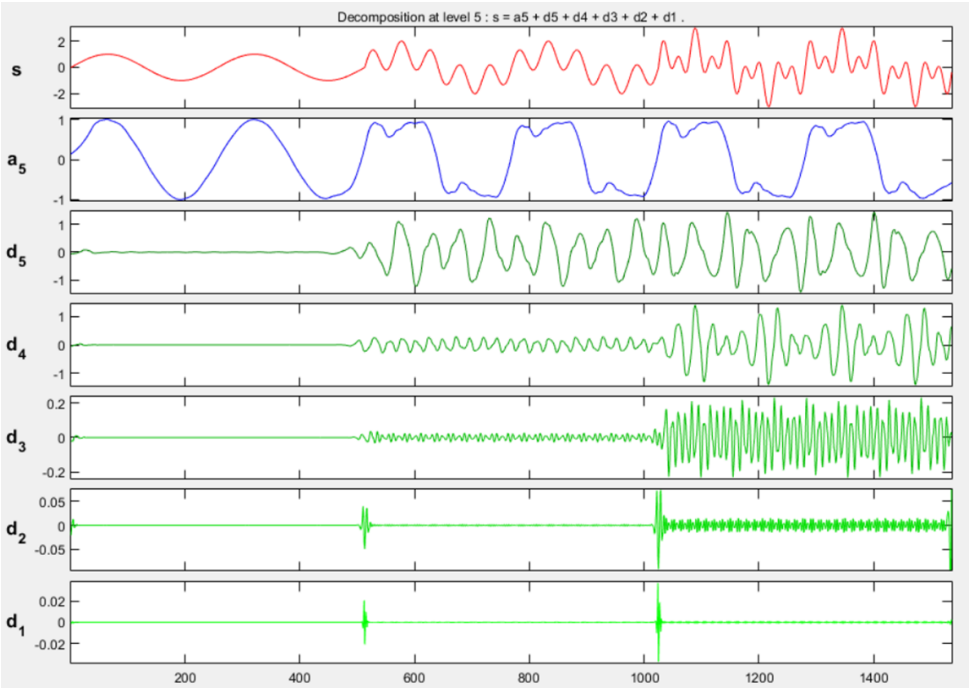

Figure 12 – DWT decomposition of 5 levels.

2.5.3 Wavelet Packet Transform (WPT)

The Wavelet's Packet Transform (WPT) uses the same DWT filter equations. The difference is that both the approximation coefficients and the detail coefficients are decomposed. The result is a complete decomposition, as shown in the coefficient tree of Fig. 13.

In the decomposition using the Wavelet Packet Transform, the frequency bands are uniform in comparison to the Discrete Wavelet Transform, which is of great importance for the harmonic analysis (Fig. 14).

For this work, it was used an eight level decomposition, according to the sampling frequency of the input signal (15360Hz) and the output range of each filter corresponded to 30Hz (Fig. 15).

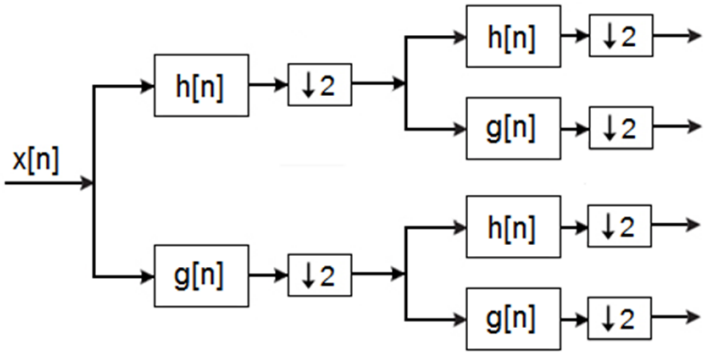

Figure 13 – Decomposition of the Wavelet Transform Package tree.

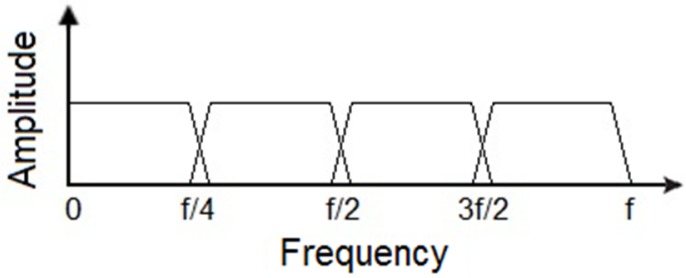

Figure 14 – WPT frequency spectrum.

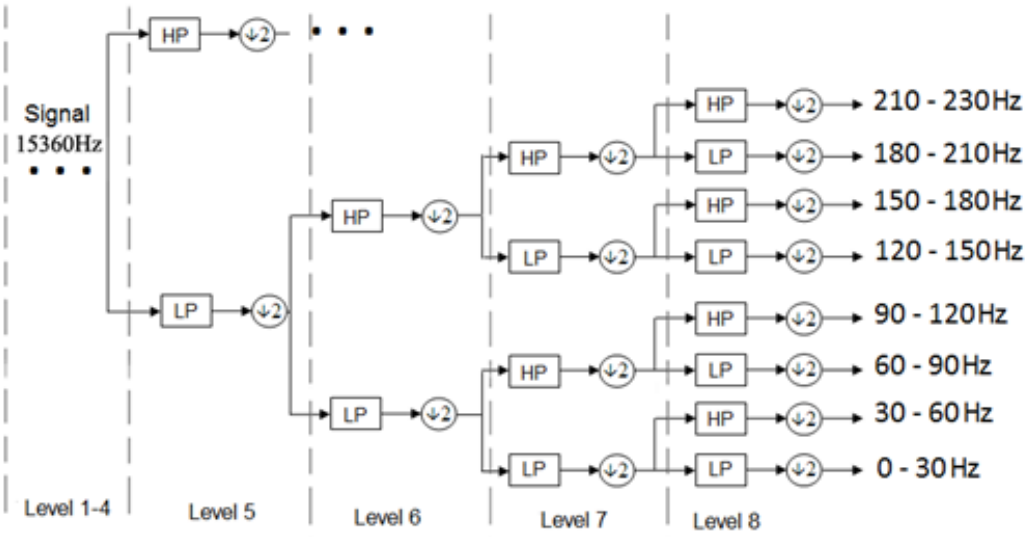

Figure 15 – WPT decomposition for 8 levels.

Using the harmonic analysis for 60Hz grids, the output of the fundamental and its respective harmonics would be located at the end of the pass-band of two adjacent filters, so the signal will spread among these filters. A wavelet packet harmonic technique has been used to decompose harmonics in this case [48]. In this technique the filter output is centralized in the desired harmonic, obtained as the sum of signals reconstruted(synthesis) by two adjacent filters (Fig. 16).

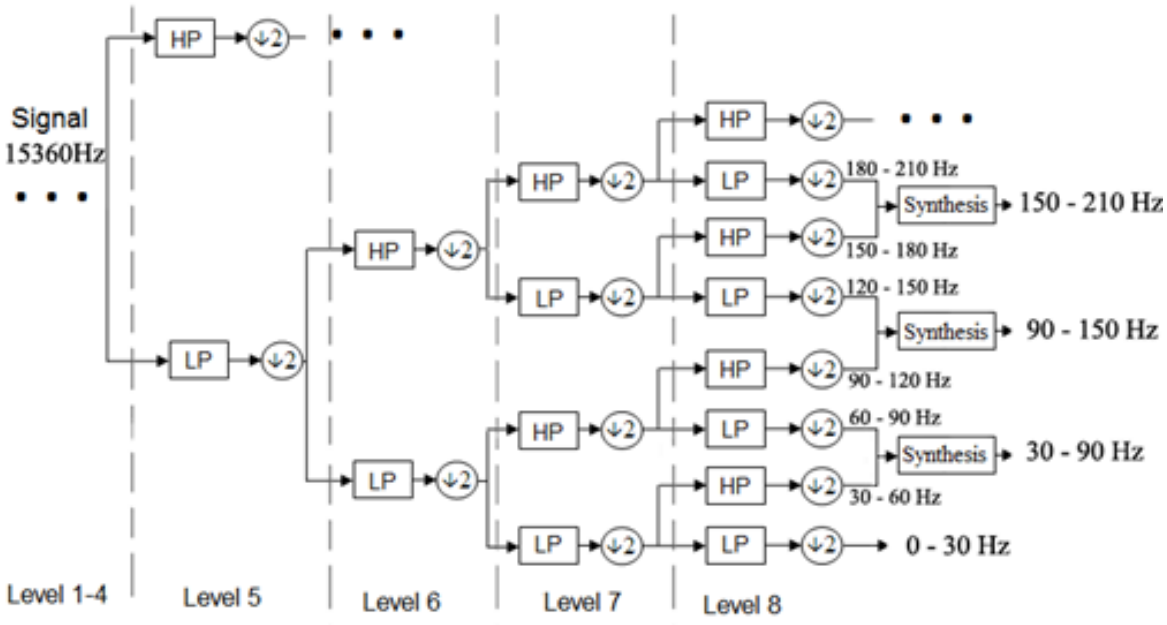

Figure 16 – Adapt WPT filters to harmonic frequencies.

3 INVERTERS

3.1 Introduction

This chapter describes three of the main different topologies of three phase inverters: the three phase H-Bridge VSI, three phase five level Cascade multilevel inverter and five level Diode Clamped multilevel inverter. The single-carrier (2L) and Multi-carrier (5L) SPWM control may be applied to the above inverters, and it‘s total harmonic distortion and spectrum can be obtained by simulations in MATLAB/Simulink. The conversion of the alternating DC current is achieved by the semiconductor switching, distributed in order to obtain an AC current. The control techniques of the semiconductor switches are discussed in the next subsection.

3.2 Sinusoidal Pulse-Width Modulation (SPWM)

There are several existing techniques for modulation control of inverters [18], each providing some improvement compared to each other [55]. One of them is the modulation by sinusoidal pulse width (SPWM). This technique allows the removal of desired of low order voltage harmonics of the inverter AC output [56]. To use this type of modulation, two voltage signals are compared: a triangular wave carrier of high frequency with amplitude $\hat{V}_c$ and frequency $\hat{f}_c$, and a signal of sinusoidal reference, with amplitude $\hat{V}_m$ and frequency $\hat{f}_m$, to generate pulses to the switches of the inverter (Fig. 17). The pulse width at the output of the modulator varies the amplitude of the reference signal compared with the carrier signal during the interval of $\hat{V}_c(t) < \hat{V}_m(t)$ in the positive cycle of $\hat{V}_m(t)$ and $\hat{V}_c(t) > \hat{V}_m(t)$ of the negative cycle of $\hat{V}_m(t)$. The output of the switch is changed when the sine wave is intercepted by the triangular wave, so the carrier frequency defines the switching frequency. The fundamental frequency is defined by modulating the amplitude of the output voltage depending on the peak value of the modulation.

3.3 Modulation Index

The modulation index is defined between the magnitude modulating wave's peak $\hat{V}_m$ by the triangular carrier wave amplitude $\hat{V}_c$ ratio, determining the pulse width and voltage RMS inverter output, with the index:

$$\hat{m}_a = \frac{\hat{V}_m}{\hat{V}_c} \tag{3.1}$$

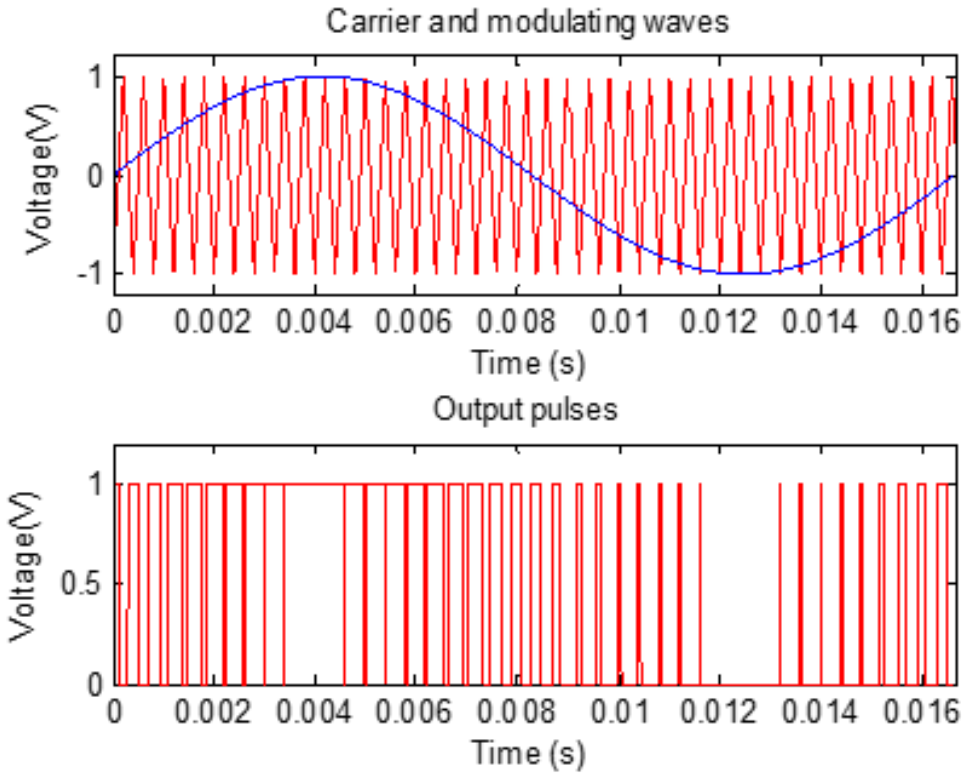

Figure 17 – Triangular carrier, sinusoidal reference and output pulses.

The frequency modulation index is represented between the carrier frequency $\hat{f}_c$ by the modulating frequency $\hat{f}_m$ ratio:

$$\hat{m}_f = \frac{\hat{f}_c}{\hat{f}_m} \tag{3.2}$$

In three phase inverters, $\hat{m}_f$ should be an odd integer (bipolar PWM) to eliminate even harmonics. For low values of $\hat{m}_f$ it should be odd and multiple of three to cancel out most dominant harmonics in the line-to-line voltage. The harmonics present in the inverter are centered around of $\hat{m}_f$ and its multiples $\hat{m}_f, 2\hat{m}_f, 3\hat{m}_f, 4\hat{m}_f \ldots$.

$$h = j\hat{m}_f \pm k \tag{3.3}$$

For odd j values harmonics exist solely to even values of k.

3.4 Three Phase H-Bridge Inverter

The three-phase inverters are used in industrial applications that require more power. Naturally, its use is more common compared to the single-phase inverters. They can be powered by PV array, batteries or rectifiers. It has three arms inverter half-bridge,

which must operate in a complementary way, totaling six pulses, two for each phase (Fig. 18). The pulses are generated using SPWM technique, but it is necessary three sinusoidal reference waves displaced from each other by 120°.

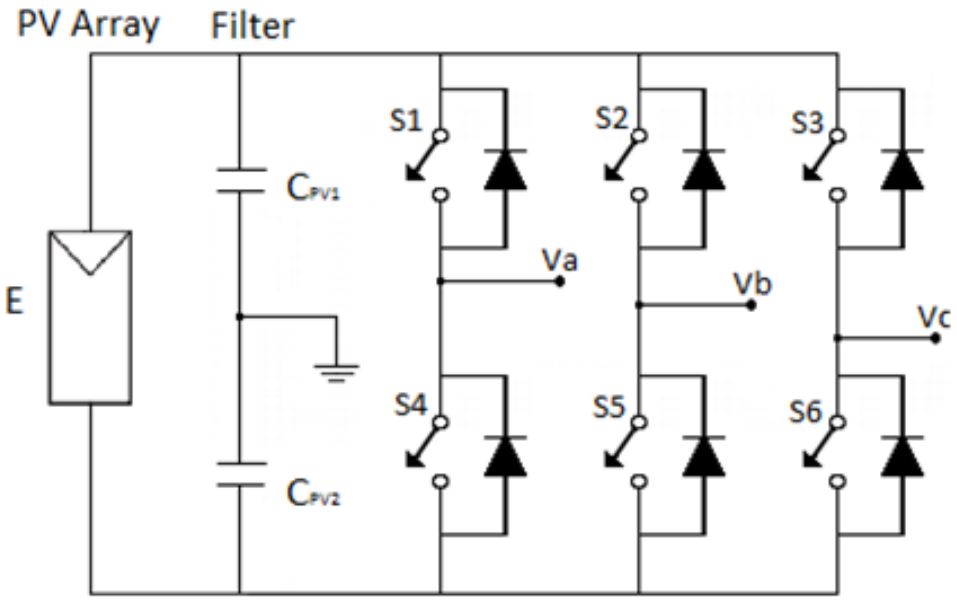

Figure 18 – Three phase H-Bridge inverter topology feed by PV array.

The switching strategy is represented in Table 1.

Table 1 – Switching Strategy And Line To Line Voltage - H-Bridge Inverter

State	S_1	S_2	S_3	V_{AB}	V_{BC}	V_{AB}
1	OFF	OFF	OFF	0	0	0
2	OFF	OFF	ON	0	-E	E
3	OFF	ON	OFF	-E	E	0
4	OFF	ON	ON	-E	0	E
5	ON	OFF	OFF	E	0	-E
6	ON	OFF	ON	E	-E	0
7	ON	ON	OFF	0	E	-E
8	ON	ON	ON	0	0	0

3.5 Diode Clamped Multilevel Inverter

The Diode Clamped topology, also known as neutral point inverters, need clamping devices. Diodes are used as clamping devices to limit the power devices voltage stress [57]. This topology uses capacitors in series to divide DC voltage at different levels. The DC power supply charges the capacitor and the levels are obtained by the switches operating strategy. To produce phase voltage an n levels inverter needs $(n-1)$ capacitors, $2(n-1)$ switching devices [58, 59]. In a three phase 5-level diode clamped multilevel needs per phase $2(n-1) = 8$ number of switches and $(n-1) = 4$ number of voltage sources. The Fig. 19 shows the leg for phase A of this topology.

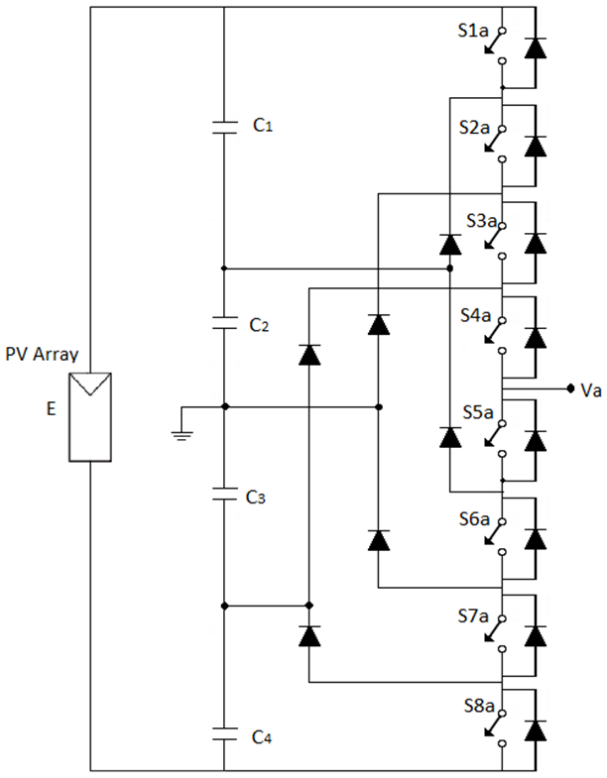

Figure 19 – Three-phase Diode Clamped 5L Multilevel Inverter Topology(One Leg).

The switches are arranged into 4 pairs $(S1a, S5a), (S2a, S6a), (S3a, S7a), (S4a, S8a)$. The pairs are triggered complementary. If a pair of switch is on, the other must be off. To form the 5 levels, four switches are triggered at any point of time. The phase A output voltage V_{AN} has five states: $E/2$, $E/4$, 0, $-E/4$ and - $E/2$. The switching strategy is represented at Table 2.

In multi-carrier modulation strategy, $(m-1)$ carriers are compared with modulating sine wave of frequency $\hat{f}_m$ to generate m-level output. All the $(m-1)$ carrier signals are of same frequency $\hat{f}_c$ and amplitude $\hat{V}_c$ and they are all in the same phase [60]. This technique is named Phase Disposition (PD) [61].

Table 2 – Switching Strategy And Line To Line Voltage - Diode Clamped Inverter

State	S_1a	S_2a	S_3a	S_4a	V_{AN}
1	ON	ON	ON	ON	E/2
2	OFF	ON	ON	ON	E/4
3	OFF	OFF	ON	ON	0
4	OFF	OFF	OFF	ON	-E/4
5	OFF	OFF	OFF	OFF	-E/2

3.6 Cascade H-Bridge Multilevel Inverter

This topology consists on connecting H-bridge inverters in series to get a sinusoidal voltage output, with separated DC voltage sources [57, 62]. The output voltage is the sum of the voltage that is generated by each cell. Number of output voltage levels are 2n+1, where n is the number of cells per phase [5]. It needs less number of components compared to the diode clamped reducing the price and the weight. The cascaded 5L inverter needs $2(n-1) = 8$ switching devices per phase. The Fig. (Fig. 20) shows an inverter cascade of 5 levels.

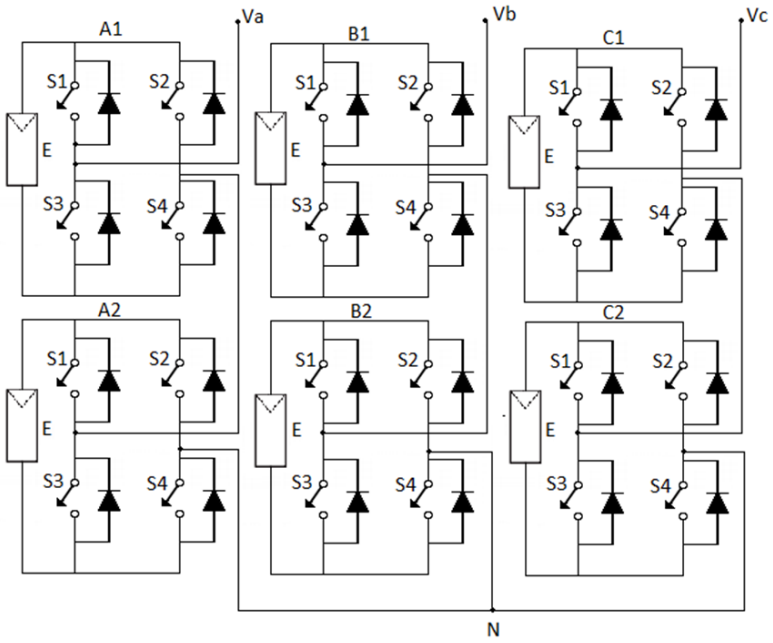

Figure 20 – Cascade Multilevel inverter.

For phase A two cells (A1 and A2) are connected in series (Fig. 20). The output voltage V_{an} has five states: $2E$, E, 0, $-E$ and -$2E$. The switching strategy is represented at Table III.

Table 3 – Switching Strategy And Line To Line Voltage - Cascade inverter

Cell A1				Cell A2				
S_1a	S_2a	S_3a	S_4a	S_1a	S_2a	S_3a	S_4a	V_{AN}
ON	OFF	OFF	ON	ON	OFF	OFF	OFF	2E
OFF	ON	OFF	ON	ON	OFF	OFF	OFF	E
OFF	ON	ON	OFF	ON	OFF	OFF	OFF	0
OFF	ON	ON	OFF	ON	OFF	ON	ON	-E
OFF	ON	ON	OFF	OFF	ON	ON	ON	-2E

4 METODOLOGY

4.1 Analysis of Inverter Topologies

Three types of multi-level inverter topologies were simulated and voltage and current harmonics were analyzed. The simulink schematic is shown in Fig 21.

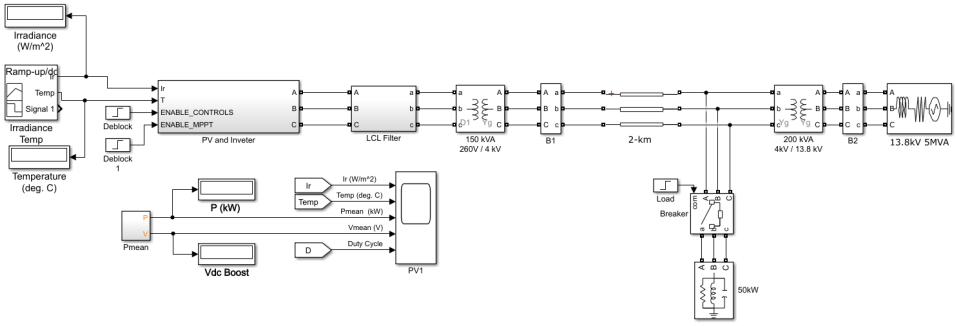

Figure 21 – Simulink schematic of simulation

The values used in the MATLAB/Simulink simulations for the inverter were:

$$m_a = 1 \tag{4.1}$$

$$\hat{f}_c = 3000Hz \tag{4.2}$$

$$\hat{f}_m = 60Hz \tag{4.3}$$

4.1.1 Three Phase H-Bridge Inverter

The simulations were performed using MATLAB / Simulink. Fig. 22 shows inverter subsystem module. The voltage supplied to the inverter is a PV Array represented by a DC source.

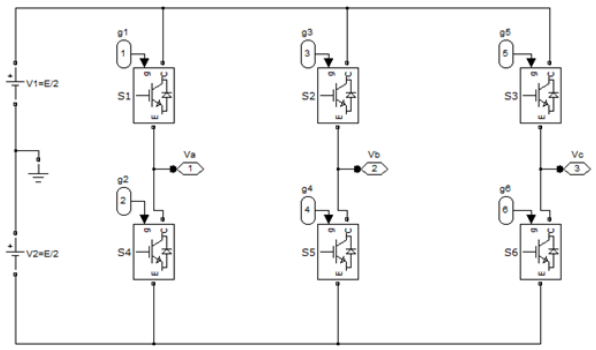

Figure 22 – Three phase H-Bridge Inverter Model.

The SPWM generator module (Fig. 23):

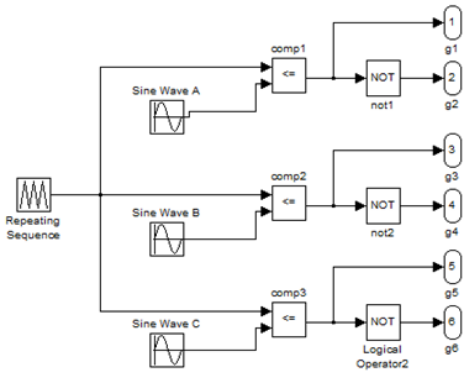

Figure 23 – SPWM Generator model for 2-Level inverter.

For 400V DC input the simulation results of output line to line voltages (Fig. 24(a)), line to neutral voltages (Fig. 24(b)) and current RL load (Fig. 26) are shown below (without LCL filter).

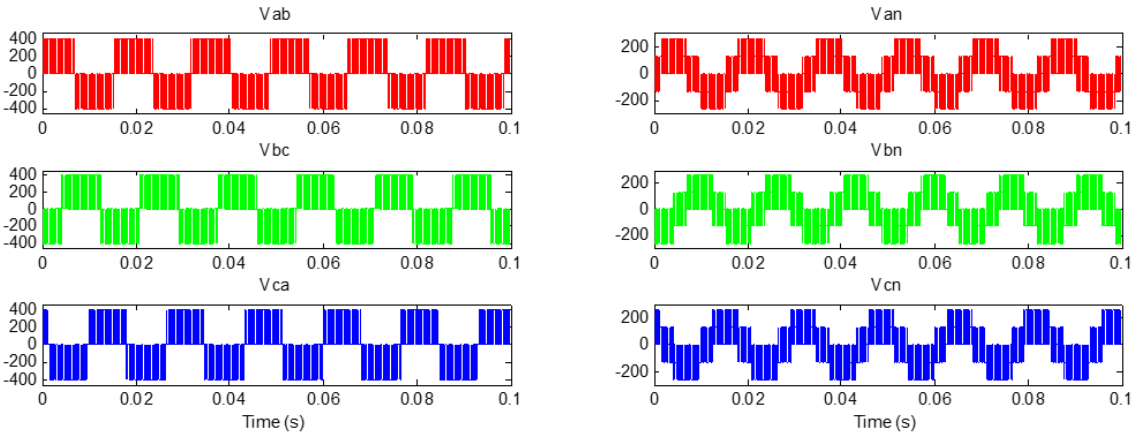

(a) Line to line voltage output.

(b) Line to neutral voltage output

Figure 24 – Three phase voltage output inverter.

Analysis of harmonic spectrum to line voltage V_{ab}:

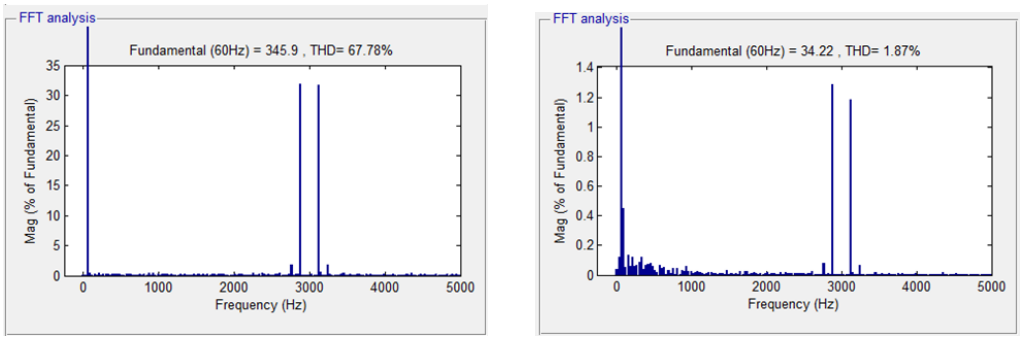

(a) Spectrum of V_{an}. (b) Spectrum of I_{an}.

Figure 25 – The harmonic spectrum of output inverter.

The fundamental component was 345.9V with a THD of 67.78% since the harmonic components appear near the switching frequency 3kHz. According to equation 3.3, the harmonics at the frequency of 3kHz, and $mf = 50$, will be located at $h = 50 \pm 2$, $h = 48th$ and $52th$, which can be seen in Fig. 25.

The waveform for the current I_a.

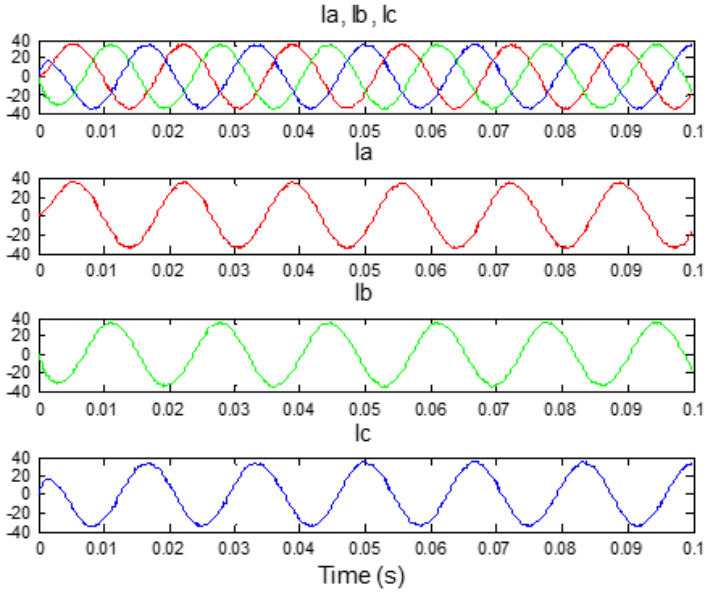

Figure 26 – Three phase line to neutral current output inverter.

The line to line voltage was filtered with LCL filter (Fig. 27(a)) and new THD is shown at Fig. 27(b):

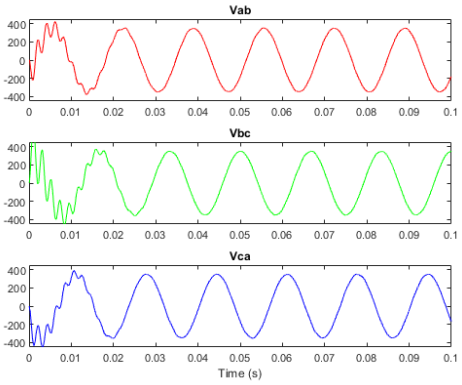

(a) V_{ab} Signal.

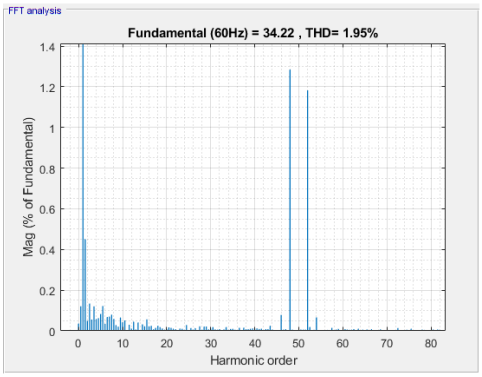

(b) Spectrum of V_{ab}.

Figure 27 – The harmonic spectrum of output inverter.

When the LCL filter were used, the output voltage appeared more like a pure sine wave and better prepared to grid connected (new THD is 1.95%). Similar results were obtained with LCL filter for the other topologies and will not be described.

4.1.2 Diode Clamped Multilevel Inverter

The Fig. 29(a) shows the Simulink model and Fig. 29(b) the output pulses with the multi-carrier waves.

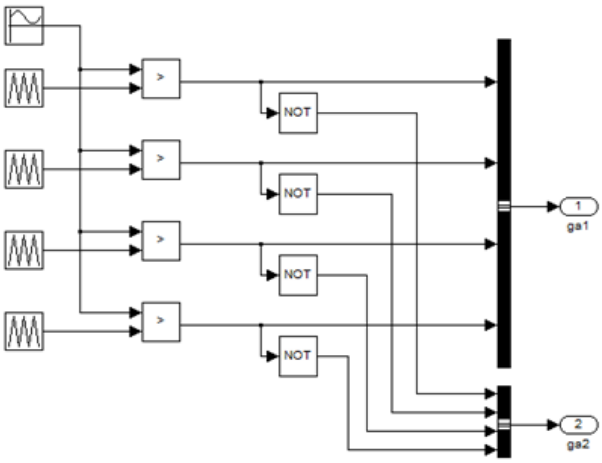

(a) Multi-carrier SPWM Generator model for one leg (5L).

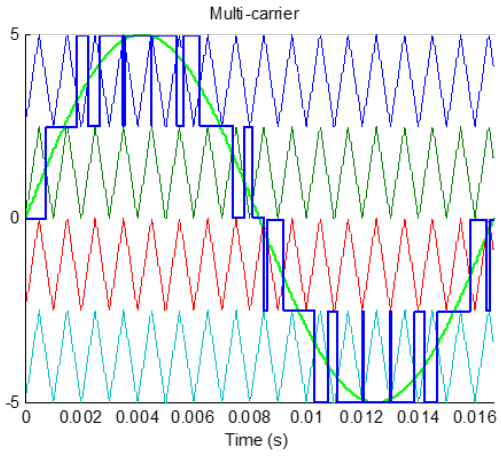

(b) Carrier, modulating and output voltage waves.

Figure 28 – The harmonic spectrum of output inverter.

The Matlab/Simulink schematics:

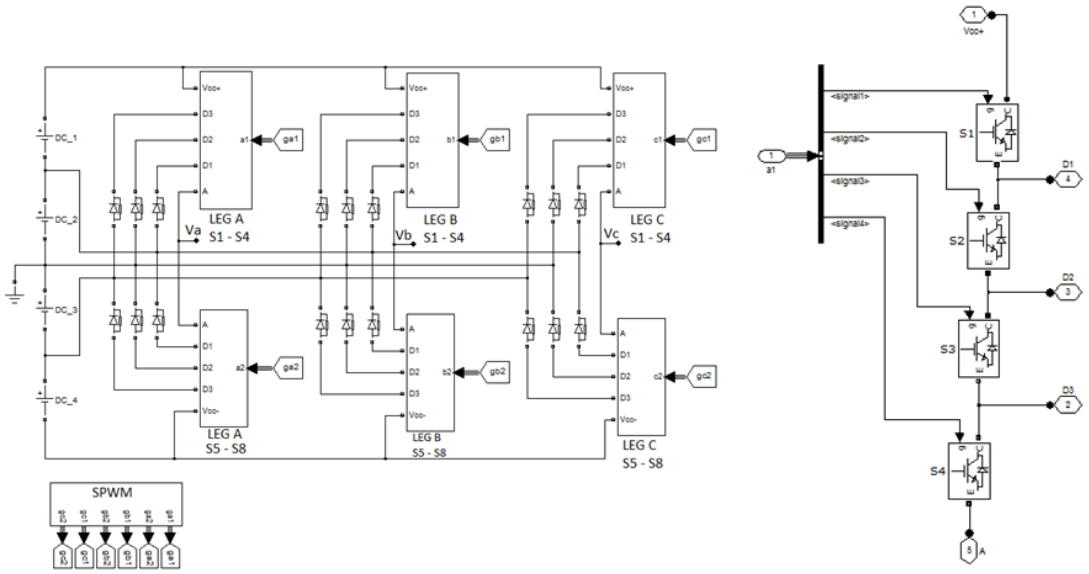

(a) Three phase Diode Clamped 5L Multilevel inverter topology in Simulink.

(b) Subsystem for one switch leg.

Figure 29 – Diode Clamped Topology.

For 400V DC input the simulation results of output line to line voltages (Fig. 30(a)), line to neutral voltages (Fig. 30(b)) (without LCL Filter).

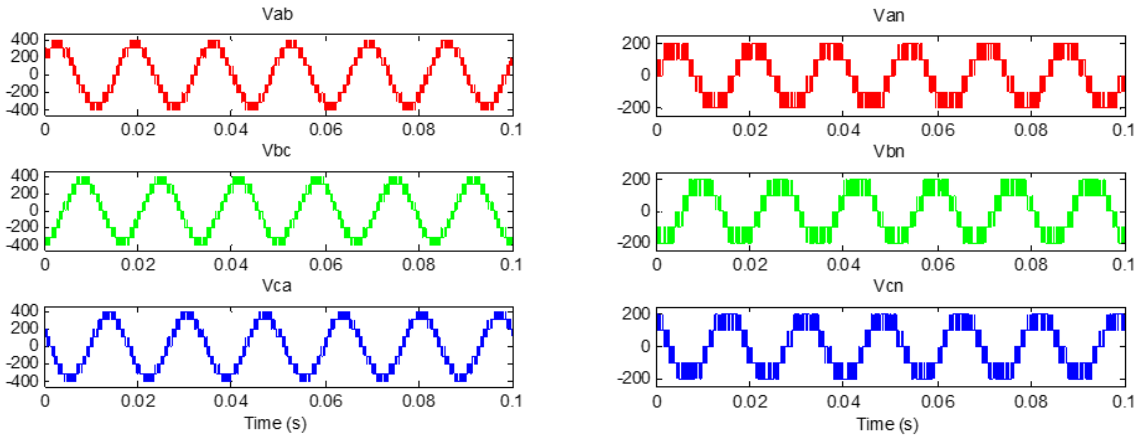

(a) Line to line voltage. V_{an}.

(b) Line to neutral voltage.

Figure 30 – Diode Clamped 5L multilevel Inverter.

The fundamental component was 346.7V with THD of 16.81%. The analysis (Fig. 31 shows that a high number of harmonics spectrum are concentrated on the switching frequency.

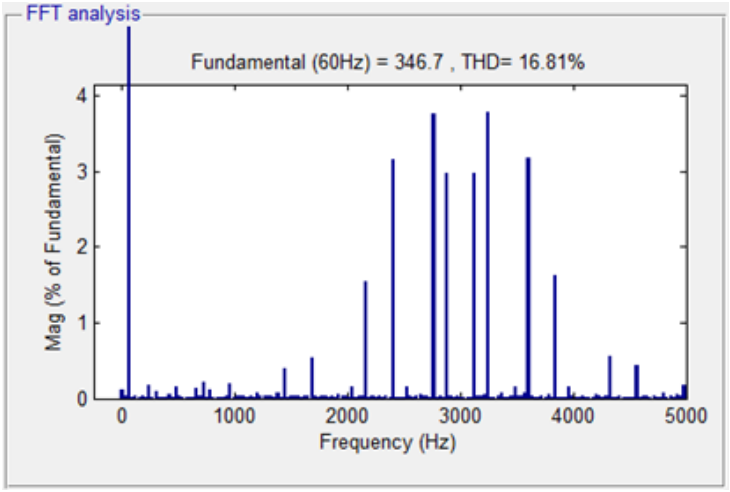

Figure 31 – The harmonic spectrum of inverter voltage output (Diode Clamped 5L multilevel Inverter).

4.1.3 Cascade H-Bridge Multilevel Inverter

The input DC voltage sources value per cell is 100V. The output inverter is 200Vac line to ground and 400Vac for line to line. Simulink models is shown at Fig. 32. There are three generators inside the module of SPWM Generator for legs A, B and C.

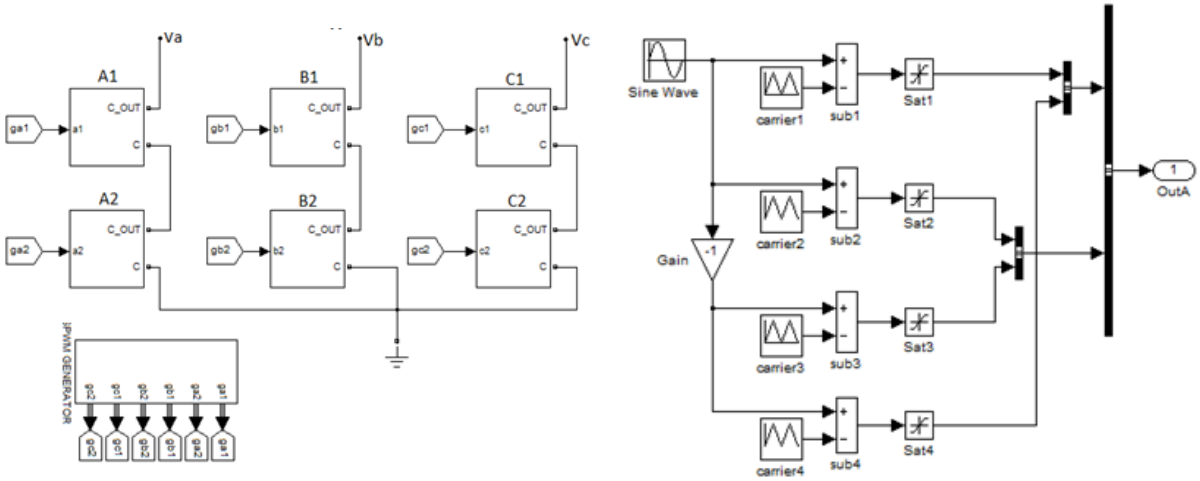

(a) Simulink Cascade Inverter. (b) SPWM Generator.

Figure 32 – 3-ph Cascade 5L and SPWM Model topology in Simulink.

The results of output line to line voltages (Fig. 33(a)), line to neutral voltages (Fig. 33(b)) (without LCL Filter):

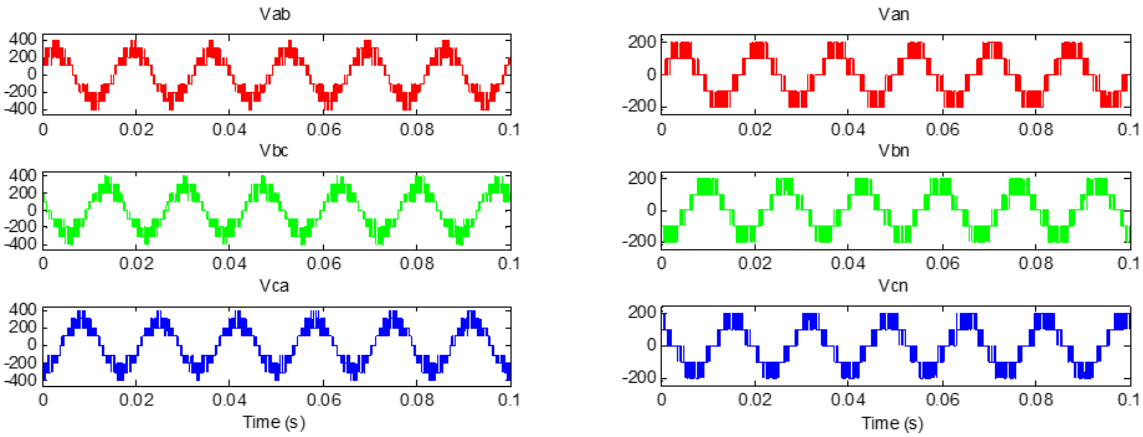

(a) Line to line voltage.

(b) Line to neutral voltage.

Figure 33 – Cascade 5L multilevel Inverter.

In analysis of harmonic spectrum to line voltage V_{ab} (Fig. 34), the fundamental component was 284.8v with THD of 19.95%. The analysis shows a large number of harmonics, especially around the switching frequency.

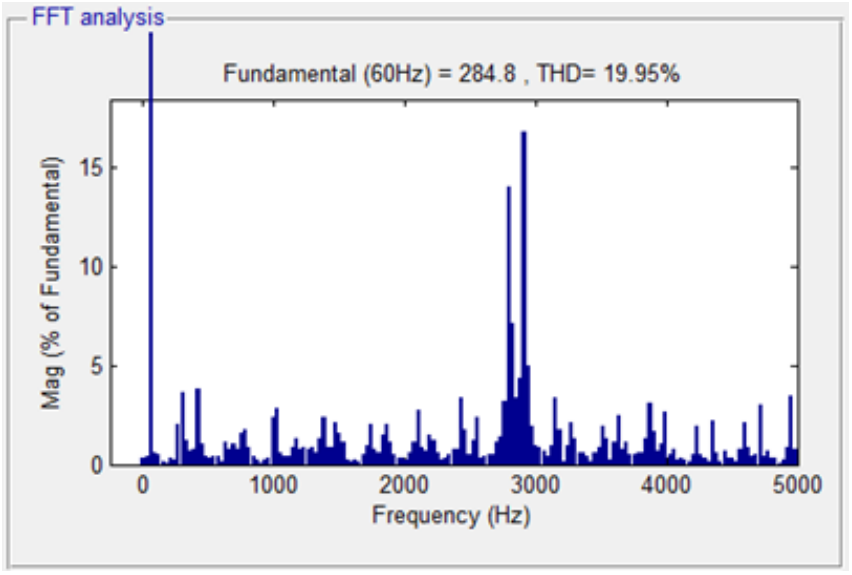

Figure 34 – Harmonic spectrum of inverter output voltage.

4.1.4 Results

The harmonic spectrum was extracted by using the FFT analysis. The definition of the total harmonic distortion (THD) is a percentage of how close a wave is to the fundamental signal. The THD for the three topologies is shown at Table 4.

As seen on the table, the voltage output of five level inverter is closer to sine wave than the output of 2-level inverter. Comparing the analysis of the simulation of the three phase VSI, three phase five level Cascade inverter and five level Diode Clamped, it‘s

Table 4 – Comparison of total harmonic distortion

3-Phase Inverter	Levels	THD (Line to Line)
VSI	2L	67.78%
Cascaded Mulilevel	5L	19.95%
Diode Clamped Multilevel	5L	16.81%

observed that the total harmonic distortion decreases as the number of level increases, due to the fact that the output voltage waveform appears like a sine wave. The SPWM technique used also contributes to reduce the level of harmonic, especially the low-order harmonics, leading to a decrease in filter requirements, recommended for applications that require low THD values. The harmonic's spectrum of the three topologies concentrate around the 50th harmonic (switching frequency). The harmonics content present in the output voltage can be eliminated either by using a filter circuit such as LC or LCL. The 3-ph Diode Clamped presents high complexity in hardware implementation, having a higher cost followed by 3-ph Cascade Multilevel inverter and 3-ph H-Bridge inverter.

4.2 Devices and Measurements

The data used in this work refers to the building (Fig. 35(a)) of the Federal University of Itajubá located in Itajubá, Brazil, which is connected to a three-phase medium voltage system (13.8 kV) by a 150 kVA transformer (Fig. 37) and has a PV System with a production capacity of 27 kWp/day (Fig. 35(b)). The typical loads in the building are computers, printers, lighting, refrigerators, RTDS, UPS, elevator, among others.

(a) University building [63]. (b) PV System. [64].

Figure 35 – University building and PV System.

The current measurement has been performed on the building's transformer secondary portrayed by M1 at Fig. 36, and a second point of measurement was performed at the photovoltaic system inverter's output, denominated M2 (Fig. 36) to verify the effects

of the harmonic's injection produced by the inverter due to its operation, irradiation variation, etc.

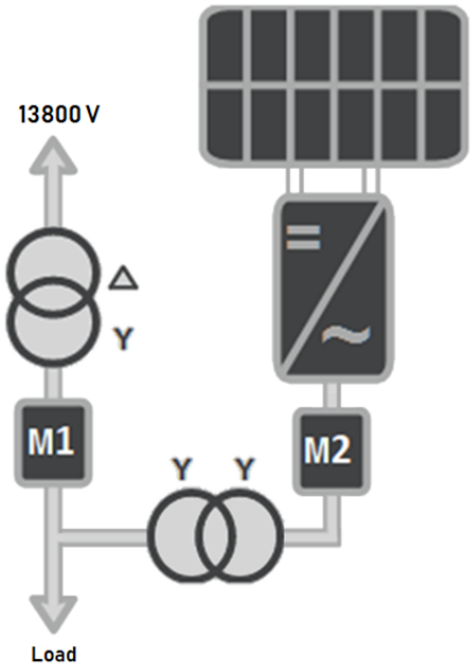

Figure 36 – Diagram of the measured system.

The measurements were performed in sequence on a typical day of work. For data acquisition a 16-bit NI USB-9162/9215 100 kS/s (Fig. 38) and LEM Flex system has been used along with an anti-aliasing filter and the sampling rate used was 15360Hz (256 points per cycle), for the electrical grid frequency of 60Hz.

Figure 37 – Medium Voltage Transformer.

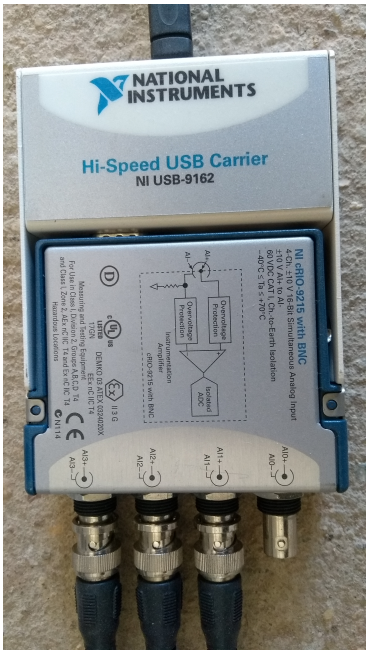

Figure 38 – NI USB-9162/9215

4.2.1 Inverters

There are two types of inverter models at the PV system from Fronius manufacture, being one 12,500W (Symo) and two 8000W (IG Plus). The two inverters models operate's automatically, connecting at dawn, provided there is enough radiation for generation, in the same way, after nightfall the inverter is turned off and completely disconnected from the grid. It's characteristics are discussed in the following subsections.

4.2.2 Fronius Symo 12.5 3M

This three-phase transformerless inverter works in a power range of 12 to 20.0 kW, has a wide input voltage range and two MPPT trackers providing flexibility in system design. It has interface connection for data collection via Wifi or Ethernet. The inverter image is shown in Fig. 39 and its characteristics at Table 5.

(a) External (b) Internal

Figure 39 – Fronius Symo 12.5 3M Inverter.

Table 5 – Inverter Technical Data - Fronius Symo 12.5 3M.

INPUT		OUTPUT	
DC maximum power	12.500 W	Max. output power	12.500 W
Nominal input voltage	200 - 1000 V	Max. output current	18.0 A
Max. input current	27.0 A	Power factor	0 - 1 ind. / cap
		Distortion	$< 2\%$

4.2.3 Fronius IG Plus 100 V-3

This three-phase HF transformer inverter works in a power range of 3.5 to 12.0 kW. It has interface connection for data collection via Wifi or Ethernet. The inverter image is shown in Fig. 40 and its characteristics at Table 6.

(a) External

(b) Internal [65]

Figure 40 – Fronius IG Plus 100 V-3 Inverter.

Table 6 – Inverter Technical Data - Fronius IG Plus 100 V-3

INPUT		OUTPUT	
DC maximum power	8.430 W	Max. output power	8.000 W
Nominal input voltage	370 V	Max. output current	11.6 A
Max. input current	36.7 A	Power factor	0.75 – 1 ind. / cap
		Distortion	$< 3\%$

5 RESULTS

5.1 Analysis of Photovoltaic Inverters

Time-frequency techniques are used to analyze the behavior of harmonics in the system and at PV inverters output. The operating conditions of the inverters were analyzed under regular conditions, startup, shutdown and during irradiation variations. Current measurement was performed at M2 (Fig. 36), for each model (Symo and IG Plus) separately.

5.1.1 Regular Condition Analysis

Current measurement was performed with 1 minute(60s) for Symo and 5 minutes duration(300s) for IG PLus at each inverter output. Measurements were performed on a sunny day of August, at 11:00 a.m, with irradiance of 680 W/m^2, panel temperature 49° and 28° ambient temperature, with Fronios Symo power of 9 kW/12.5 kW (75%) and IG Plus 11.2/16 kW (5.6 kW + 5.6kW) (70%). The three-phase current for Fronius Symos inverter is shown at Fig. 41.

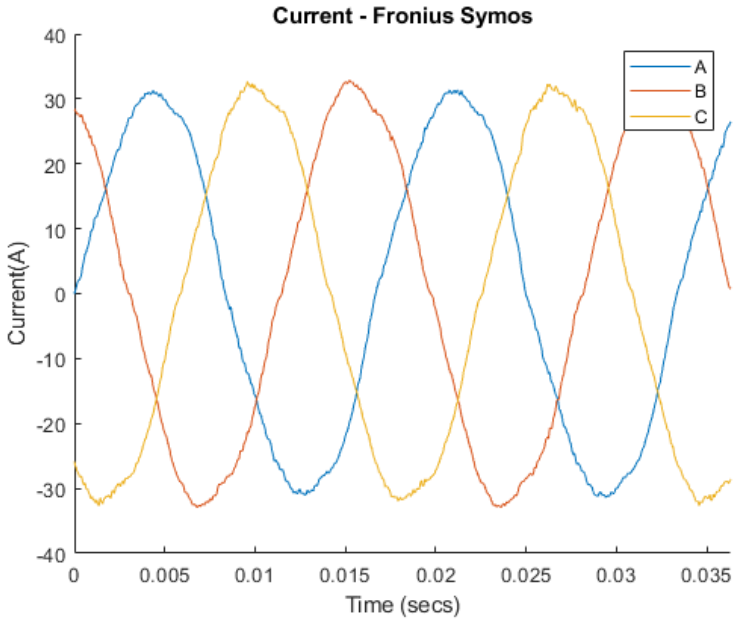

Figure 41 – Three-phase output currents at the Symo inverter.

The harmonic content was extracted using the FFT with 12 cycles at the sampled signal. This inverter has a low harmonic content, composed by the third and fifth harmonics and the other frequencies with low amplitude (Fig. 42). THD value is 3.90%.

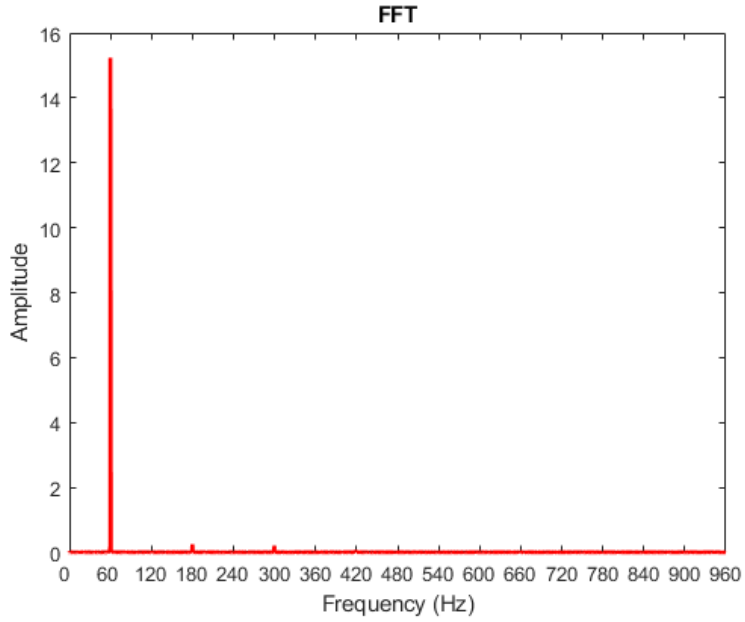

Figure 42 – FFT at Symo inverter current signal.

STFT is used to verify the presence of time varying harmonics in the signal (Fig. 43).

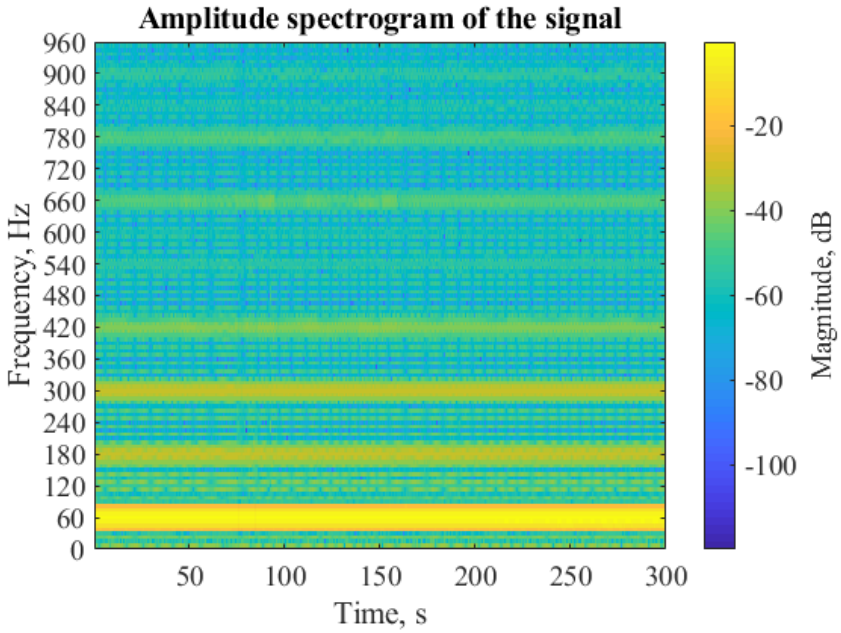

Figure 43 – STFT at Symo inverter current signal.

In agreement with FFT results, the STFT shows the constant presence of the third and fifth harmonic components, and the other frequencies with low amplitude of the entire signal.

The DWT was used to analyze the events of frequency changes in the signal (Fig. 44). The mother wavelet for all analysis was db4.

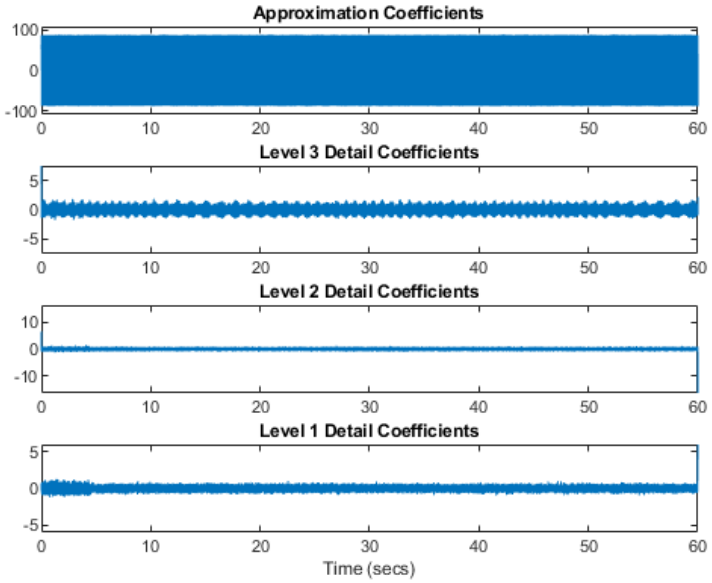

Figure 44 – DWT at Symo inverter current signal.

No significant changes were found in the details of DWT decomposition that suggest events of sudden frequency changes.

The harmonics were decomposed using the WPT as signal synthesis was performed and the graph of each harmonic at time was extracted. The mother wavelet for all analysis was db45. Fig. 45(a) shows the fundamental component of the extracted signal and (b) a zoom in of that signal. Since there is little harmonic incidence, the decomposed component overlaps the original signal.

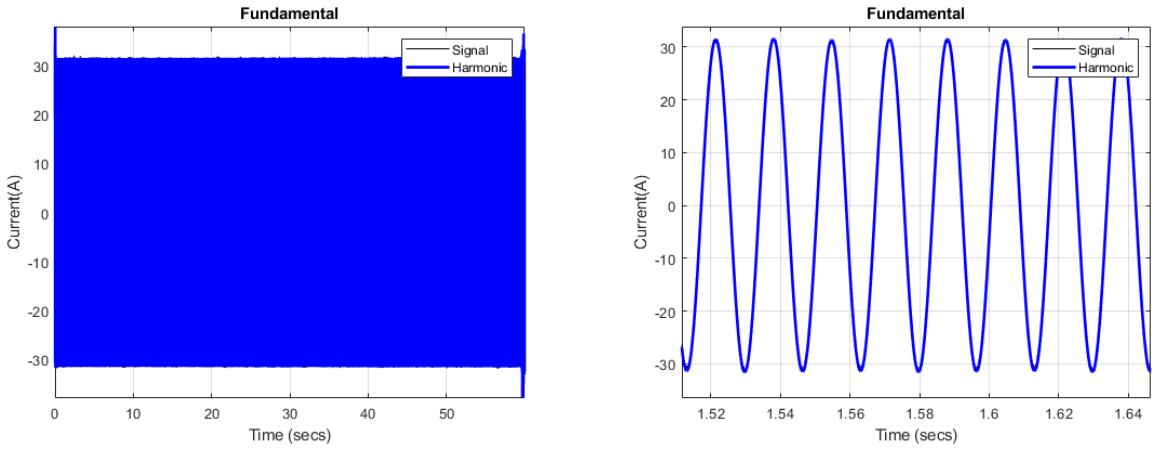

(a) Fundamental (b) Zoom

Figure 45 – Fundamental component.

The other harmonic components are shown at Fig. 46. Odd components were highlighted because other components did not present significant values.

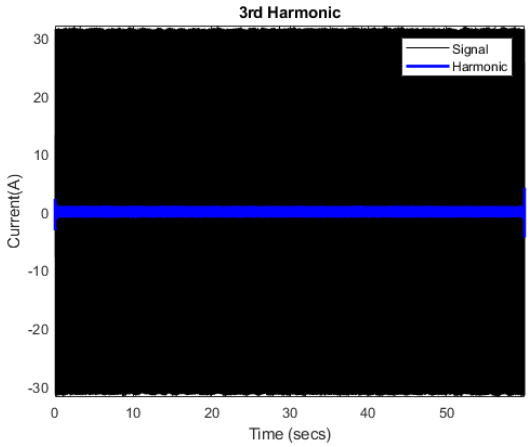

(a) Third

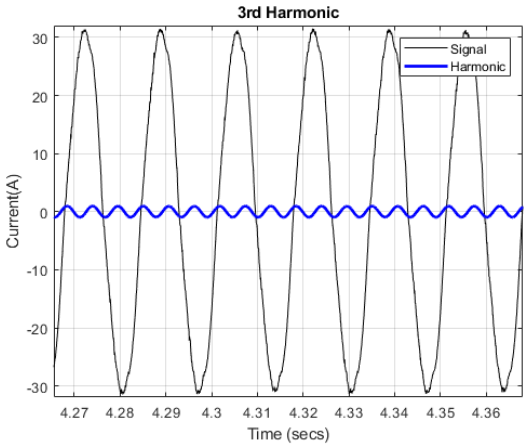

(b) Third (Zoom).

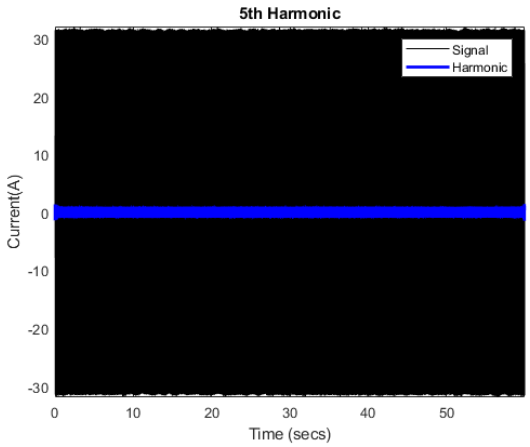

(c) Fifth

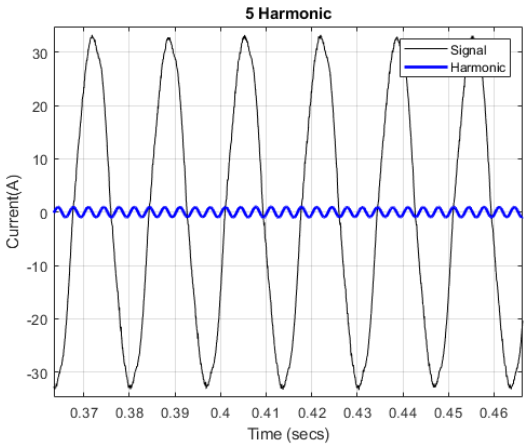

(d) Fifth (Zoom).

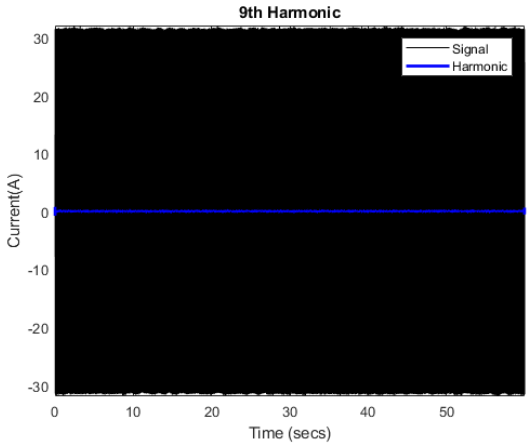

(e) Ninth.

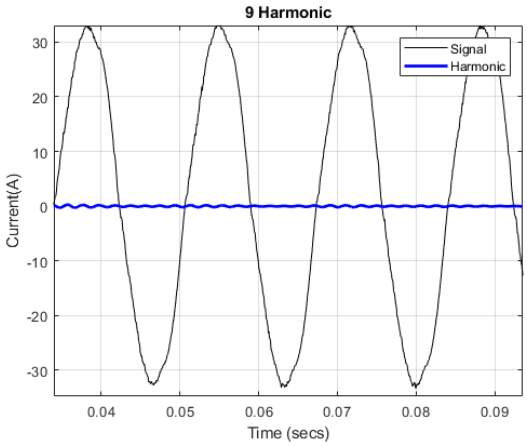

(f) Ninth (Zoom).

Figure 46 – Harmonic components synthesis over time.

The same analysis was performed on the Fronius IG Plus inverter under the same conditions (two inverters):

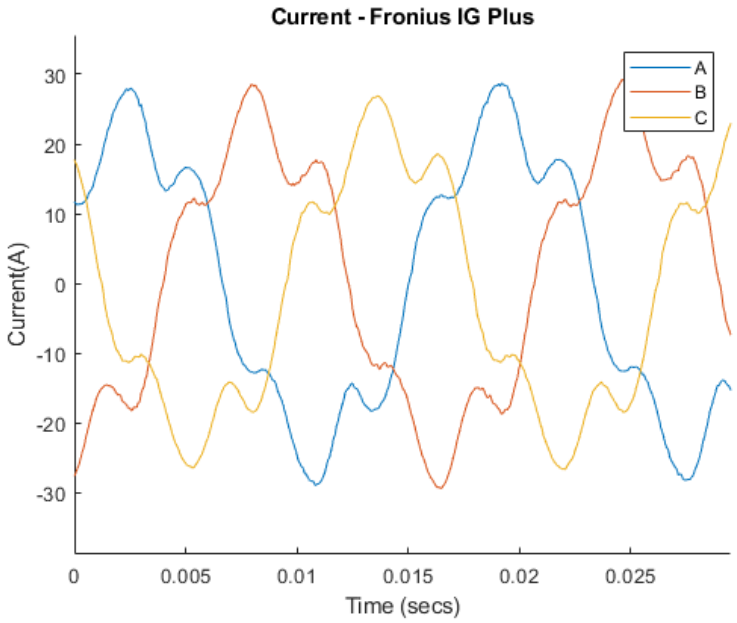

Figure 47 – Three-phase output currents at the IG Plus inverter.

At Fig. 47 it is possible to perceive a high content of harmonics in comparison to Fronius Symo, as the sine wave appears with perceptible deformations.

The harmonic content was extracted using FFT at the sampled signal (Fig. 48).

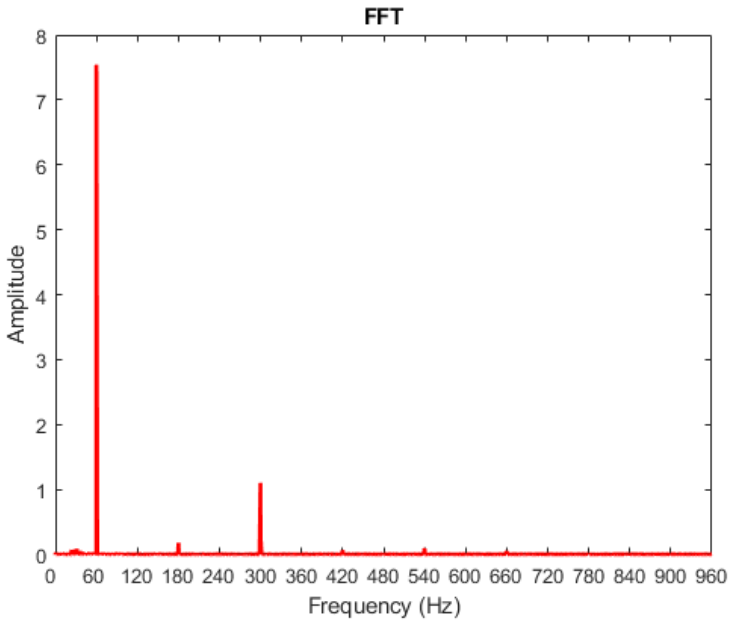

Figure 48 – FFT at IG Plus inverter current signal.

This inverter in general has low overall harmonic content but contains a higher portion of the third and fifth harmonics. THD value is 21.84%.

A STFT results (Fig. 49):

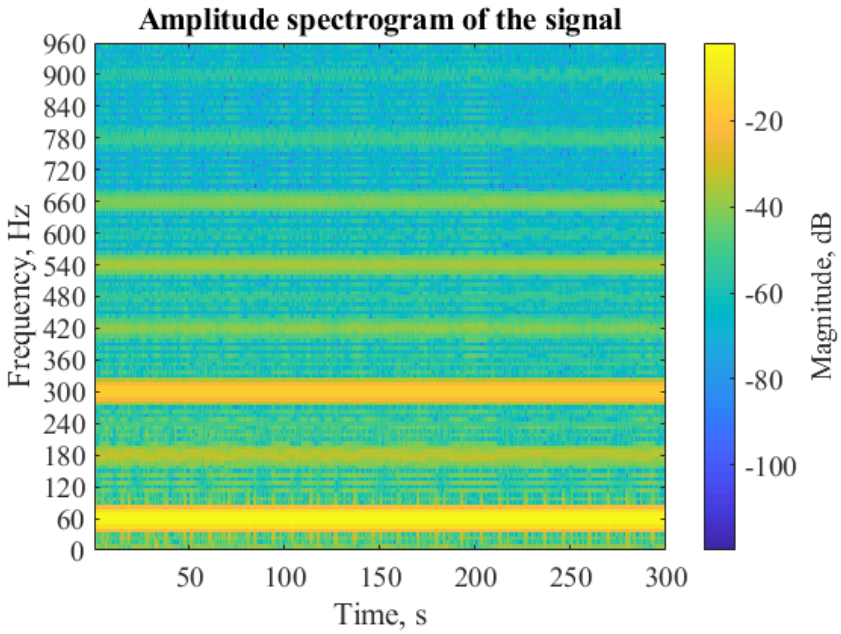

Figure 49 – STFT at current signal in IG Plus inverter .

In agreement with FFT, STFT results shows high presence of third and fifth harmonic components, and the other frequencies with low amplitude throughout the signal. The DWT results: (Fig. 50).

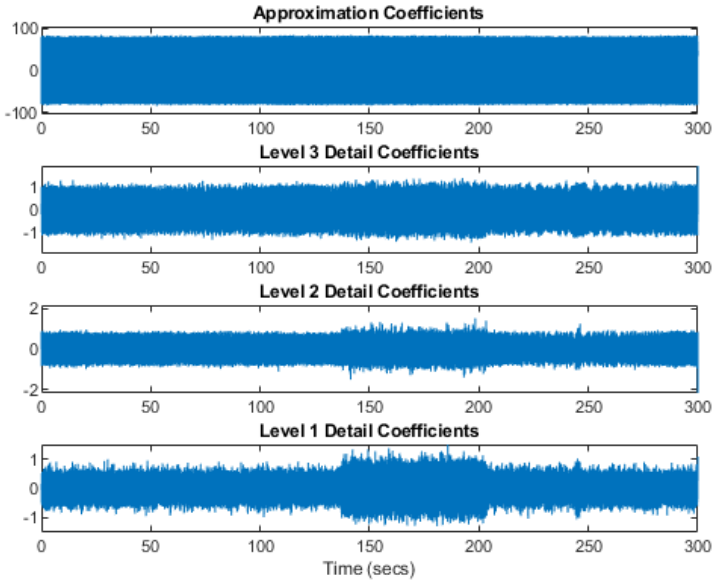

Figure 50 – DWT at IG Plus inverter current signal.

As well as Symo inverter, IG Plus did not show visible changes in DWT due to frequency changes. However it presented an increase of detail energy due to irradiation momentary variation.

In harmonic decomposition using WPT the harmonic components of the signal were extracted. The fundamental is shown in Fig. 51.

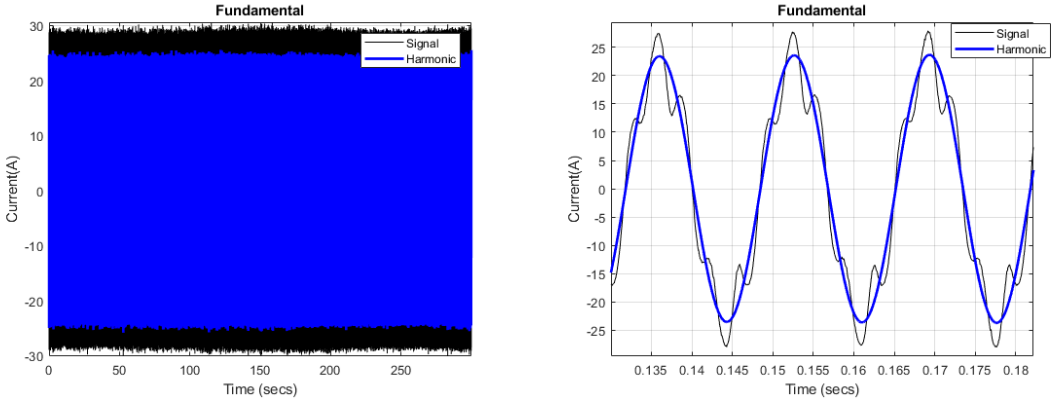

(a) Fundamental (b) Zoom

Figure 51 – Fundamental component.

The other harmonic components are shown in Fig. 52. Odd components were highlighted because other components did not present significant values.

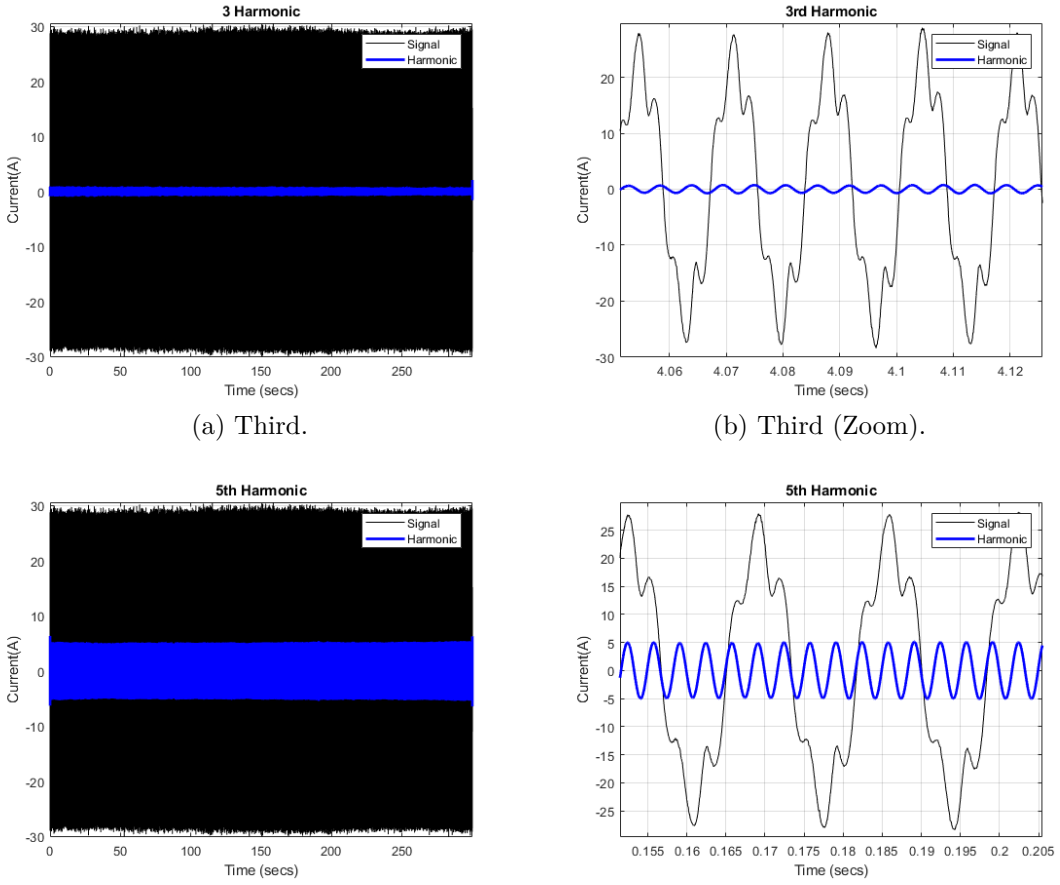

(a) Third. (b) Third (Zoom).

(c) Fifth. (d) Fifth (Zoom).

Figure 52 – Harmonic synthesis components.

5.1.2 Startup Analysis

In this section experiments were performed with inverter startup and shutdown in order to evaluate the impacts of their harmonic content. In startup measurements loads were disconnected from the building substation.

Current measurement was performed with 5 minute(300s) for Symo and 5 minutes duration(300s) for IG PLus at each inverter output. Measurements were performed on a sunny day of August, at 12:00 a.m, with irradiance of 715 W/m^2, panel temperature 51° and 29° ambient temperature, with Fronios Symo power of 9450 kW/12.5 kW (75.6%) and IG Plus 11.6/16 kW (5.8 kW + 5.8kW)(72.5%).

The Fig. 53 represents startup cycle of Fronius Symo inverter:

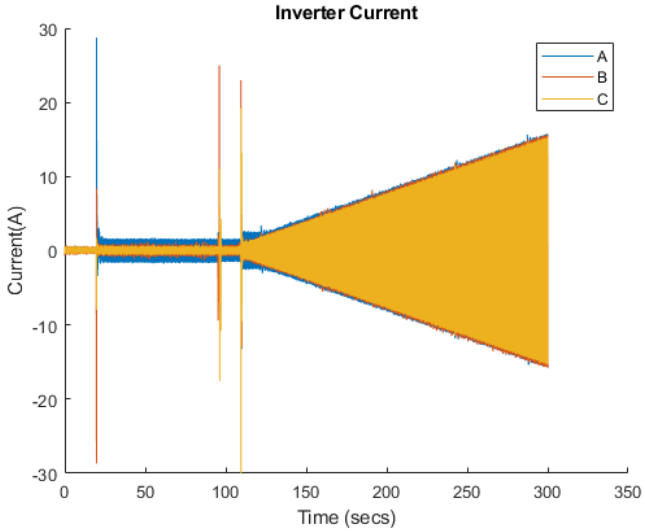

Figure 53 – Three-phase currents at the inverter output.

In Fig. 54 each phase was represented separately for a better visualization:

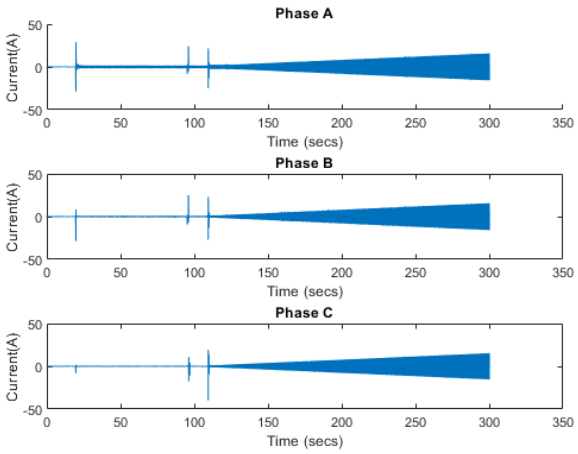

Figure 54 – Three-phase currents per phase.

The starting cycle of the Fronius Symo is shown in Fig 53 and Fig. 54 the inverter was turned on 20s after the start of the measurement, causing a current peak and remaining stable for 75s when two peaks of current occurring 15s apart. After this cycle, the inverter starts to gradually increase output current. This type of control with smooth entry in the grid avoids possible problems caused by lack of energy or abrupt variations in the irradiation, where it prevents the sudden injection of a high current in the grid of the building, preserving the equipment and protection devices connected to it.

Using the STFT, the time-varying harmonics can be checked at inverter start: (Fig. 55).

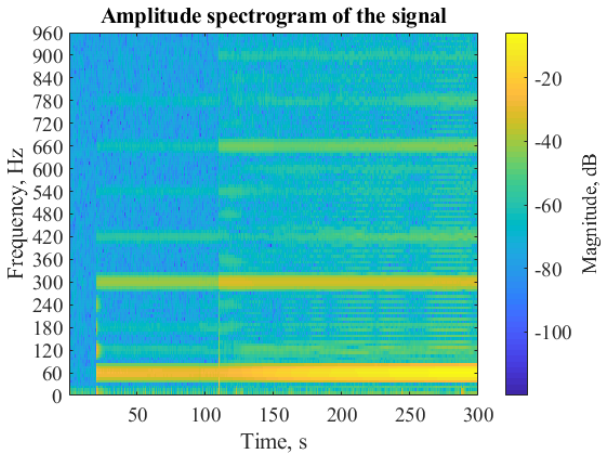

Figure 55 – FFT result for the startup of the Symo inverter.

The graph shows the instants in which the greater component (fifth harmonic) was inject, but there is not a good resolution to know exactly the moment of the events occurred, only the moments in which the components entered the system.

The DWT has better resolution to analyze these types of events, as can be observed in the (Fig. 56).

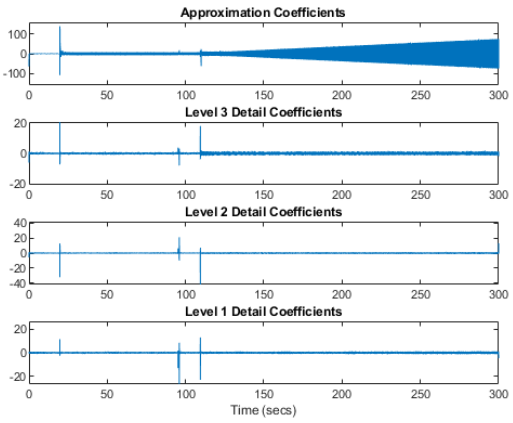

Figure 56 – DWT applied at the Symo inverter.

At Fig. 56, the time of the events of the three peaks are clearly visualized, showing this tool identification capacity of events in power systems.

With the use of WPT the evolution of the harmonics in the time during the starter of the inverter is observed. The third and fifth harmonics increase as the current is injected into the system. At Fig. 57 shows the harmonic components of the signal.

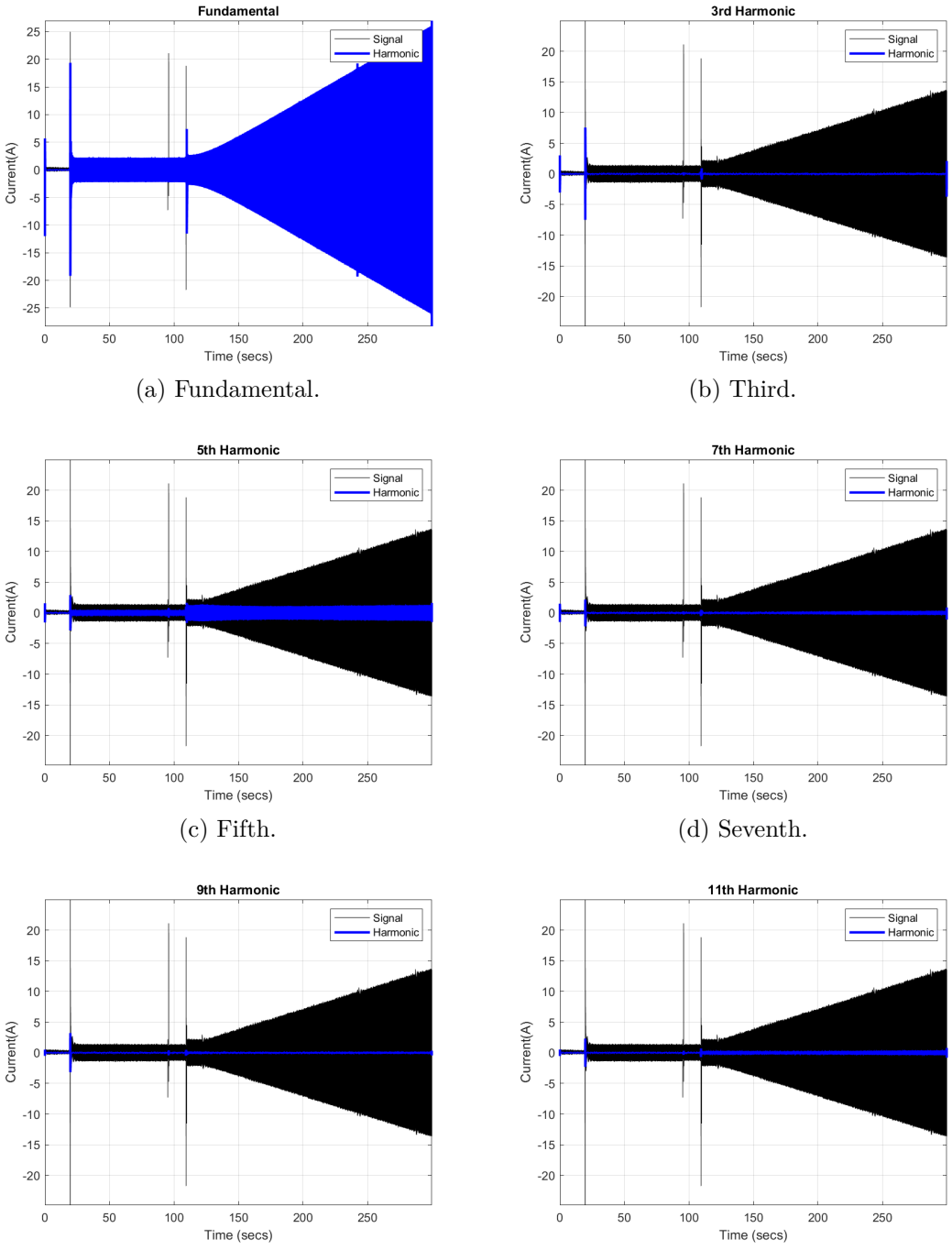

(a) Fundamental.

(b) Third.

(c) Fifth.

(d) Seventh.

(e) Ninth.

(f) Eleventh.

Figure 57 – Harmonic components decomposed by WPT.

For the IG Plus inverter the measurement of its starting cycle is shown in Fig. 58 (two inverters):

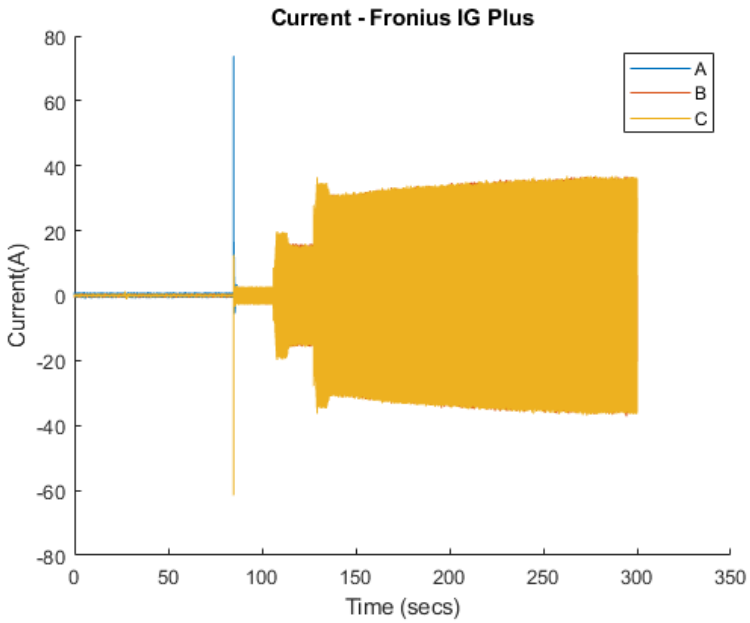

Figure 58 – Three-phase currents at IG Plus inverter output.

In Fig. 59 each phase was represented separately for a better visualization:

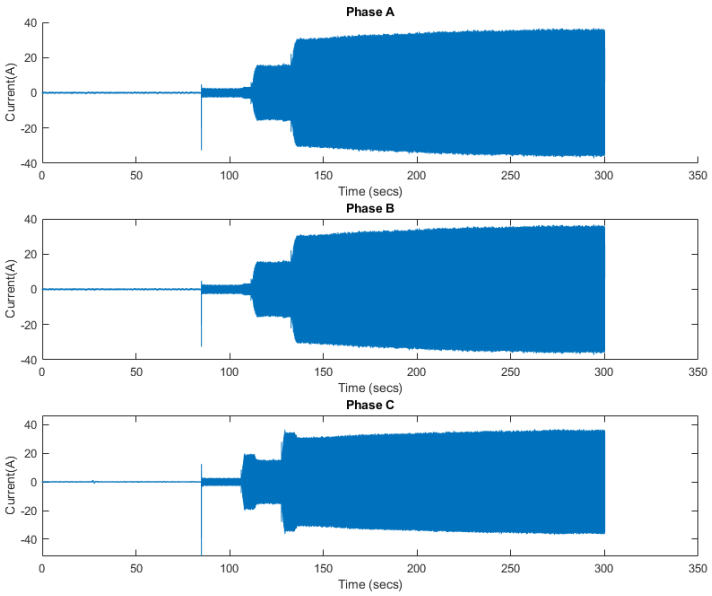

Figure 59 – Three-phase currents per phase.

The starting cycle of the Fronius IG Plus is shown in Fig. 58 and Fig. 59, the inverter has been turned on 85s after the start of the measurement, in a first step, the cycle causes a current peak and is stable for 75s, with the insertion of a low current(2A). After 20s a second starting step occurs, increasing the current output by a factor of 10

(20A) and finally after 20s there is a 70 % increase in current (34A). The complete starting cycle of this inverter is composed of 3 stages, with a total duration of 60s. Compared to Symo, its starting process is more abrupt in relation to the progression of injection in the grid, but its process is faster.

Using STFT, time-varying harmonics can be checked at inverter startup (Fig. 60).

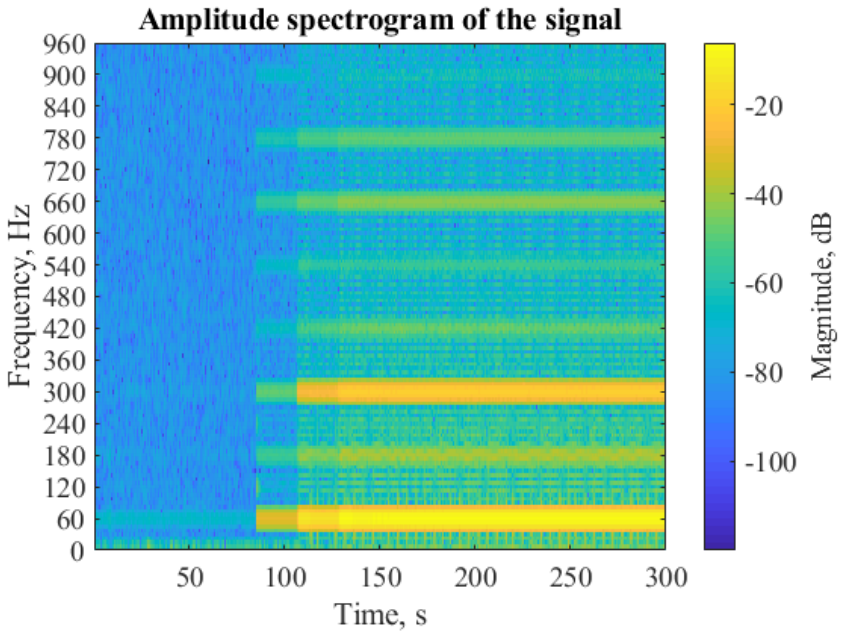

Figure 60 – STFT result at startup of the IG Plus inverter.

The graph shows the instant in which the most obvious component (fifth harmonic) enters the system, but there is not a good resolution to know exactly the moment of the events occurred, only the moments in which the components entered the system.

The DWT analysis is shown in (Fig. 61)

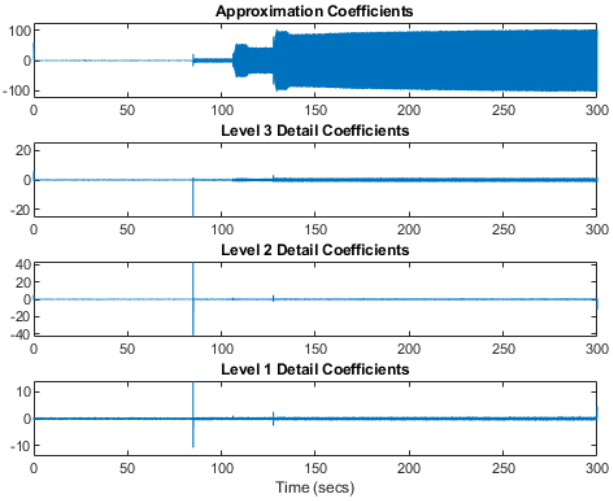

Figure 61 – DWT applied for IG Plus inverter.

At Fig. 61 the time at which the 3 stages of the start has been identified, although steps 2 and 3 result in a small variation in the image.

With the use of WPT the evolution of harmonics in the time during inverter startup is observed. At Fig. 62 shows the main harmonic components of the signal. As discussed earlier, the third and fifth harmonics increase as the current is injected into the system.

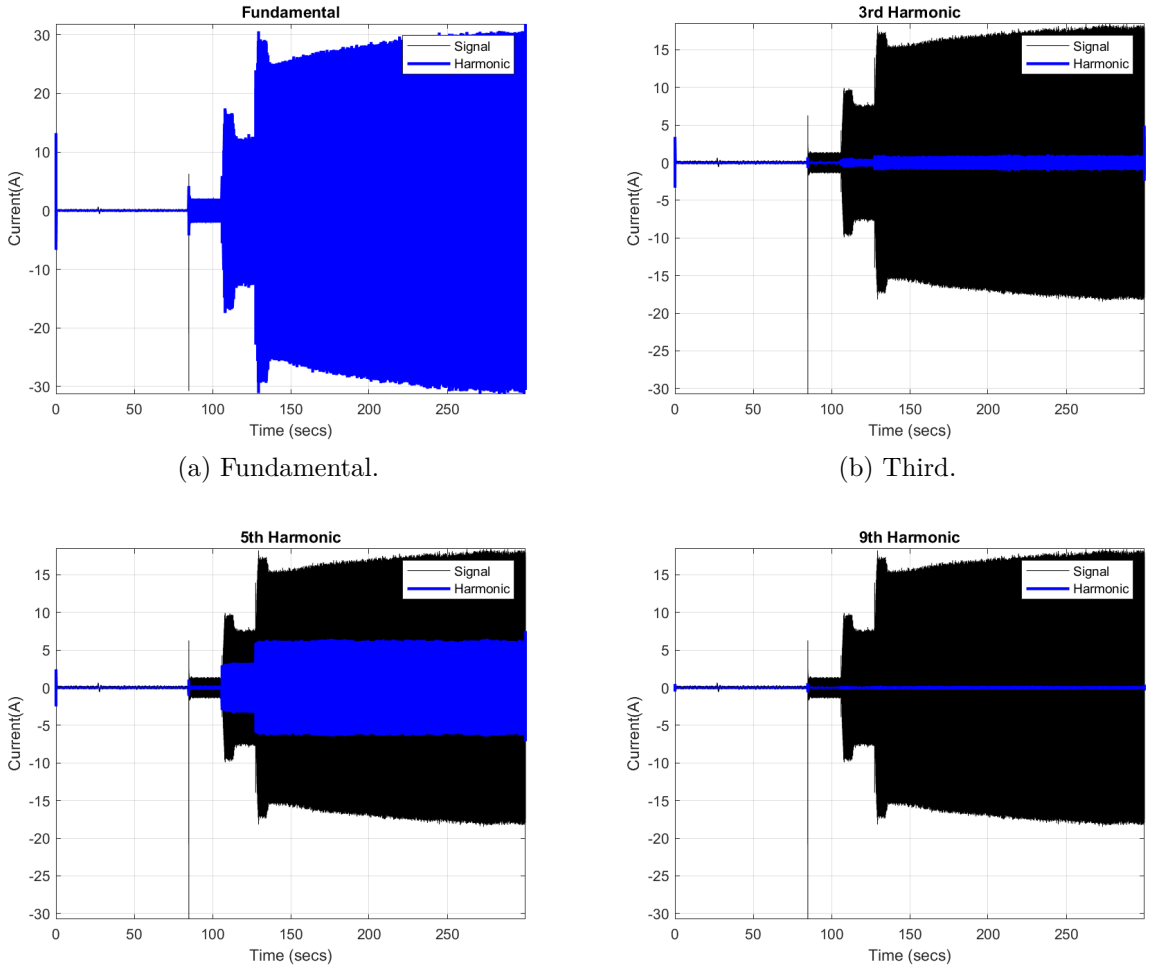

(a) Fundamental.

(b) Third.

(c) Fifth.

(d) Ninth.

Figure 62 – Startup - Harmonic Synthesis components decomposed by WPT.

Evaluating inverter shutdown only makes sense in the context of the system, ie, the measurement must be performed at the building substation transformer secondary where PV generated energy is injected. In this experiment, at the beginning of the measurements both inverters are already connected and in steady state. Two measurements were performed, one of 16 minutes (960 sec) and one of 5 minutes (300 sec.). The table 7 contains the actions and time it was performed (seconds):

Table 7 – Experiment Procedures

Action	Measurement I	Measurement II
Shutdown IG Plus	230s	
Startup IG Plus	430s	
Shutdown Symo	560s	
Startup Symo	705s	
Shutdown Both	845s	75s
Startup Both		265s

First measurement is shown at Fig. 63. The actions of the first column of the Table 7 were performed.

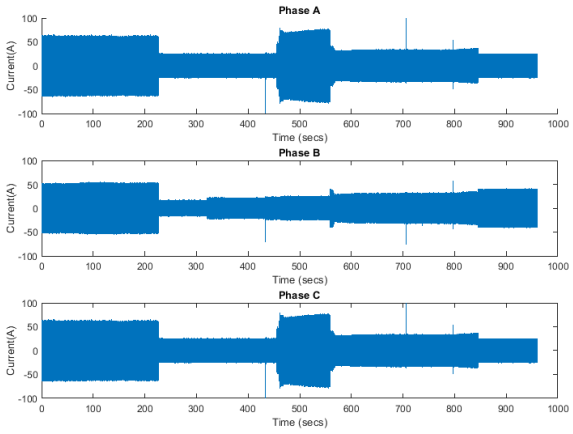

Figure 63 – Three-phase currents during startup and shutdown inverters.

DWT applied is shown at Fig. 64. In this case DWT failed to perform in identifying the events startup.

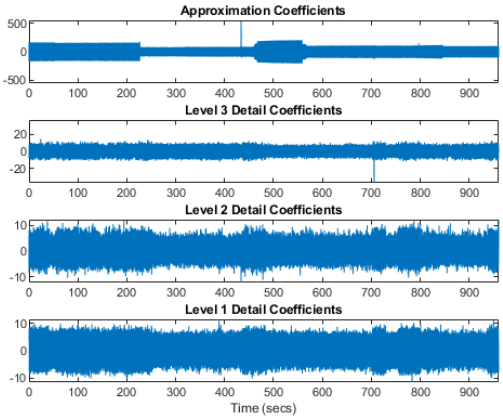

Figure 64 – DWT for startup and shutdown inverters.

Fig. 65 shows the decomposition using WPT where the points used in the following analysis are marked. At the instant of time 226s the inverter IG Plus is turned off, leading to a reduction in the mains current, it remains constant until the moment 433s where the inverter is reconnected, starting its startup process, seen in the previous analyzes, there is a current peak, followed by two steps, where the injected current is increased. At instant 557s the inverter Symo is turned off, also causing a reduction of the current system. At the instant 706s the inverter Symo is switched on, causing a current peak and then starts its starting cycle, where after a certain period, at approximately instant 800, the second stage occurs and the process of gradual increase of the current is initiated. Finally, both are turned off at the moment 845s, the effect is a reduction of the odd harmonics in the system, especially the fifth harmonic, having the inverters as its main source.

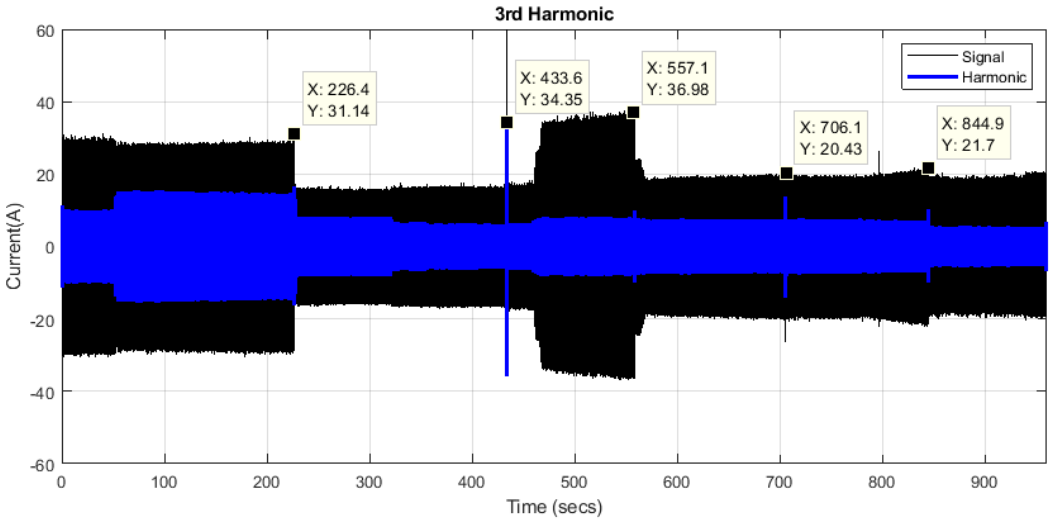

(a) Third

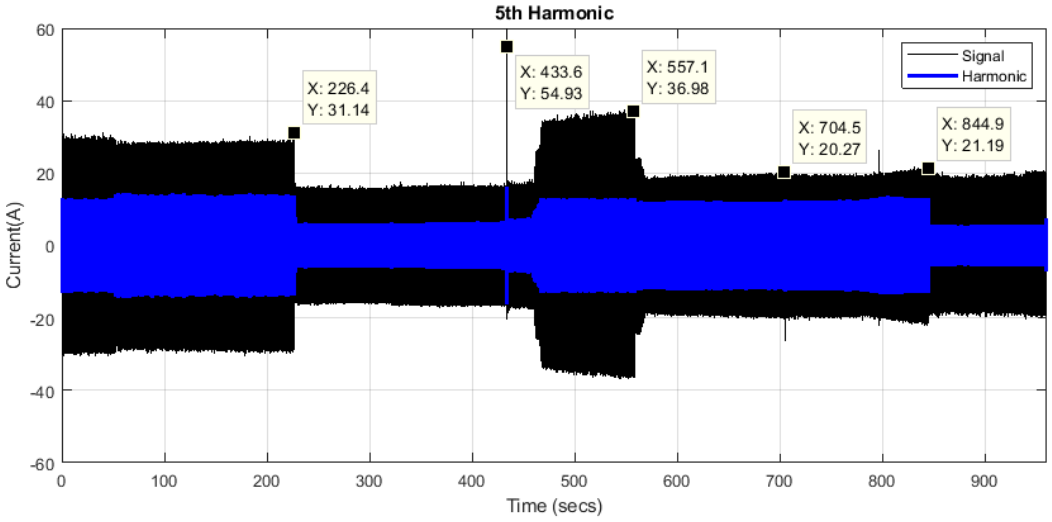

(b) Fifth

Figure 65 – Harmonics referring to the in/out inverters of system.

For the second experiment, was used the 5 minutes measurement, the time of the actions are in the third column of the Tab. 7. The sample image of the experiment is shown in Fig. 66.

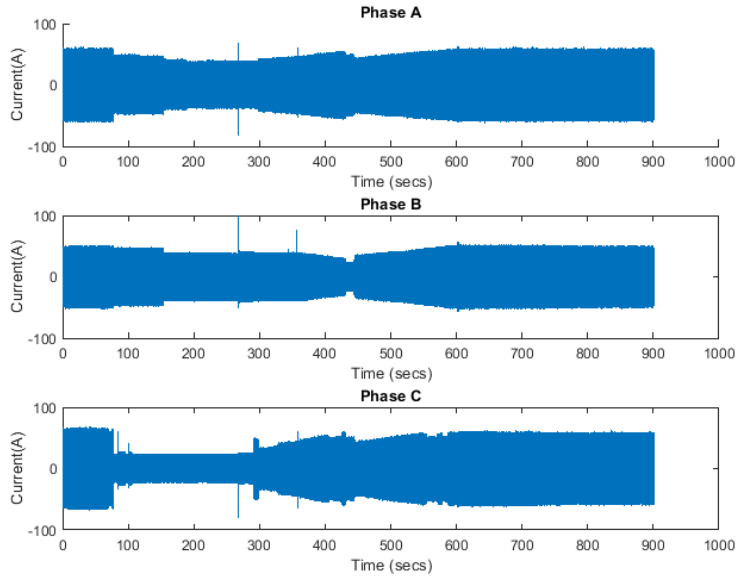

Figure 66 – Three-phase currents at the inverter output.

The DWT for the experiment is shown in Fig. 67. In this case, DWT was able to pick up the starter events from the IG Plus and Symo inverter in the level 2 detail component.

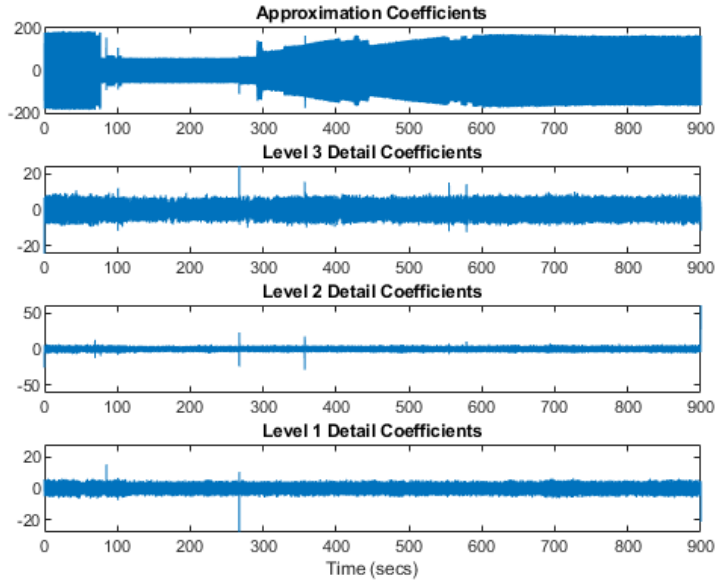

Figure 67 – DWT for irradiance variation.

At Fig. 68 shows the decomposition using the WPT, where the points used in

the following analysis are marked. At the instant of time 76s both inverters are turned off, causing the reduction of circulating current in the system, and consequently of the harmonics generated by them. At the instant 267s both inverters are reconnected and the starting point is performed, between the moments 300s and 400s, the IG Plus cycles in stages and in parallel the flow of the Symo gradually enters, at the instant 600s both inverters have completed their cycle and are operating in regime.

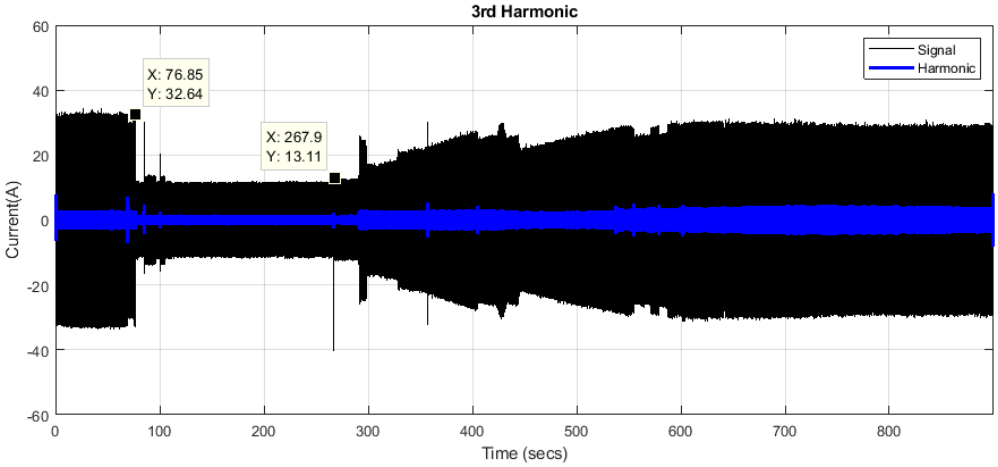

(a) Third

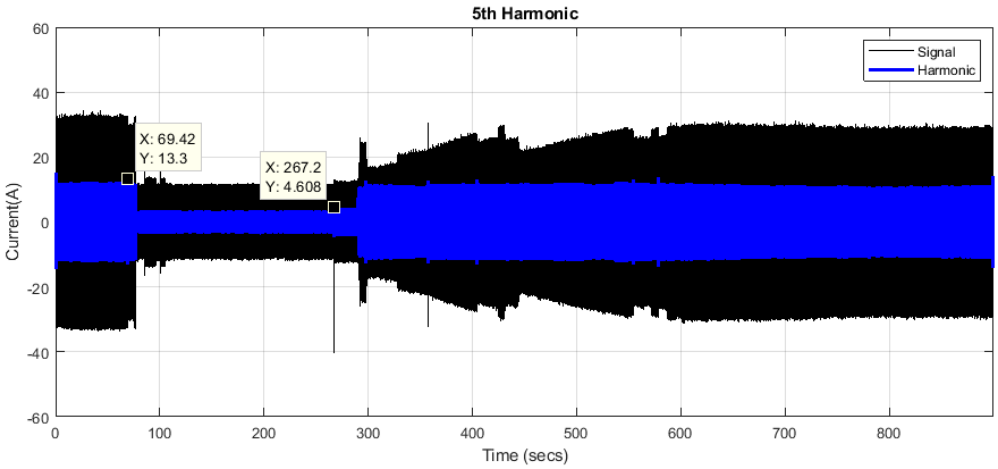

(b) Fifth

Figure 68 – Harmonics referring to the in/out inverters of system.

5.1.3 Generation Variation Analysis

In this section measurements were made when the inverter operated under conditions of variation in the solar irradiation on the panels due to the presence of transient shading (clouds). Two conditions were analyzed for each inverter.

The first measurement for variations in Symo irradiation was performed with 5 minutes duration (300s). Measurements were performed on a sunny day of August, at 12:00 p.m., panel temperature 48° and 26° ambient temperature. The irradiance and power

data were obtained from the inverter's API in real time, and this communication has a response delay time ranging from 5 to 10 seconds between the responses from the data collection request, thus, the irradiation's variation and its effect at the current are not synchronized at Fig. 69.

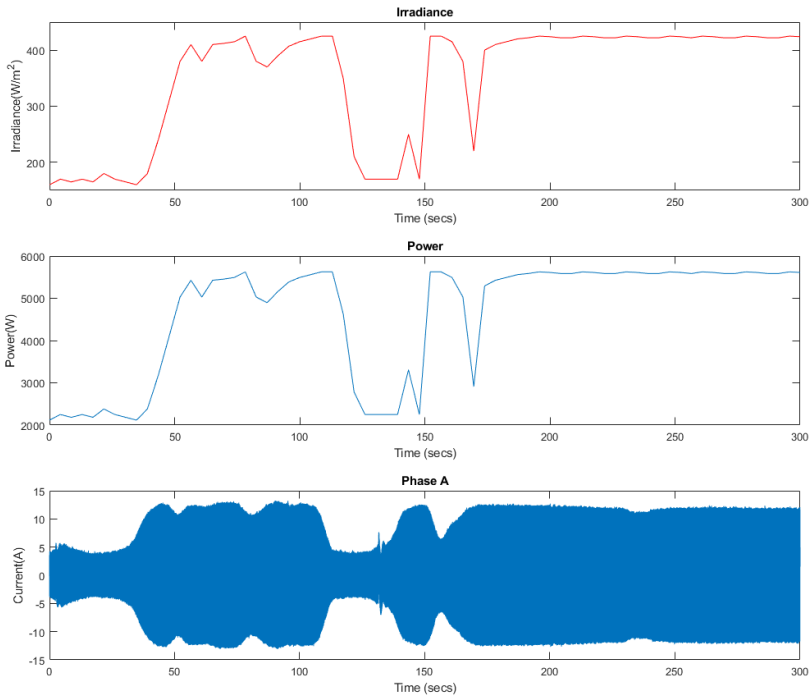

Figure 69 – Irradiance, Power and Current under generation variation effect.

For the Symo inverter Fig. 70 shows the current for the three phases during irradiation variation.

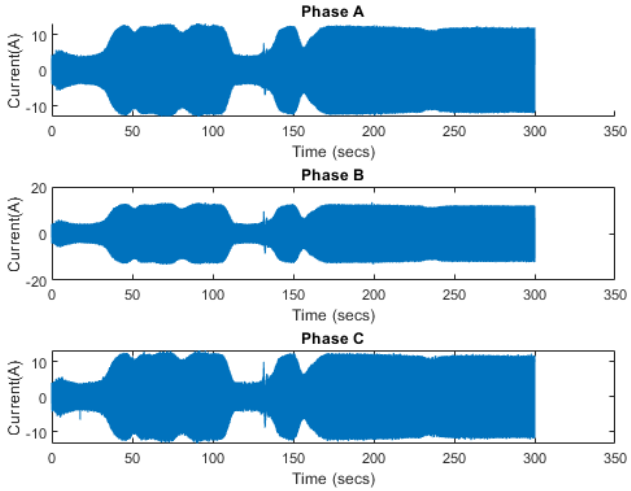

Figure 70 – Currents under generation variation effect.

The STFT shows that the harmonics are present throughout the signal, and it presents the variation of the magnitude of the harmonics (Fig. 55).

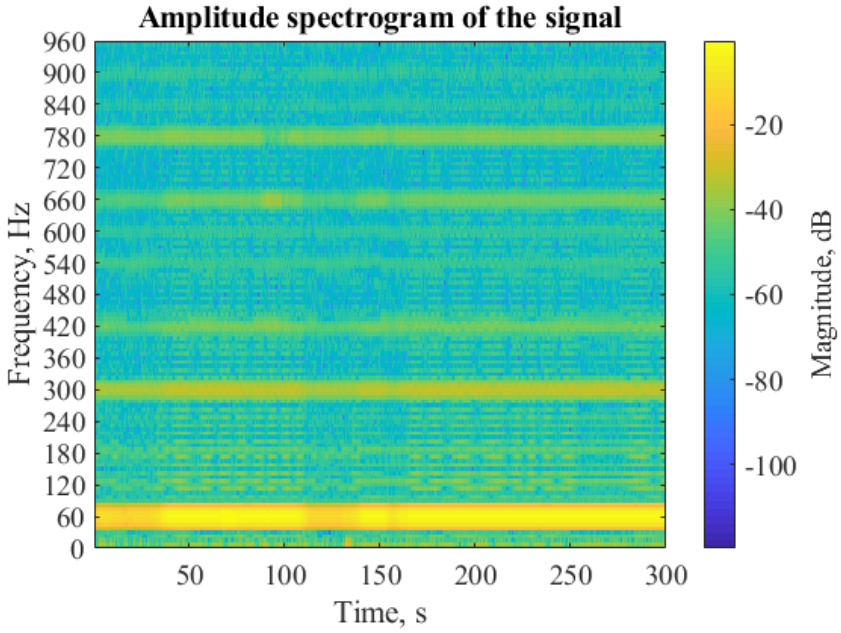

Figure 71 – STFT for irradiance variation.

The DWT for this analysis is shown in Fig. 72. In this case the DWT failed to perform well in identifying the events in the inverter generation variation due to changes in solar irradiance.

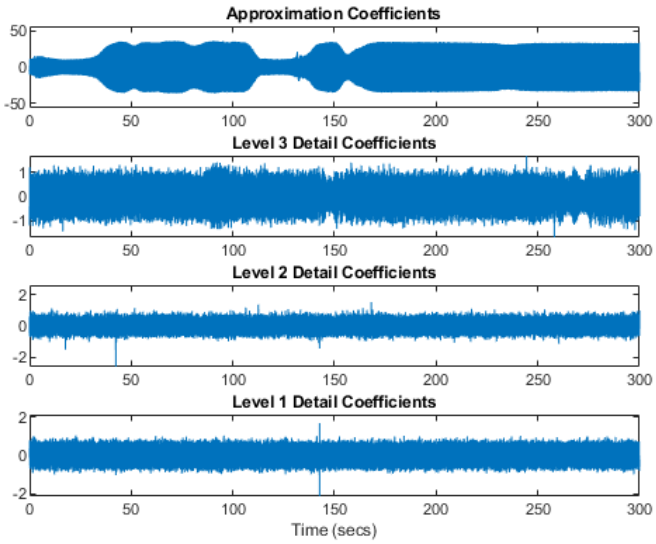

Figure 72 – DWT for irradiance variation.

In the WPT analysis there was no significant variations in the system harmonics (Fig. 73), the result was a decrease or increase proportional to the variation of the generation due to the variation in the irradiation in the solar panels.

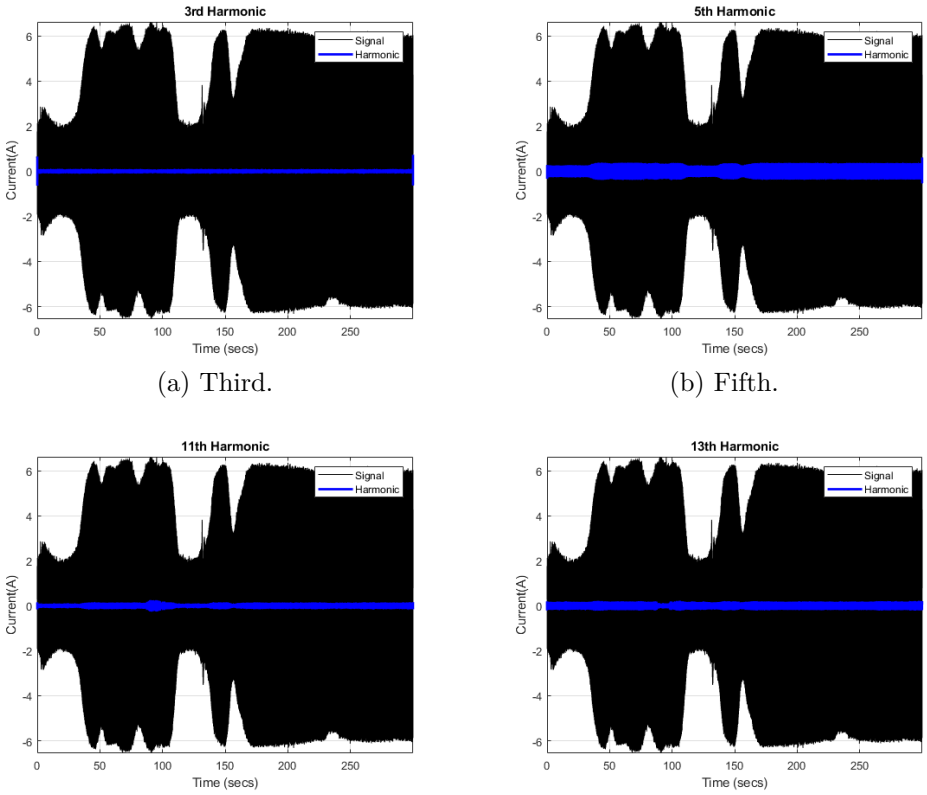

(a) Third. (b) Fifth.

(c) Eleventh. (d) Thirteenth.

Figure 73 – Harmonics referring to variation generation at inverters.

Second measurement for variations in Symo irradiation was performed with 10 minutes duration (600s). Measurements were performed on a sunny day of August, at 12:20 p.m., panel temperature 51° and 31° ambient temperature.The irradiance and power data were obtained from the inverter's API in real time, and this communication has a response delay time ranging from 5 to 10 seconds between the responses from the data collection request, thus, the irradiation's variation and its effect at the current are not synchronized at Fig. 75. Fig. 74 illustrate the currents at the three phases.

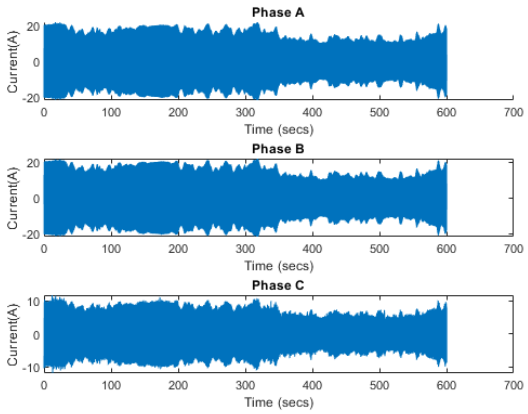

Figure 74 – Currents under generation variation effect.

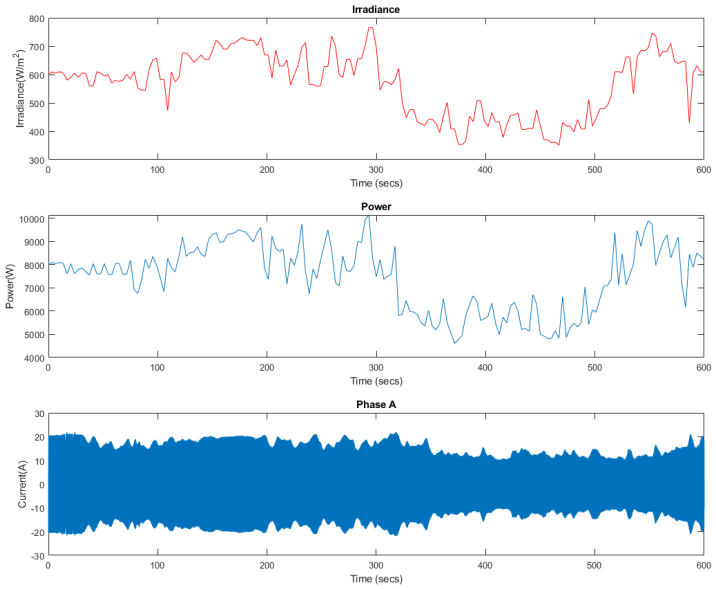

Figure 75 – Irradiance, Power and Current under generation variation effect.

Similar to the previous case there are no significant modifications in the harmonics of this inverter(Fig. 76):

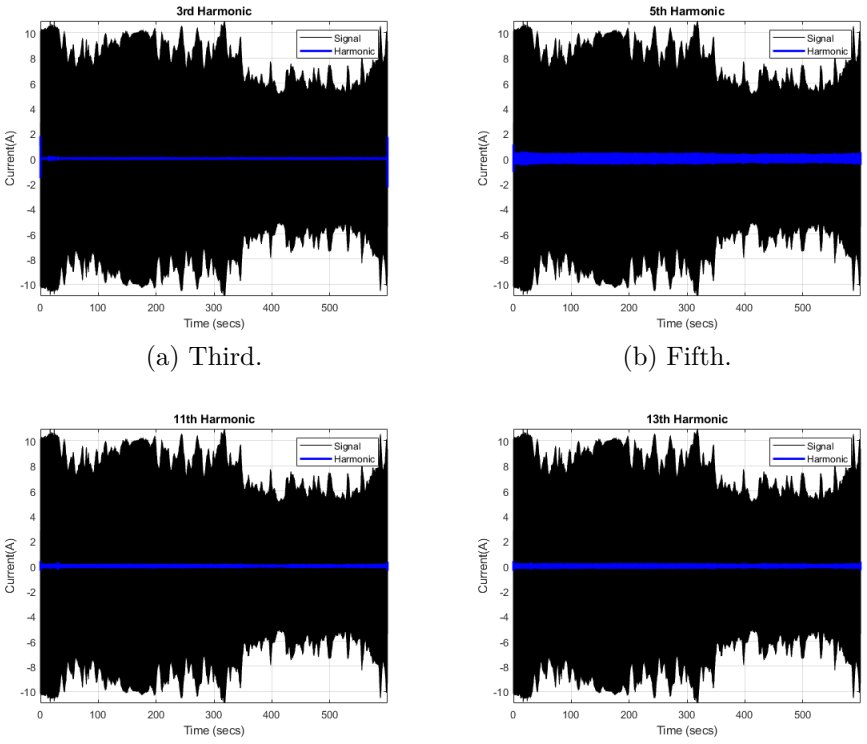

(a) Third. (b) Fifth.

(c) Eleventh. (d) Thirteenth.

Figure 76 – Harmonics referring to variation generation at inverters.

The same procedures were performed for the IG Plus inverter, 2 minutes measurement duration (120s), at 12:20 p.m., panel temperature 51° and 29° ambient temperature.

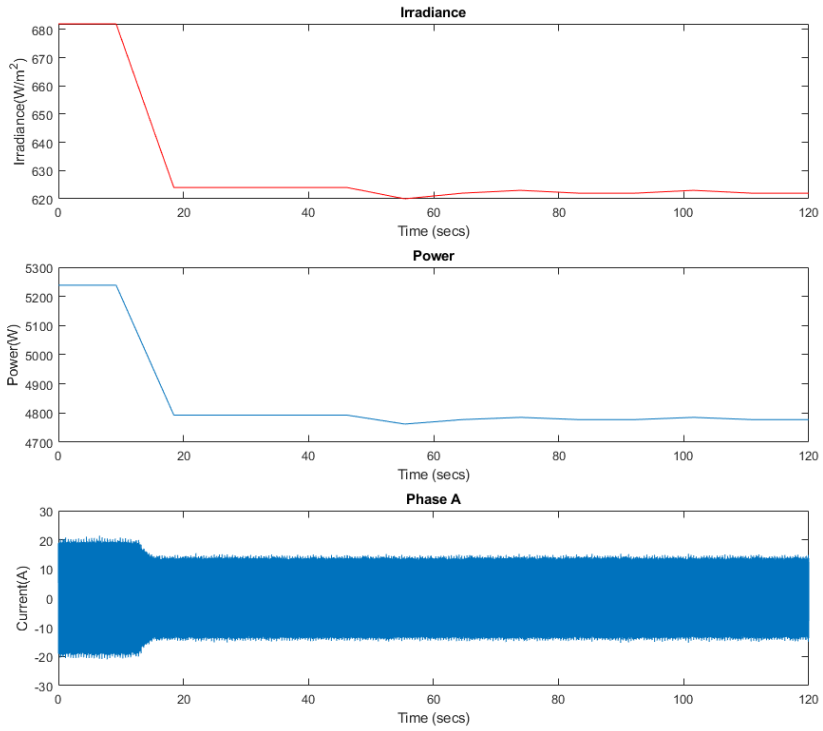

Figure 77 – Irradiance, Power and Current under generation variation effect.

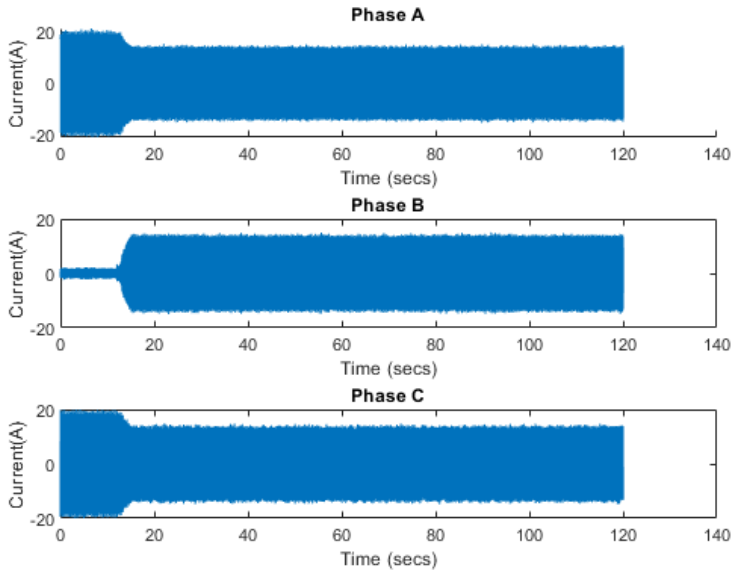

Figure 78 – Currents under generation variation effect at IG Plus.

STFT with constant harmonic frequencies (Fig. 79).

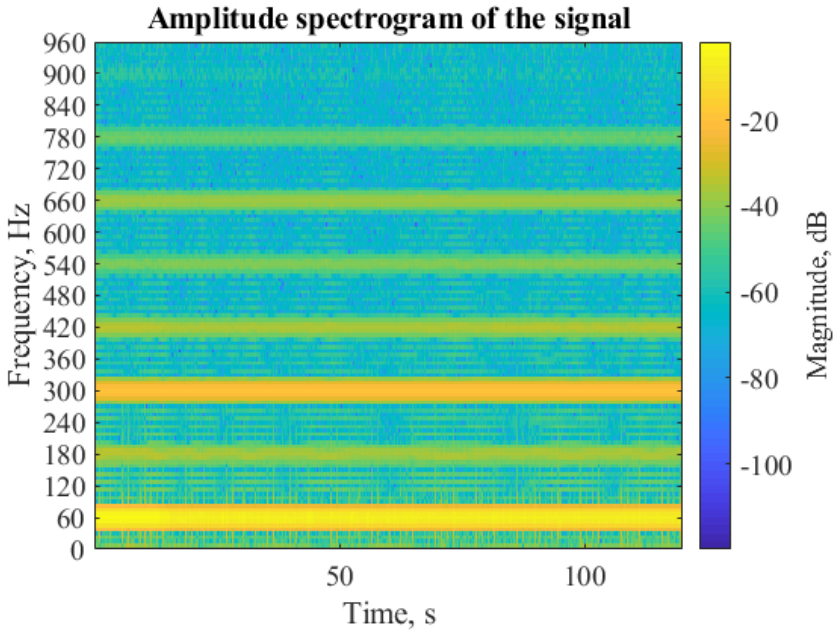

Figure 79 – STFT for irradiance variation.

DWT without significant changes in decomposition details (Fig. 80).

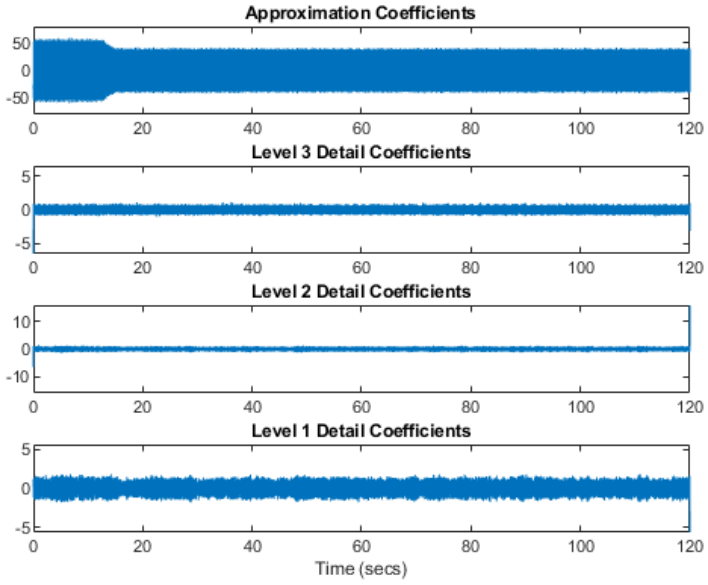

Figure 80 – DWT for irradiance variation.

The same goes for analysis using WPT (Fig 81).

A characteristic observed in this inverter is until it reaches a minimum level of generation it maintains one phase with low current, while increasing the current of the other two phases. This behavior is generally not specified by the manufacturer and may cause an imbalance in the system of the building in which the generation is located. Fig. 78 and Fig. 82 and 83 exhibits this phenomenon (Phase B).

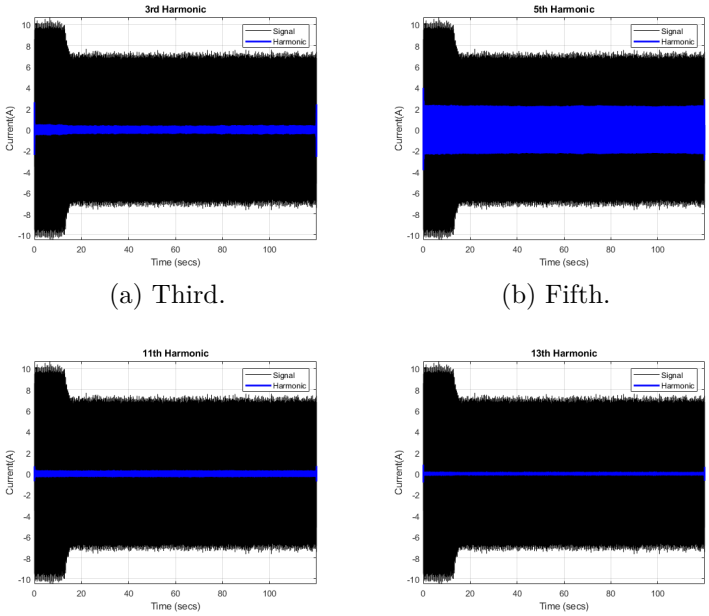

(a) Third. (b) Fifth.

(c) Eleventh. (d) Thirteenth.

Figure 81 – Harmonics referring to generation variation in inverters.

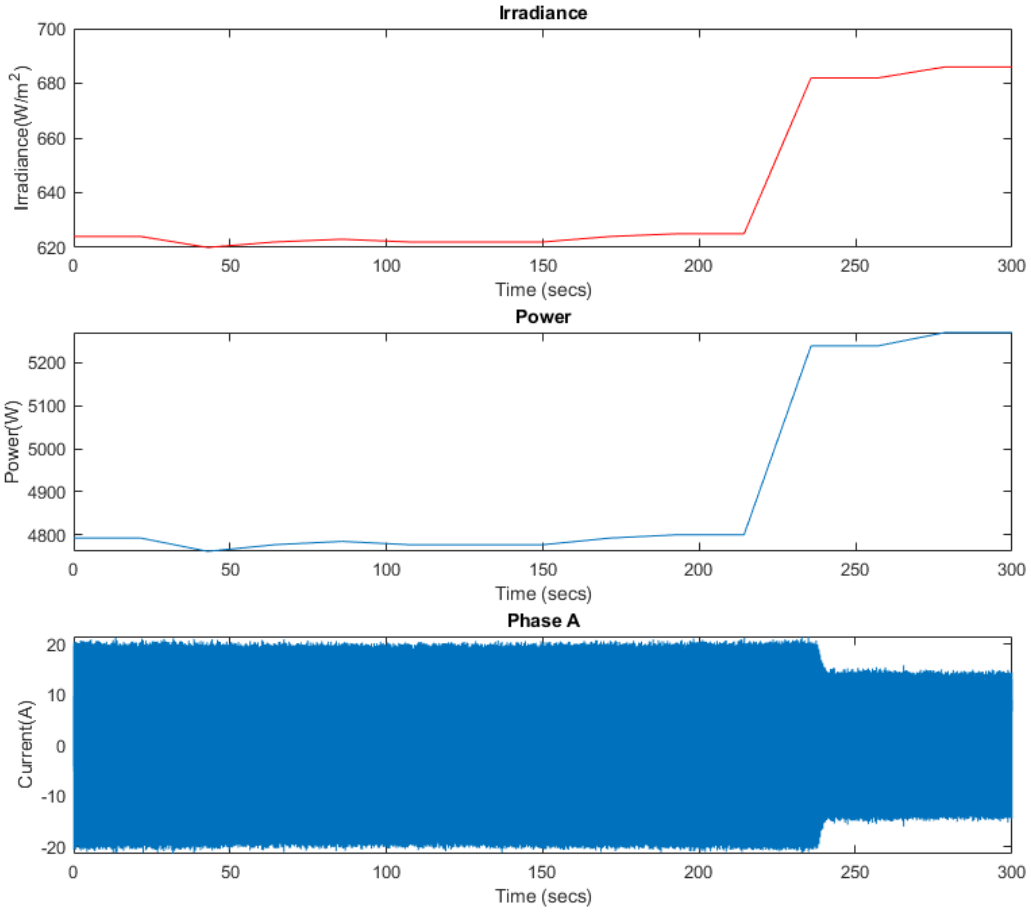

Figure 82 – Irradiance, Power and Current under generation variation effect.

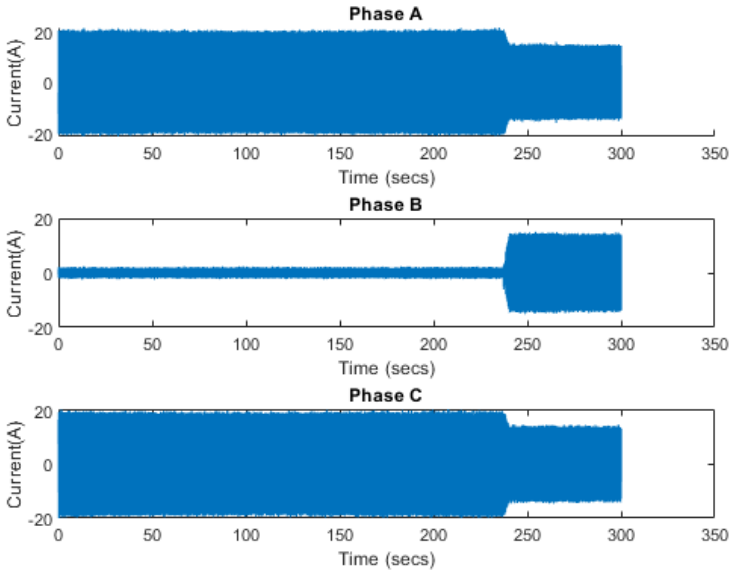

Figure 83 – Three-phase currents at the inverter output under generation variation.

Second measurement for IG Plus under condition of generation variation, signal sampled is shown at Fig. 84):

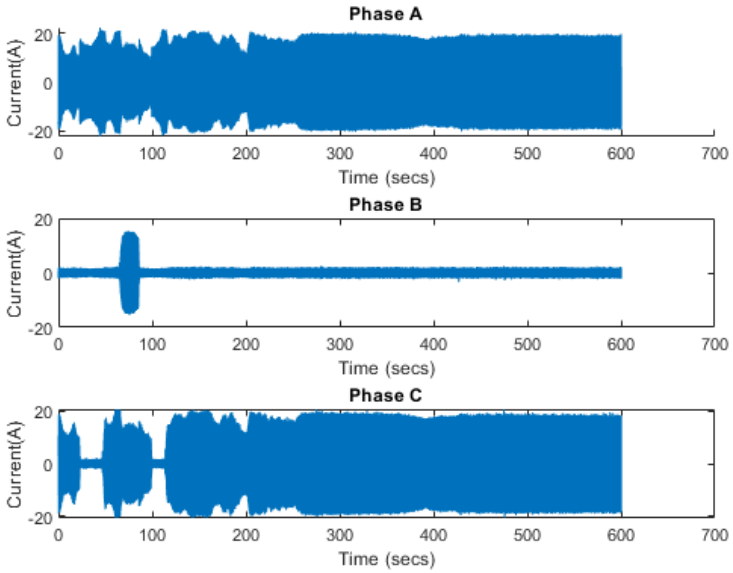

Figure 84 – Three-phase currents at the inverter output.

DWT was able to identify the sudden changes of the variations, since the irradiation reached low indices compromising the generation in some moments.

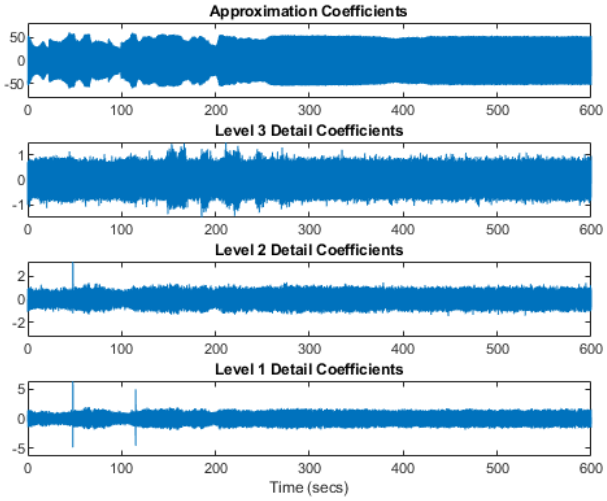

(a) Phase A

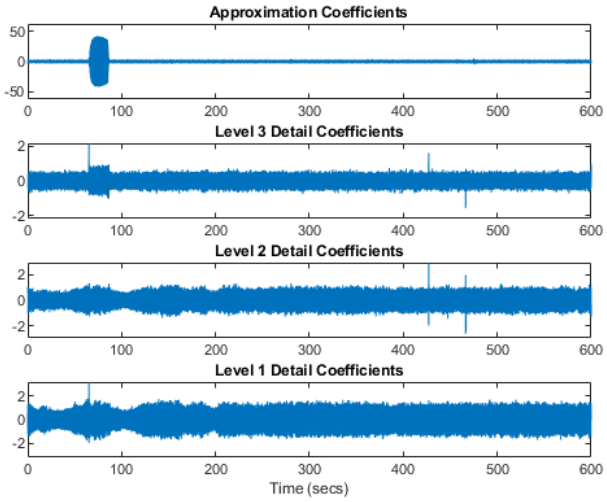

(b) Phase B

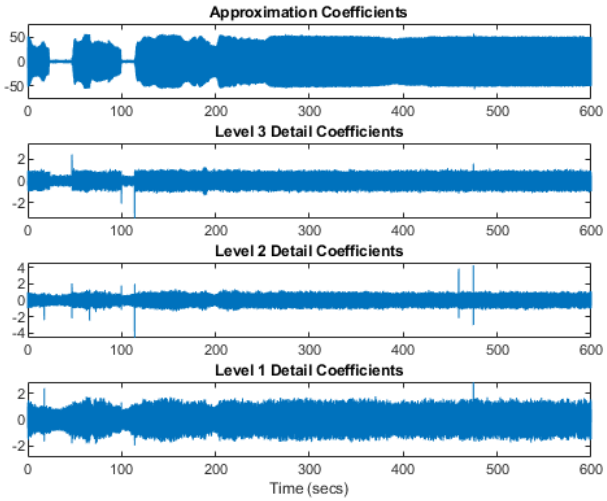

(c) Phase C

Figure 85 – DWT of each output current phase.

Harmonic decomposition of the three phases using WPT (Fig. 86):

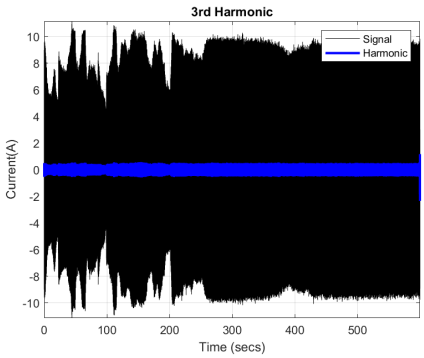

(a) Third - Phase A.

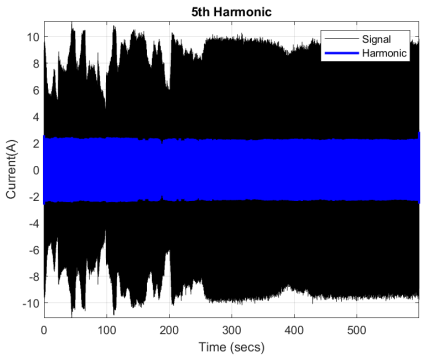

(b) Fifth - Phase A.

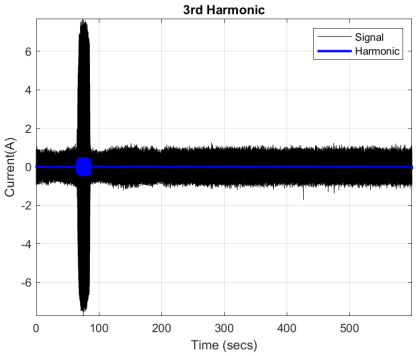

(c) Third - Phase B.

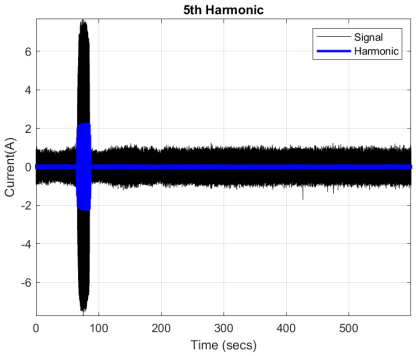

(d) Fifth - Phase B.

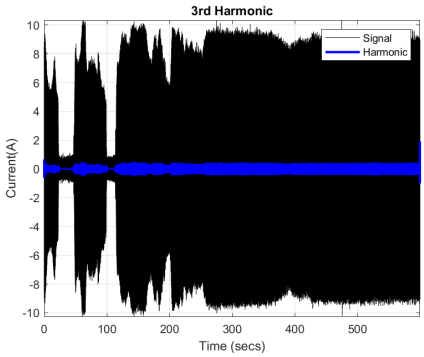

(e) Third - Phase C.

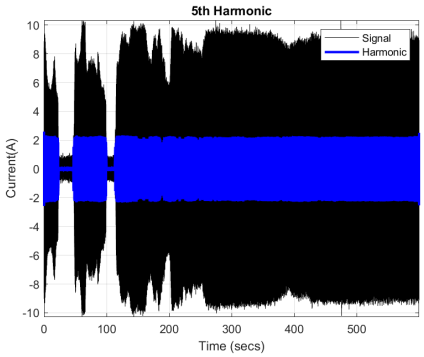

(f) Third - Phase C.

Figure 86 – Harmonics referring to generation variation at inverter.

In this section, two models of inverters from the same manufacturer were analyzed, both models presented different behavioral characteristics for the presented scenarios, being the starter strategies of the inverters, being stepwise or gradual, the behavior against generation variances, one reducing a phase of the system and increasing the others and finally the quality of the form of the injected sinewave in the system, being one of the inverters to have high index of injection of fifth harmonic.

5.2 PV System Connection Analysis

A final analysis was performed using two measurements at the building substation. Both made in sequence. First was taken with no PV connected at the grid and second after the PV inverter startup and stabilization. Measurements were performed on a sunny day of August, at 13:30 p.m., with irradiance of 700 W/m^2, panel temperature 51° and 31° ambient temperature. with Fronios Symo power of 9250 kW/12.5 kW (74%) and IG Plus 11.4/16 kW (5.7 kW + 5.7kW)(71.2%). Voltage waveforms are shown in Fig. 87.

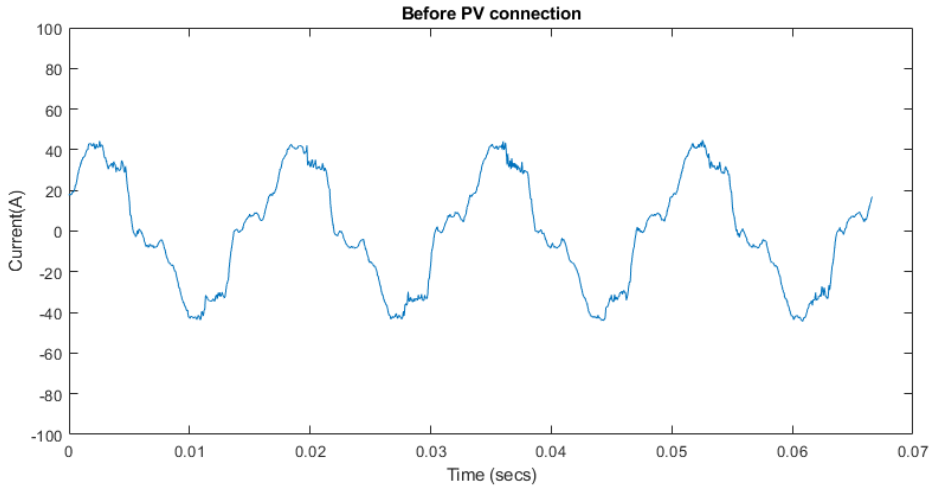

(a) Before connection.

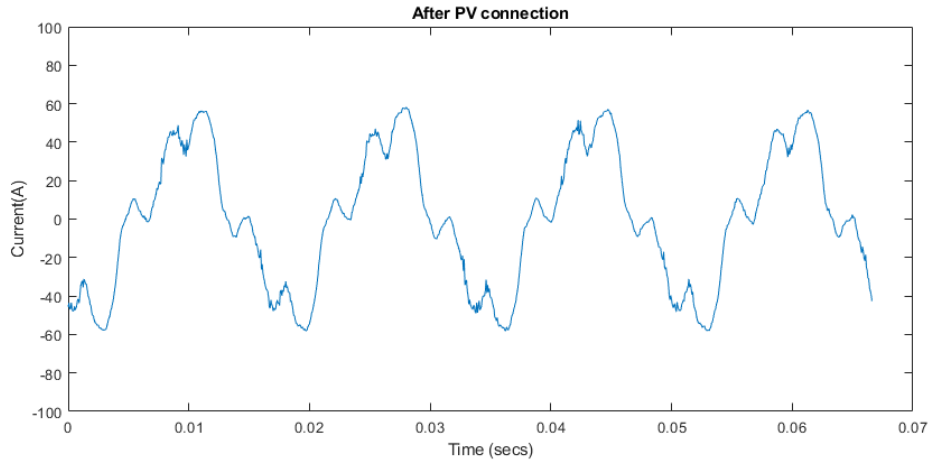

(b) After connection.

Figure 87 – System current wave before and after PV connection.

FFT and THD were extracted using 12 cycles of each signal. The FFT is shown in Fig. 88.

The Table 8 shows the percentage relation of the odd harmonics of the systems, before and after the connection. A small reduction in all harmonics is observed except in the 5th harmonic, having an increase of 14%.

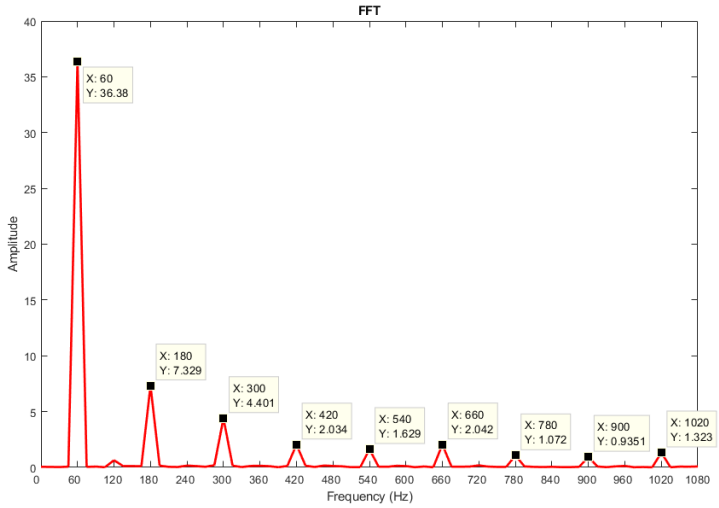

(a) Before connection.

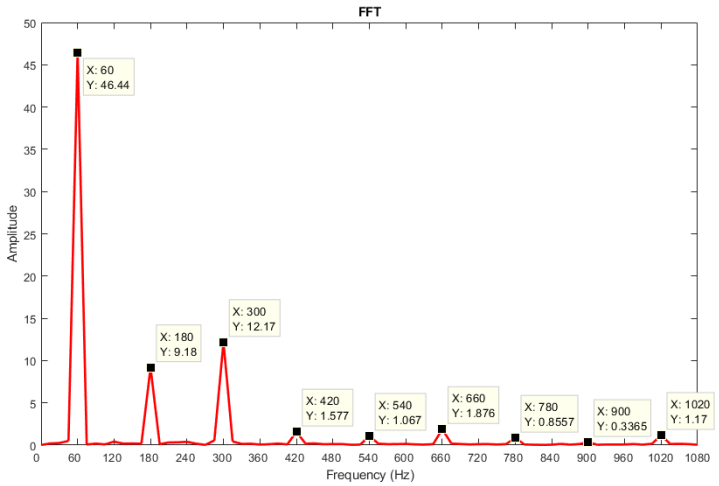

(b) After connection.

Figure 88 – FFT before and after PV connection.

Table 8 – Harmonic comparison before and after pv connection.

	Before PV		After PV	
Harmonic frequency(Hz)	Current (A)	%	Current (A)	%
60Hz	36.38A	100,00%	46.44A	100,00%
180Hz	7.33A	20,15%	9.18A	19,72%
300Hz	4.40A	12,10%	12.17A	26,21%
420Hz	2.03A	5,59%	1.58A	3,40%
540Hz	1.63A	4,48%	1.07A	2,30%
660Hz	2.04A	5,61%	1.88A	4,04%
780Hz	1.07A	2,95%	0.86A	1,84%
900Hz	0.94	2,57%	0.34A	0,79%
1020Hz	1.32A	3,64%	1.17A	2,52%

The THD for the current in the system without generation was 40.72%, with the PV system connected the THD was of 47.26%. An increase of approximately 7%.

5.3 Events Identification

During the analysis of the various measurements made, a recurrent signal was found in some measurements. This signal appeared even in the direct measurements at the output of the inverters and the same at maximum generation capacity and with the day totally sunny, which was not being associated with being produced by the inverter. This signal can be visualized on the seventeenth harmonic of a sampling of the output of the inverter Symo (Fig. 89).

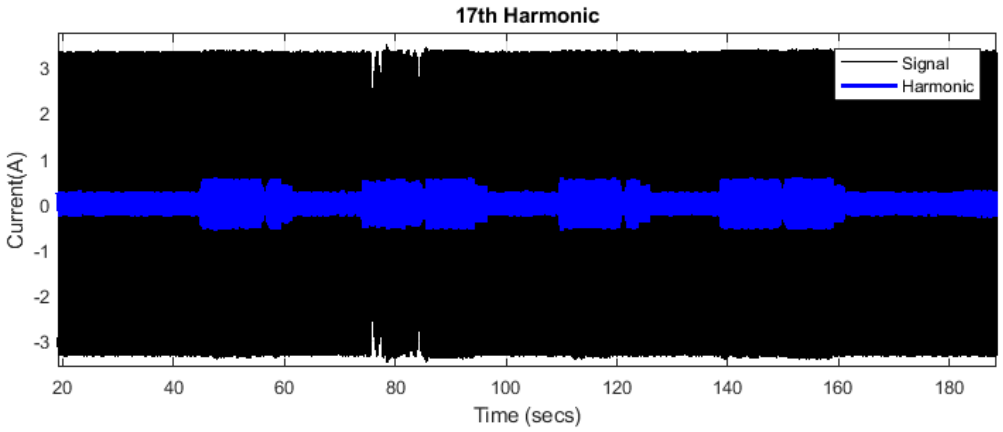

Figure 89 – Recurrent harmonic signal.

In this way loads that could generate high harmonics in the system were carried out, such as AC units, elevators, irrigation pumps, PCs, among others. Time of measurements were carried out between 10:30 a.m. to 1:30 p.m., departure time for lunch in the building, and in this way increased use of the elevator. Thus, further investigation was carried out on this specific load.

The elevator has been activated six times for the measure at M1 (Fig. 36) and two times for the measure at M2 (Fig. 36), within five minutes (300 seconds) of measurement. The Fig. 90 shows the the measure at M1 (substation transformer) and Fig. 91 at M2 (output inverter).

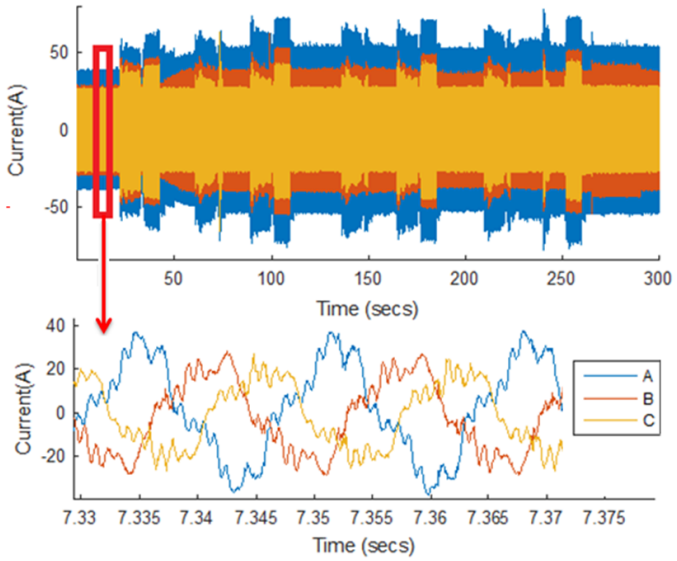

Figure 90 – Current in phases A, B and C at M1.

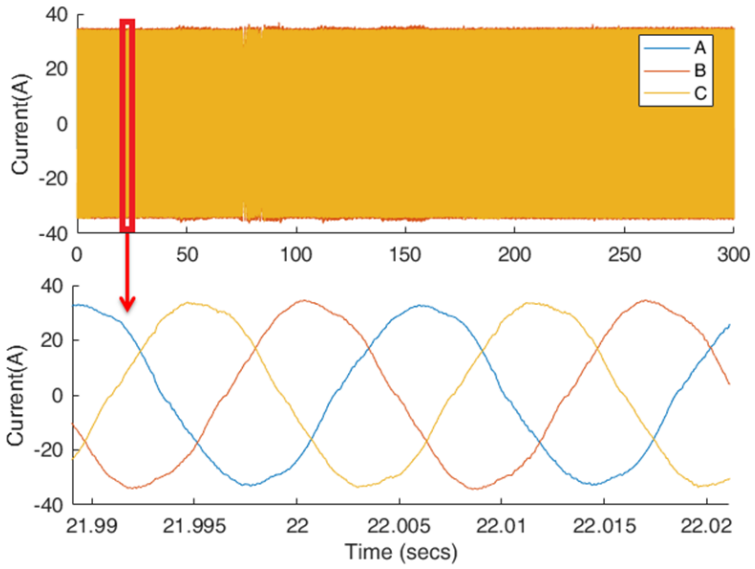

Figure 91 – Current in phases A, B and C at inverter's output (M2)

The mentioned techniques were applied to verify the behavior and characteristics caused by the elevator's activation event in the harmonic currents. From the results, analyzes were carried out to identify the elevator's activation events through the harmonic signature of the load and a qualitative comparison of the techniques used. When the elevator load is activated, the frequency inverter that controls its activation injects different harmonics in the grid. These harmonics vary over the time, as can be seen at Fig. 92. This figure shows the waveform of the phase A current, highlighting the waveform before and during an activation.

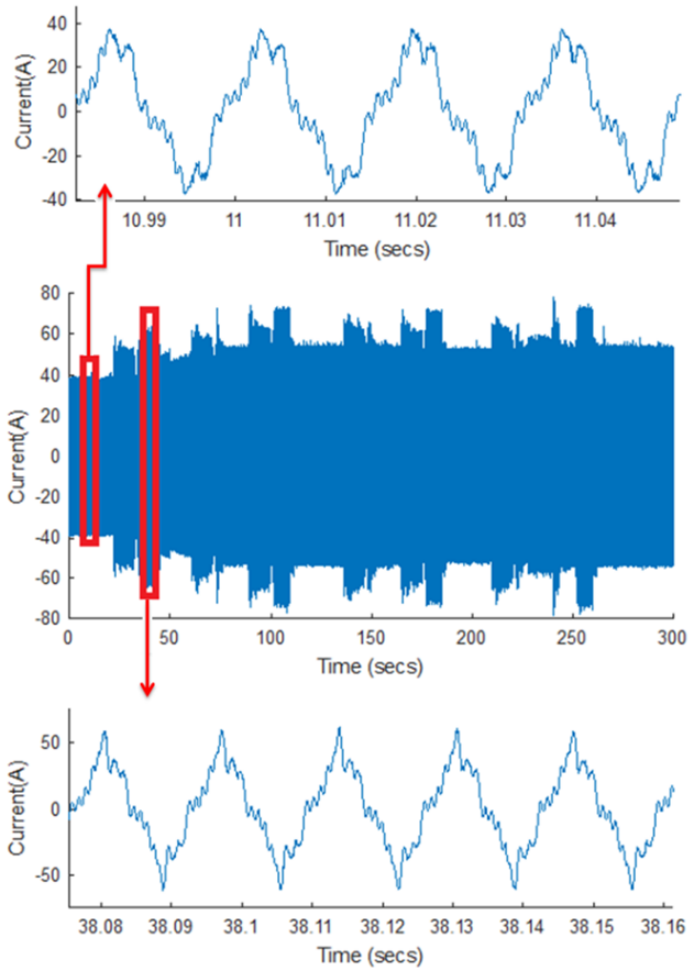

Figure 92 – Current in phases A, details before and during an activation.

5.3.1 FFT

Since the analyzed signal has variable frequencies in time, the FFT is not recommended for this analysis, however, it can be used to measure which harmonic components are present in the signal before the activation's, at the steady state. Thus, an FFT has been performed using 12 cycles. Figure 93 shows the spectrum of the harmonic frequencies.

As expected, odd harmonics are predominant, which is consistent because they are common to the load types presented at the analyzed environment.

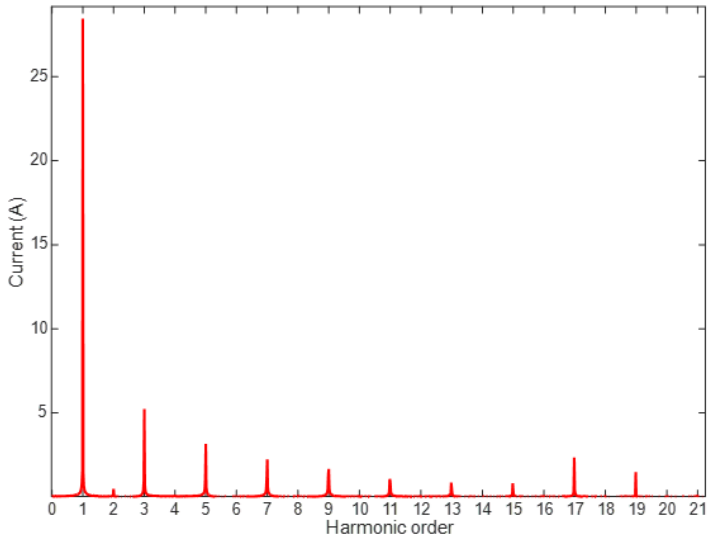

Figure 93 – FFT for 12 cycles.

5.3.2 STFT

By using the STFT, it was not possible to observe significant changes for different windows at the spectrogram, since through the FFT performed it is noticed that odd harmonics are present at all time, thus, with the activation of the load, the injection of harmonics were not relevant enough to cause changes in the spectrogram shown in Fig. 94 for the measurement at M1 and at Fig. 95, for the measurement at M2.

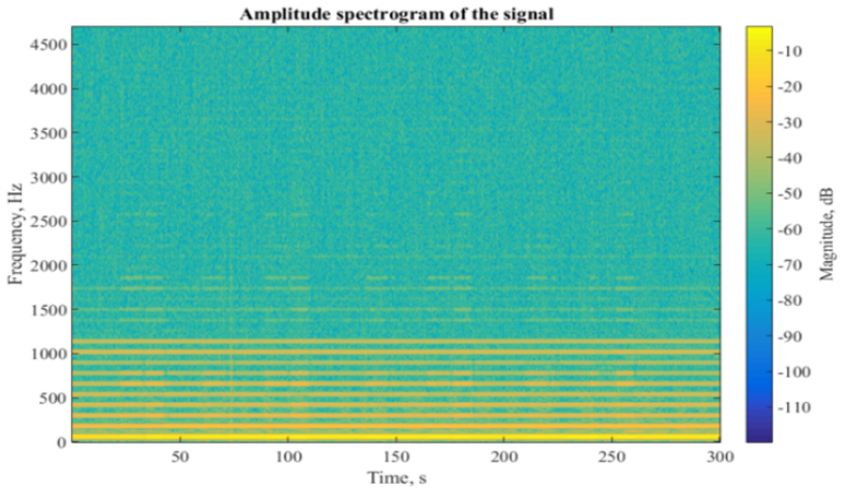

Figure 94 – Spectrogram using STFT at M1.

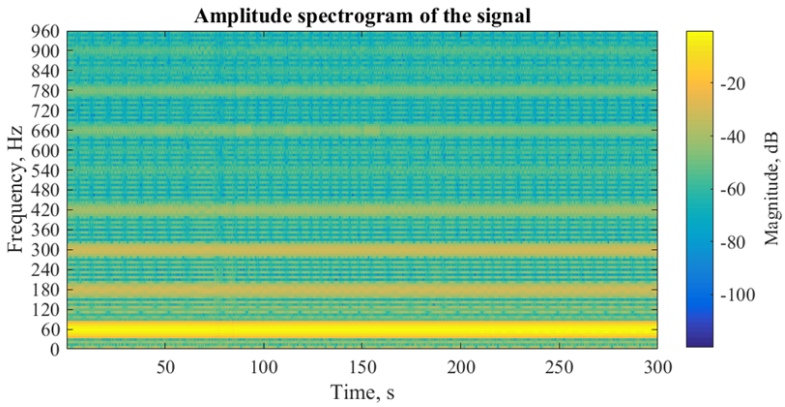

Figure 95 – Spectrogram using STFT at M2.

5.3.3 Wavelet

The wavelet transform provides good results for frequency changes and disturbances detection [46]. The DWT has been applied using the wavelet mother db4 to 5 levels of decomposition at the measurement of M1 (Fig. 96).

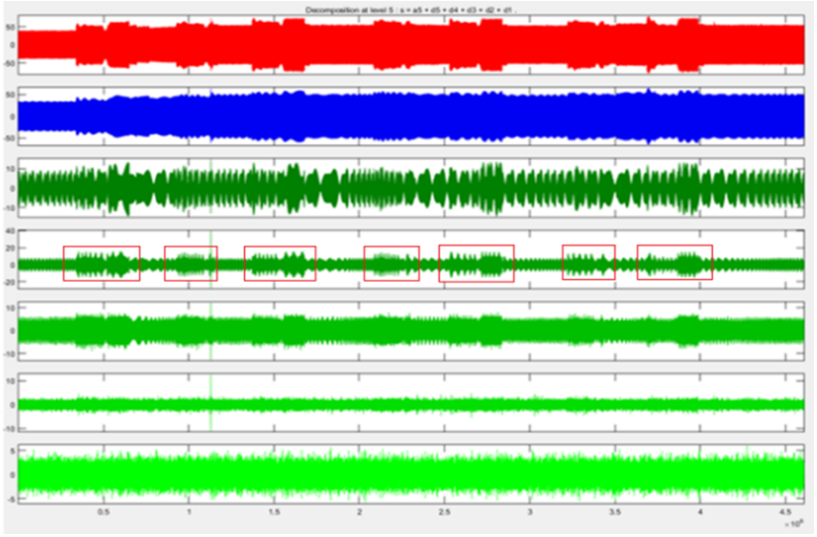

Figure 96 – 5-level wavelet decomposition (M1).

The details levels d3 and d4 which provide information about frequency variation behavior during the elevator's activation. The activations can be visualized with more details at level d4, where is detected the moment of the activation. In this specific case, it wasn't possible to distinguish between different types of activations, such as the elevator's ascend or descent. Fig. 97 shows the measurement at M2, and at the levels decomposition alteration can be observed at two points of the waveform. A study of the original waveform did not show perceptible visual alterations and there were no variances at the irradiance values verification. Therefore, the phenomena resulted of the harmonics propagation due to the elevator's activation at the grid.

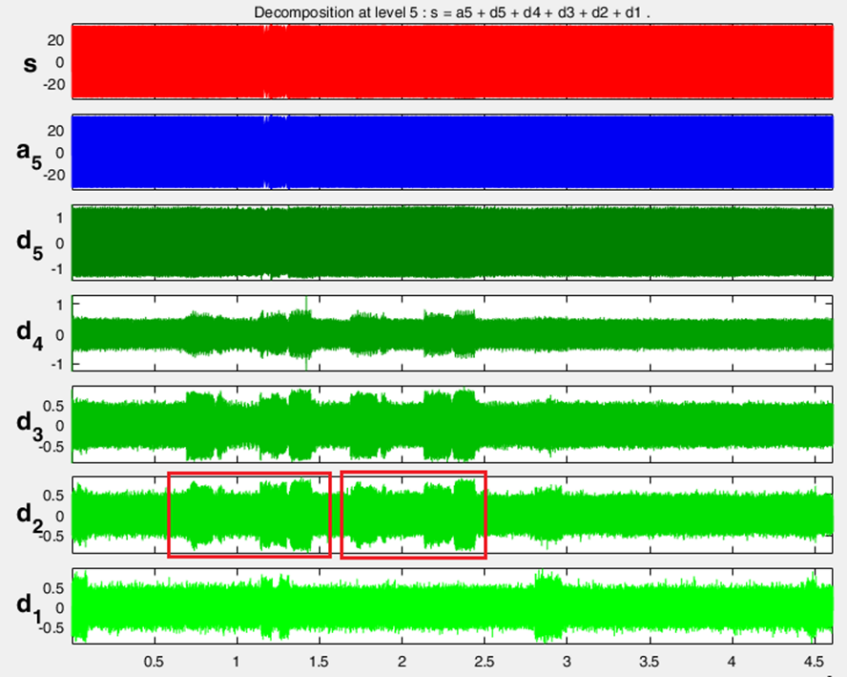

Figure 97 – 5-level wavelet decomposition (M2).

5.3.4 Wavelet Packet

The wavelet packet transform has been applied for an 8-level decomposition and mother wavelet was db45. The filter's synthesis result in the harmonics analysis was extracted, so it can be possible to analyze the waveform in each of the harmonics separately. Fig. 98 shows the extracted fundamental component.

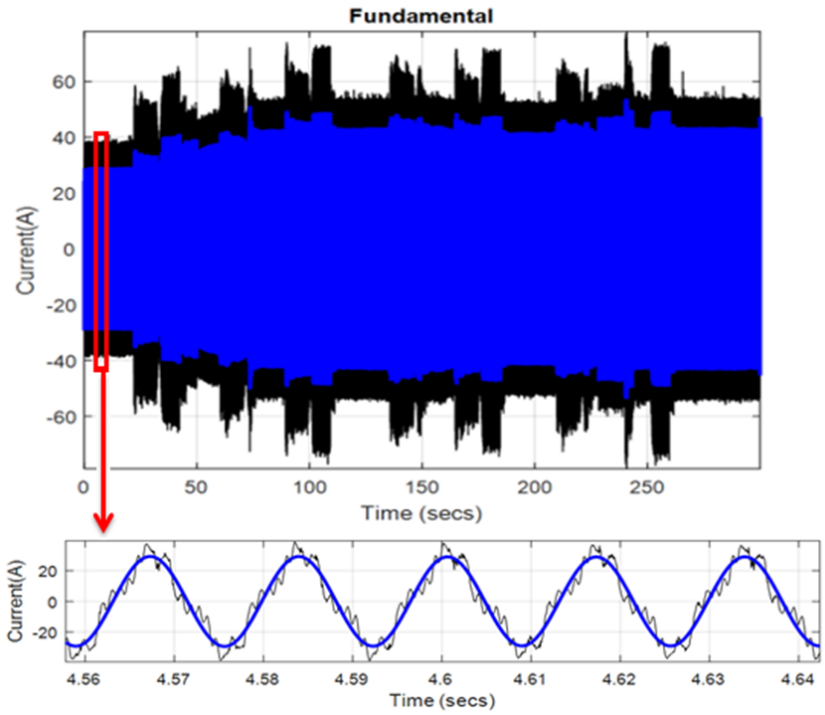

Figure 98 – Current waveform and fundamental component.

The third, seventh and ninth harmonics did not show significant variations with the elevator's activation events, maintaining their constant behavior. Fig. 99 shows the third harmonic. For the fifth, eleventh and thirteenth harmonic, a different type of behavior can be observed, where the changes resulting from the activation events can be clearly perceived, allowing the type of movement to be identified (ascent or descent), the duration of the activation event, besides the information in time of when the event occurred. Fig. 100 shows the eleventh harmonic.

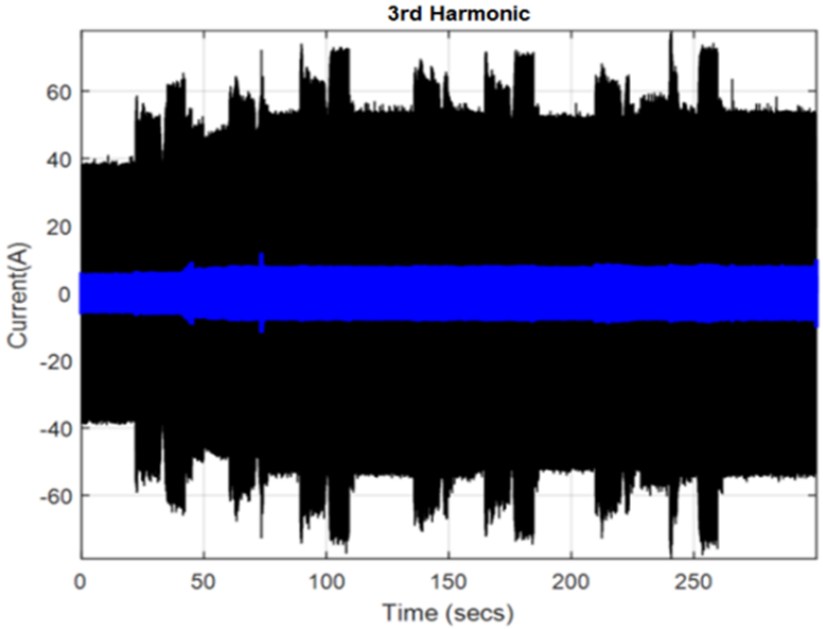

Figure 99 – Current waveform and third harmonic component.

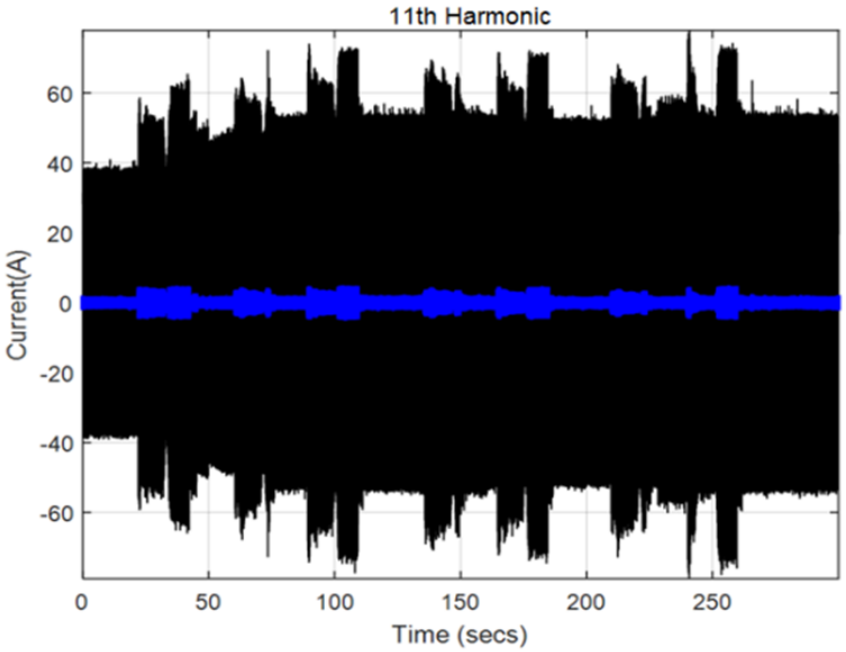

Figure 100 – Current waveform and eleventh harmonic component.

Fig. 101 shows the identified pattern for the eleventh harmonic, where the ascent and descent movements are differentiated. The elevator's ascent has a 16s duration, and the descent 24s.

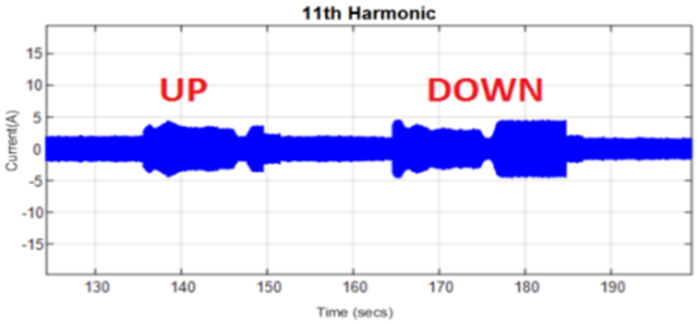

Figure 101 – Detail of the signature of elevator going up and down in the 11th harmonic.

It is possible to specify the exactly instants of the elevator's activation in the sampled signal from the identified patterns, which are 5 downward movements and 3 upward movements (Fig. 102).

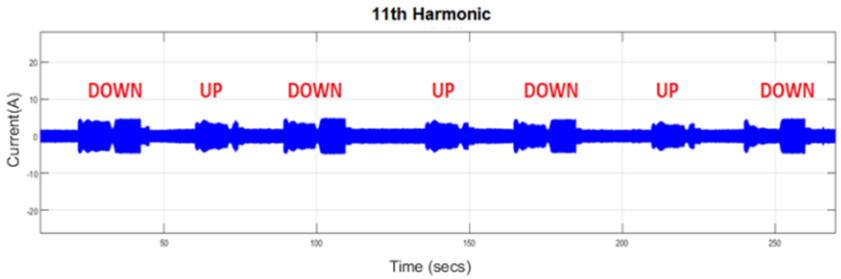

Figure 102 – Identification of elevator going up and down using the 11th harmonic.

The same study was performed using the wavelet packet at the measurement at M2 (Fig. 103), and the same pattern was identified. Therefore, proving that the harmonics are a result of the load's activation and not generated by solar inverter.

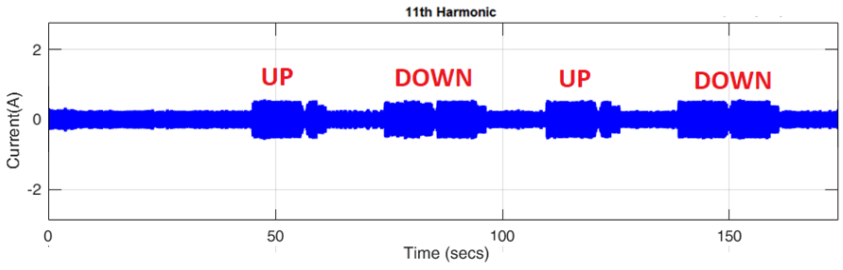

Figure 103 – Current waveform and eleventh harmonic component.

The results demonstrate the efficiency of the wavelet as a tool to study the impacts caused by the load at the system. In this work, a propagation of the harmonics produced by the load's activation measured at the inverter (M2) was verified, which could cause a measurement interpretation error, in case such harmonics were attributed to the inverter.

5.3.5 Results

The time-frequency analysis techniques were used to enlighten our understanding of a load behavior. The STFT did not provide the desired results because the behavior of the load did not present variations of frequencies different from those that already existed in the system. The wavelet transform provided effective for determining the activation desired moments, however it wasn't possible to distinguish between them. Lastly, the wavelet packet was efficient for this study objective, making it possible to identify the elevator's activation moments, and to obtain the duration and distinction of the ascent and descent events. These analyzes can be expanded to other types of loads (such as air conditioning, pumps, compressors, UPS, etc).

In addition to the obtained information, the wavelet packet provides important information such as the time-dependent harmonic spectrum, allowing a more complete impact analysis of harmonic distortion on an electric grid.

6 CONCLUSION

The main objective of this work is to carry out a study with PV inverters in a real system in order to compare the harmonic distortion impacts caused by these inverters under stationary and transient conditions. And also check if the data provided by the manufacturer really were equivalent to the actual measured in the system.

The first study had the objective to provide more details of understanding the harmonic contribution of an inverter connected to the grid, taking into account its topologies and control methods. Thus, in the practical analysis the results were better understood.

The Symos inverter have a more sinusoidal shape and overall lower harmonic components. However a it increases the insertion of 3rd and 5th harmonics in the system. It's startup process is smoother, increasing the output of the inverter gradually, the time for operation in full generation is greater compared to the other inverter analyzed. This feature helps decreasing impacts on loads and protections of systems connected to the building's substation.

The IG Plus inverter has a faster start-up, but with more sudden input in the system, there are three stages for the complete start-up. This inverter has an interesting particularity, where when it does not reach a minimum value of irradiation for generation, it turns off one of the phases, increasing the current in the others. This can cause unbalance between system phases. In both inverters, there are no significant changes in harmonic production due to the variation of solar irradiation, that is, the increase of a specific harmonic or the insertion of new harmonics that are not present in the system.

The analysis of power quality in buildings that contain solar generation is of essential, given that the electrical system has been designed to contain a certain level of distortion due to the expected loads, such as the use of non-linear loads as computers, etc. With addition of the generation the contribution of the inverter can influence the power quality of the system, as verified in this work the injection of some specific higher harmonics in the system.

The THD data obtained in the analysis of measurements differed from those presented by the manufacturer. Where it has been found that both inverters, more specifically the IG Plus inverter is a great generator of harmonics for the system, especially the 5th harmonic, which can be detrimental to rotating systems fed by the grid. time-frequency analysis have proved to be effective, helping on a better understanding of an inverter operation under regular and transient conditions, so it is possible to expand these analyzes for large generations in order to design protections and preventive procedures for such systems.

With the techniques it was possible to identify a use pattern for an elevator located at the building site, with a harmonic signature, allowing identification of the moment, duration and type of usage. In addition, the results obtained show an interesting result on harmonic propagation in the system, where the harmonics generated by the drive inverter of an elevator were detected at the output of a PV inverter. When analyzed in isolation as it was performed, this harmonic can be erroneously associated to the inverter and in the analysis of other loads of the system.

Among the used signal processing techniques, the Wavelet Packet presented the best results for this work's proposal, owing to its capacity to analyze each harmonic separately. It was possible to verify the harmonic's behavior during the different tests performed, providing a better understanding of the used inverter's particularities.

The case study in inverters showed good results and contributions for power quality analysis, showing that some characteristics of the inverters are associated to the type of control and construction of these equipment's, which can vary between manufacturers and models.

7 FUTURE WORK

The performed analysis can be applied to any photovoltaic generation, thus, for the continuity of this work:

- Analyze different manufacturers and other inverters models.
- Apply these tools at larger photovoltaic plants where there is a greater number of inverters.
- Use artificial intelligence techniques to detect the harmonic signature of loads in the system.

BIBLIOGRAPHY

[1] Sharma, H.; Rylander, M.; Dorr, D. Grid impacts due to increased penetration of newer harmonic sources. *IEEE Transactions on Industry Applications*, v. 52, n. 1, p. 99–104, Jan 2016. ISSN 0093-9994. Cited on the page 12.

[2] Rad, M. S. et al. Analysis of the grid harmonics and their impacts on distribution transformers. p. 1–5, Feb 2012. Cited 2 times on the page 12 and 14.

[3] Bravo, R. J. Solar pv power plants harmonics impacts. In: *2018 IEEE/PES Transmission and Distribution Conference and Exposition (T D)*. [S.l.: s.n.], 2018. p. 1–9. ISSN 2160-8563. Cited on the page 12.

[4] Agrawal, A.; Singh, D. K. Harmonic impact of grid connected photovoltaic system on low voltage power system. In: *2018 3rd International Conference for Convergence in Technology (I2CT)*. [S.l.: s.n.], 2018. p. 1–5. Cited 2 times on the page 12 and 13.

[5] Panagis, P. et al. Comparison of state of the art multilevel inverters. *IEEE Power Electronics Specialists Conference*, p. 4296–4301, June 2008. Cited 2 times on the page 12 and 30.

[6] Goyal, G. N.; Aware, M. V. A comparative performance of six-phase nine switch inverter operation with spwm and svpwm. In: *2012 IEEE International Conference on Power Electronics, Drives and Energy Systems (PEDES)*. [S.l.: s.n.], 2012. p. 1–6. Cited on the page 12.

[7] Xu, W. Applying harmonic standards to time-varying harmonics. In: *IEEE Power Engineering Society General Meeting, 2005.* [S.l.: s.n.], 2005. p. 2407–2409 Vol. 3. ISSN 1932-5517. Cited on the page 12.

[8] Grötzbach, M.; Redmann, R. Line current harmonics of vsi-fed adjustable-speed drives. *IEEE Trans. Ind. Appl*, v. 36, p. 683–690, March/April 2000. Cited on the page 13.

[9] Zeng G. H. Tan, J. Z. W. F. P.; Ji, Y. C. Novel single-phase five-level voltage-source inverter for the shunt active power filter. *IET Power Electronics*, v. 3, n. 4, p. 480–489, July 2010. Cited on the page 13.

[10] Bhattacharya, S. Series connected igct based high power three-level neutral point clamped voltage source inverter pole for facts applications. *IEEE 36th Power Electronics Specialists Conference*, v. 3, n. 4, p. 2315–2321, July 2005. Cited on the page 13.

[11] Borowy, B. S.; Salameh, Z. M. Methodology for optimally sizing the combination of a battery bank and pv array in a wind/pv hybrid system. *IEEE Transactions on Power Electronics*, v. 11, n. 2, p. 367–375, Jun 1996. Cited on the page 13.

[12] Qudsi, O. A. et al. Optimized gdpwm based on spontaneous evolutionary ga for reducing switching losses on inverter. *Information Technology and Electrical Engineering (ICITEE)*, p. 391 – 396, Oct 2013. Cited on the page 13.

[13] Peng J. S. Lai, J. W. M. F. Z.; VanCoevering, J. A multilevel voltage-source inverter with separate dc sources for static var generation. *IEEE Transactions on Industry Applications*, v. 32, n. 5, p. 1130–1138, Sep/Oct 1996. Cited on the page 13.

[14] Alepuz, S. B. S. et al. Interfacing renewable energy sources to the utility grid using a three-level inverter. *IEEE Transactions on Industrial Electronics*, v. 53, n. 5, p. 1504–1511, Oct 2006. Cited on the page 13.

[15] Dogga, R.; Pathak, M. Recent trends in solar pv inverter topologies. *Solar Energy*, v. 183, p. 57 – 73, 2019. ISSN 0038-092X. Disponível em: <http://www.sciencedirect.com/science/article/pii/S0038092X19301999>. Cited on the page 13.

[16] Rani, P. S.; Prasadarao, K. V. S.; Subbarao, K. R. N. V. Comparison of symmetrical and asymmetrical multilevel inverter topologies with reduced number of switches. In: *2014 International Conference on Smart Electric Grid (ISEG)*. [S.l.: s.n.], 2014. p. 1–5. Cited on the page 13.

[17] Amamra, S. et al. Multilevel inverter topology for renewable energy grid integration. *IEEE Transactions on Industrial Electronics*, v. 64, n. 11, p. 8855–8866, Nov 2017. ISSN 0278-0046. Cited on the page 13.

[18] Boonmee, C.; Wajanatepin, N. Comparison of using carrier-based pulse width modulation techniques for cascaded h-bridge inverters application in the pv energy systems. *Electrical Engineering Congress (iEECON)*, v. 53, n. 5, p. 1–4, Oct 2014. Cited 2 times on the page 13 and 26.

[19] Kerekes, T. et al. A new high-efficiency single-phase transformerless pv inverter topology", in ieee transactions on power electronics. *IEEE Transactions on Power Electronics*, v. 58, n. 1, p. 184–191, Jun 2009. Cited on the page 13.

[20] Fekete, K.; Klaic, Z.; Majdandzic, L. A new high-efficiency single-phase transformerless pv inverter topology", in ieee transactions on power electronics. *Renewable Energy*, v. 43, p. 140–148, Dec 2011. Cited on the page 13.

[21] Ueda, Y. et al. Analysis results of output power loss due to the grid voltage rise in grid-connected photovoltaic power generation systems. *IEEE Transations on Industrial Electronics*, v. 55, n. 7, p. 1–3, Jul 2008. Cited on the page 14.

[22] Cabral, J. B. R. et al. A new high gain non-isolated dc-dc boost converter for photovoltaic application. *Brazilian Power Electronics Conference*, p. 569–574, 2013. Cited on the page 14.

[23] Begum, B. A.; Vasanth, J. A. Mppt based photovoltaic boost half bridge converter for grid connected system. *Green Computing Communication and Electrical Engineering (ICGCCEE)*, p. 1–6, March 2014. Cited on the page 14.

[24] Kwon, J. M.; Kwon, B. H.; NAM, K. H. Three-phase photovoltaic system with three-level boosting mppt control. *IEEE Transactions on Power Electronics*, v. 23, n. 5, p. 2319–2327, Sept 2008. Cited on the page 14.

[25] Jung, D.; Nguyen, H. H.; Yau, D. K. Y. Tracking appliance usage information using harmonic signature sensing. p. 459–465, Nov 2015. Cited on the page 14.

[26] Subhashree, R.; Preethi, C. S.; Supriya, P. Fault distance identification in transmission line using stft algorithm. *2016 International Conference on Computer Communication and Informatics (ICCCI)*, p. 1–4, Jan 2016. Cited on the page 14.

[27] Bhattacharjee, R.; De, A. A robust stft based algorithm for detection of symmetrical fault during power swing. In: *2016 IEEE 7th Power India International Conference (PIICON)*. [S.l.: s.n.], 2016. p. 1–5. Cited on the page 14.

[28] Barros, J.; Ramón, D. Detection and analysis of time-varying harmonics in power systems using wavelets. *6th WSEAS IASME Int. Conf. on Electric Power Systems, High Voltages*, Dec 2006. Cited on the page 14.

[29] Okumus, H.; Nuroglu, F. M. Power system event classification based on machine learning. In: *2018 3rd International Conference on Computer Science and Engineering (UBMK)*. [S.l.: s.n.], 2018. p. 402–405. Cited on the page 14.

[30] Zaro, F. R.; Abido, M. A. Real-time detection and classification for voltage events based on wavelet transform. In: *2019 IEEE Jordan International Joint Conference on Electrical Engineering and Information Technology (JEEIT)*. [S.l.: s.n.], 2019. p. 872–877. Cited on the page 14.

[31] Singh, A. K.; Fozdar, M. Supervisory framework for event detection and classification using wavelet transform. In: *2017 IEEE Power Energy Society General Meeting*. [S.l.: s.n.], 2017. p. 1–5. ISSN 1944-9933. Cited on the page 14.

[32] Prates, M. O. et al. Power system impedance measurement based on wavelet voltage imposed. In: *2014 16th International Conference on Harmonics and Quality of Power (ICHQP)*. [S.l.: s.n.], 2014. p. 798–802. ISSN 2164-0610. Cited on the page 14.

[33] Hafiz, F. et al. Power quality event identification using wavelet packet transform: A comprehensive investigation. In: *TENCON 2017 - 2017 IEEE Region 10 Conference*. [S.l.: s.n.], 2017. p. 2978–2983. ISSN 2159-3450. Cited on the page 14.

[34] Singh, A. K.; Fozdar, M. A wavelet-based event detection and location framework for enhanced situational awareness in power system. *2016 IEEE Annual India Conference (INDICON)*, p. 1–6, Dec 2016. ISSN 2325-9418. Cited on the page 14.

[35] Silva, S. et al. High impedance fault detection in power distribution systems using wavelet transform and evolving neural network. *Electric Power Systems Research*, v. 154, p. 474 – 483, 2018. ISSN 0378-7796. Disponível em: <http://www.sciencedirect.com/science/article/pii/S0378779617303644>. Cited 2 times on the page 14 and 20.

[36] Do, H. T. et al. Wavelet packet-based passive islanding detection method for grid connected photovoltaic inverters. *2016 IEEE 8th International Power Electronics and Motion Control Conference (IPEMC-ECCE Asia)*, p. 1566–1570, May 2016. Cited on the page 14.

[37] Ersoy, O. K. A comparative review of real and complex fourier-related transforms. *Proceedings of the IEEE*, v. 82, n. 3, p. 429–447, March 1994. ISSN 0018-9219. Cited on the page 16.

[38] Panchbhai, A.; Parmar, S.; Vaghasiya, C. Thd comparison for power quality (matlab simulation amp; hardware). In: *2016 IEEE 1st International Conference on Power Electronics, Intelligent Control and Energy Systems (ICPEICES)*. [S.l.: s.n.], 2016. p. 1–4. Cited on the page 16.

[39] Yu, Y.; Xu, Y.; Liu, X. Research of improved iterative dft method in harmonic current detection. *2011 Asia-Pacific Power and Energy Engineering Conference*, p. 1–4, March 2011. ISSN 2157-4847. Cited on the page 16.

[40] Ribeiro, P. F.; Belchior, F. N.; Marques, F. C. Comparative analysis of instruments measuring time varying harmonics. *International Journal of Emerging Electric Power Systems*, v. 17, 2016. Cited on the page 17.

[41] Marques, C. A. et al. Parameters estimation of time-varying harmonics. In: *Power Quality Issues*. [S.l.]: IntechOpen, 2013. Cited on the page 18.

[42] Romero-Quete, A. A. et al. Time-varying harmonic analysis of electric power systems with wind farms, by employing the possibility theory. *Dyna*, 2006, Revista DYNA, v. 82, n. 192, p. 185–194, 2015. Cited on the page 18.

[43] Liboni, L. H. et al. Efficient signal processing technique for information extraction and its applications in power systems. *Electric Power Systems Research*, v. 141, p. 538 – 548, 2016. ISSN 0378-7796. Disponível em: <http://www.sciencedirect.com/science/article/pii/S0378779616303200>. Cited 2 times on the page 18 and 21.

[44] Gabor, D. Theory of communication. part 1: The analysis of information. *Journal of the Institution of Electrical Engineers - Part III: Radio and Communication Engineering*, v. 93, n. 26, p. 429–441, November 1946. Cited on the page 18.

[45] Portnoff, M. Time-frequency representation of digital signals and systems based on short-time fourier analysis. *IEEE Transactions on Acoustics, Speech, and Signal Processing*, v. 28, n. 1, p. 55–69, February 1980. ISSN 0096-3518. Cited on the page 18.

[46] Carvalho, T. C. O. et al. Review of signal processing techniques for time-varying harmonic decomposition. *2012 IEEE Power and Energy Society General Meeting*, p. 1–6, July 2012. ISSN 1932-5517. Cited 2 times on the page 20 and 76.

[47] Frunt, J.; Kling, W. L.; Ribeiro, P. F. Wavelet decomposition for power balancing analysis. *IEEE Transactions on Power Delivery*, v. 26, n. 3, p. 1608–1614, July 2011. ISSN 0885-8977. Cited on the page 20.

[48] Thangaraj, K.; Archana, R.; Begam, S. A. Analysis and estimation of harmonics using wavelet packet transform. *2016 International Conference on Emerging Trends in Engineering, Technology and Science (ICETETS)*, p. 1–5, Feb 2016. Cited 2 times on the page 20 and 25.

[49] Nagata, E. A. et al. Voltage sag and swell detection and segmentation based on independent component analysis. *Electric Power Systems Research*, v. 155, p. 274 – 280, 2018. ISSN 0378-7796. Disponível em: <http://www.sciencedirect.com/science/article/pii/S0378779617304352>. Cited on the page 20.

[50] Escudero, R. et al. Microgrid fault detection based on wavelet transformation and park's vector approach. *Electric Power Systems Research*, v. 152, p. 401 – 410, 2017. ISSN 0378-7796. Disponível em: <http://www.sciencedirect.com/science/article/pii/S0378779617303139>. Cited on the page 20.

[51] Thirumala, K. et al. Visualizing time-varying power quality indices using generalized empirical wavelet transform. *Electric Power Systems Research*, v. 143, p. 99 – 109, 2017. ISSN 0378-7796. Disponível em: <http://www.sciencedirect.com/science/article/pii/S037877961630414X>. Cited on the page 20.

[52] Babacan, Y. et al. Wavelet analysis of a memristor emulated model proposed for compact fluorescent lamp operated systems. *Electric Power Systems Research*, v. 160, p. 56 – 62, 2018. ISSN 0378-7796. Disponível em: <http://www.sciencedirect.com/science/article/pii/S0378779618300385>. Cited on the page 20.

[53] Zubić, S.; Balcerek, P.; Zeljković Čedomir. Speed and security improvements of distance protection based on discrete wavelet and hilbert transform. *Electric Power Systems Research*, v. 148, p. 27 – 34, 2017. ISSN 0378-7796. Disponível em: <http://www.sciencedirect.com/science/article/pii/S037877961730113X>. Cited on the page 20.

[54] Qi, P. et al. Discrete wavelet transform optimal parameters estimation for arc fault detection in low-voltage residential power networks. *Electric Power Systems Research*, v. 143, p. 130 – 139, 2017. ISSN 0378-7796. Disponível em: <http://www.sciencedirect.com/science/article/pii/S0378779616304059>. Cited on the page 20.

[55] Bellini, A.; Bifaretti, S. Comparison between sinusoidal pwm and space vector modulation techniques for npc inverters. *IEEE Power Tech*, v. 53, n. 5, p. 1–7, Oct 2005. Cited on the page 26.

[56] Huang, J.; Xiong, R. Study on modulating carrier frequency twice in spwm single-phase inverter. *IEEE Transactions on Power Electronics*, v. 29, n. 7, p. 3384–3392, July 2014. Cited on the page 26.

[57] Fri, A.; Bachtiri, R. E.; Ghzizal, A. E. A comparative study of three topologies of three-phase (5l) inverter for a pv system. *Energy Procedia*, v. 42, p. 436 – 445, 2013. ISSN 1876-6102. Mediterranean Green Energy Forum 2013: Proceedings of an International Conference MGEF-13. Cited 2 times on the page 29 and 30.

[58] Rodriguez, J. et al. A survey on neutral-point-clamped inverters. *IEEE Trans on Ind. Electronics*, v. 57, n. 7, p. 2219–2230, July 2010. Cited on the page 29.

[59] Rodriguez, J. et al. Multilevel voltage-source-converter topologies for industrial medium-voltage drives. *IEEE Trans. Ind. Electron.*, v. 54, n. 6, p. 2930–2945, Dec 2007. Cited on the page 29.

[60] McGrath, B.; Holmes, D. Multicarrier pwm strategies for multilevel inverters. *IEEE Trans. Ind. Electron.*, v. 49, n. 4, p. 858–867, Aug 2002. Cited on the page 29.

[61] Lezana, P.; Aceiton, R.; Silva, C. Phase disposition pwm implementation for a hybrid multicell converter. *IEEE Transactions on Industrial Applications*, v. 60, n. 5, p. 1936–1942, May 2013. Cited on the page 29.

[62] Penga, F. Z.; Mckeever, J. W.; Adams, D. J. A power line conditioner using cascade multilevel inverters for distribution systems. *IEEE Transactions on Industrial Applications*, v. 34, n. 6, p. 1293–1298, Nov/Dec 1998. Cited on the page 30.

[63] Unifei. *Universidade Federal de Itajubá*. 2017. [Online; accessed July 22, 2019]. Disponível em: <https://unifei.edu.br/isee/wp-content/uploads/sites/33/2017/08/qmap-768x384.jpg>. Cited on the page 39.

[64] Unifei. *Universidade Federal de Itajubá*. 2017. [Online; accessed July 22, 2019]. Disponível em: <https://qmap.unifei.edu.br/wp-content/uploads/2017/09/IMG_0549.jpg>. Cited on the page 39.

[65] Ebay. *Internal Fronius IG Plus*. 2017. [Online; accessed July 22, 2019]. Disponível em: <https://i.ebayimg.com/images/g/E2EAAOSwkZxdH4Km/s-l1600.jpg>. Cited on the page 42.

APPENDIX A – PUBLISHED PAPERS

GOMES, R. O.; RIBEIRO, P. F. ; DUQUE, C. A. ; BELCHIOR, F. . IDENTIFICAÇÃO DO COMPORTAMENTO DA CARGA UTILIZANDO PROCESSAMENTO DIGITAL DE SINAIS COM HARMÔNICOS VARIANTES NO TEMPO. In: Conferência Brasileira sobre Qualidade de Energia Elétrica, 2017, Curitiba. CBQEE, 2017.